3D SITE RESPONSE ANALYSIS

SHIMA SADEGHZADEH

ÖZYEĞİN UNIVERSITY

JANUARY, 2025

3D SITE RESPONSE ANALYSIS

by
Shima Sadeghzadeh

Dissertation
Submitted in Partial Fulfillment of the
Requirements for the Degree of

Doctor of Philosophy

in
Civil Engineering

Advisor: Prof. Dr. Atilla Ansal

Graduate School of Science and Engineering
Özyeğin University
İstanbul

January, 2025

3D SITE RESPONSE ANALYSIS

Approved by:

Professor Dr. Atilla Ansal, Advisor
Department of Civil Engineering
Özyeğin University

Dr. Okan İlhan
Department of Civil Engineering
Ankara Yıldırım Beyazıt University

Professor Dr. S. Feyza Çinicioğlu
Department of Civil Engineering
Özyeğin University

Professor Dr. Ayfer Erken
Department of Civil Engineering
Doğuş University

Dr. Gökçe Tönük
Department of Civil Engineering
MEF University

Approval Date: December 23, 2024

To ...

To the cherished memory of my beloved mother and dear brother.

To my supportive father, my compassionate sister, and my dearest husband.

DECLARATION OF ORIGINALITY

I hereby declare that I am the sole author of this thesis and that this is the true copy of my thesis, including the final revisions, approved by my thesis committee. All data and information have been obtained, produced, and presented in accordance with the rules of research ethics and principles of academic honesty. As required by these rules, to the best of my knowledge I have acknowledged ideas, thoughts, and any copyrighted material in accordance with the standard referencing rules. I certify that any part of this thesis has not been submitted for a degree or diploma in another educational institution.

Shima Sadeghzadeh

ABSTRACT

Site response analysis (SRA) is a critical component of geotechnical earthquake engineering, used to evaluate how local soil conditions modify seismic waves from bedrock to the ground surface. While traditional one-dimensional (1D) SRA methods provide valuable insights into vertical wave propagation, they simplify real conditions by neglecting the full range of seismic input components that can influence ground motion characteristics. This study presents a comparative analysis of multidirectional site response modeling for a series of well-instrumented downhole arrays in Anchorage, Alaska, United States, and the Zeytinburnu soil profile in Istanbul, Türkiye, subjected to various recorded earthquake events. By incorporating all three earthquake components (East–West, North–South, and Vertical) into a multidirectional SRA framework, the research aims to achieve more accurate estimates of site amplification. The results reveal distinct differences in modeled ground motions between three-dimensional and one-dimensional analyses at various soil depths, demonstrating the enhanced reliability offered by a multidirectional approach. These findings underscore the necessity of employing more comprehensive modeling strategies in regions with high seismicity. Furthermore, an optimization study was performed as part of the research to reduce uncertainties in input parameters, with a primary focus on shear wave velocity (Vs) and the stiffness modulus derived from it. Comparisons between unoptimized and optimized models show that the optimized profile more closely aligns with recorded ground motions. This improvement highlights the framework's ability to refine key soil properties, ultimately resulting in enhanced predictive accuracy at the ground surface.

Keywords: Site response analysis (SRA), Multidirectional modeling, Geotechnical earthquake engineering, Soil amplification, Parameter optimization

ÖZET

Zemin tepki analizi (SRA), geoteknik deprem mühendisliğinin kritik bir bileşenidir ve yerel zemin koşullarının sismik dalgaları temel kayadan yüzeye kadar nasıl değiştirdiğini değerlendirmeyi amaçlar. Geleneksel tek boyutlu (1B) SRA yöntemleri, düşey dalga yayılımına dair değerli içgörüler sunsa da, zemin hareketi özelliklerini etkileyebilecek tüm sismik girdi bileşenlerini göz ardı ederek gerçek koşulları basitleştirir. Bu çalışma, Amerika Birleşik Devletleri'nin Alaska eyaletine bağlı Anchorage bölgesindeki iyi enstrümantasyona sahip derin sondaj dizileri ile İstanbul, Türkiye'deki Zeytinburnu zemin profili üzerinde kaydedilmiş çeşitli deprem verilerini kullanarak çok yönlü zemin tepki modellemesinin karşılaştırmalı bir analizini sunmaktadır. Doğu–Batı, Kuzey–Güney ve Düşey olmak üzere tüm üç deprem bileşenini çok yönlü SRA çerçevesine dahil ederek, bu araştırma, saha büyütme tahminlerinin doğruluğunu artırmayı hedeflemektedir. Elde edilen sonuçlar, farklı derinliklerdeki üç boyutlu (3B) ve tek boyutlu (1B) analizler arasında belirgin farklılıklar olduğunu göstererek, çok yönlü yaklaşımın sunduğu daha yüksek güvenilirliği ortaya koymaktadır. Bu bulgular, yüksek sismisiteye sahip bölgelerde daha kapsamlı modelleme stratejilerinin benimsenmesinin önemini vurgulamaktadır. Ayrıca, çalışma kapsamında yürütülen bir optimizasyon çalışması, özellikle kayma dalgası hızı (Vs) ve bu hızdan türetilen rijitlik modülü olmak üzere, girdi parametrelerindeki belirsizlikleri azaltmaya odaklanmıştır. Optimizasyon öncesi ve sonrası modellerin karşılaştırılması, optimize edilen profilin kaydedilmiş yer hareketleri ile daha uyumlu olduğunu göstermiştir. Bu iyileşme, çerçevenin temel zemin özelliklerini rafine edebilme kabiliyetinin altını çizerek, yer yüzeyindeki zemin hareketlerinin tahmininde artan bir doğruluk sağlamaktadır.

Anahtar Kelimeler: Zemin tepki analizi (SRA), Çok yönlü modelleme, Geoteknik deprem mühendisliği, Zemin büyütmesi, Parametre optimizasyonu.

ACKNOWLEDGEMENTS

I would like to express my deepest gratitude to my advisor, Prof. Dr. Atilla Ansal, for his exceptional guidance and mentorship throughout my research journey. His unwavering support, insightful feedback, and dedication to my academic and professional growth have been invaluable, and I am profoundly appreciative of his contributions.

A special thanks is extended to my co-advisor, Prof. Dr. Cristoforo Demartino, whose expertise and mentorship in numerical modeling and finite element methods were instrumental in advancing my understanding of these methodologies and their application within the scope of this thesis.

I wish to express my sincere appreciation to Prof. Dr. Fabio di Trapani for his invaluable support and guidance throughout the development of this thesis. His constructive feedback and insightful suggestions have greatly enhanced the quality and clarity of this work.

Finally, I would like to extend my gratitude to Prof. Dr. Mehmet Celebi, Jaime Steidl, John Thornley, and Lisa S. Schleicher for their invaluable support in providing critical data on the Atwood building in Anchorage, Alaska, which played an essential role in my research.

TABLE OF CONTENTS

DECLARATION OF ORIGINALITY iv

ABSTRACT v

ÖZET vi

ACKNOWLEDGEMENTS vii

LIST OF TABLES xi

LIST OF FIGURES xii

LIST OF ACRONYMS AND ABBREVIATIONS xv

1 INTRODUCTION 1

1.1 Problem Description 2

1.2 Scope 3

2 LITERATURE REVIEW 4

2.1 One-Dimensional Site Response Analysis 4

2.2 Limitations of One-Dimensional Site Response Analysis 5

3 CHARACTERIZATION OF DOWNHOLE ARRAYS 10

3.1 Zeytinburnu Downhole Array 10

3.1.1 Location 11

3.1.2 Instrumentation 11

3.1.3 In-situ Tests 12

3.1.4 Selected Earthquakes 14

3.1.5 Soil Property 15

3.2 Alaska Downhole Array 16

3.2.1 Location 16

3.2.2 Instrumentation 17

3.2.3 In-situ Tests 18

3.2.4 Selected Earthquakes 19

3.2.5 Soil Property 21
4 SITE RESPONSE ANALYSIS MODELING 31
4.1 Deepsoil 33
4.1.1 Introduction to DEEPSOIL 33
4.1.2 Equivalent Linear Analysis in DEEPSOIL 34
4.1.3 Input Parameters and Configuration in DEEPSOIL 36
4.2 Plaxis3D 40
4.2.1 Introduction to Plaxis3D 40
4.2.2 Why Plaxis3D program? 41
4.2.3 Hardening Soil Model in Plaxis3D 42
4.3 OpenSeesPy 52
4.3.1 Proposed framework 52
4.3.2 Proposed FE model for predicting 3D SRA 53
5 OPTIMIZATION STUDY 62
5.1 Background of Optimization study 62
5.2 Benefits of the Optimization Study 67
5.3 Optimization Framework 67
5.3.1 Optimization in 3D site response analysis 67
5.3.2 Working Principles 68
5.3.3 Design Vector Encoding 70
5.3.4 Definition of the objective function 71
6 RESULTS 75
6.1 Zeytinburnu Soil Profile 75
6.1.1 1D site response analysis with Deepsoil 75
6.1.2 3D site response analysis with Plaxis3D 76
6.1.3 3D site response analysis with OpenSeesPy 76
6.1.4 Comparison of three methods 77
6.2 Alaska Soil profile 78
6.2.1 1D and 3D site response analysis 78

6.3 Results of Optimization study 88
7 CONCLUSIONS 95
7.1 Summary of Work 95
7.2 Key Findings 96
REFERENCES 100
VITA 112

LIST OF TABLES

Table 3.1: Summary of Kütahya earthquake in EW, NS and V directions 15

Table 3.2: Recorded Earthquakes at Atwood Building 20

Table 3.3: Recorded PGAs at three directions 20

Table 4.1: Alaska soil profile details. 39

Table 4.2: Zeytinburnu soil profile details 1. 39

Table 4.3: Hardening Soil model Required Parameters. 45

Table 4.4: Suggested Correlations for different soil types of HS model. 46

Table 4.5: Used parameters for HS model in Plaxis3D for Zeytinburnu soil profile. 47

Table 4.6: Corrected Nspt test data for Zeytinburnu soil profile. 49

Table 4.7: Zeytinburnu soil profile details 2. 56

LIST OF FIGURES

Figure 3.1: Zeytinburnu district in Türkiye 11

Figure 3.2: Accelerometers along Zeytinburnu vertical array. 12

Figure 3.3: Shear wave velocity profile obtained by PS logging test in Zeytinburnu. 13

Figure 3.4: Distance of Zeytinburnu to Kütahya Earthquake. 14

Figure 3.5: Recorded acceleration time histories at various depths and three directions. 22

Figure 3.6: Corresponding recorded spectra accelerations at various depths and three directions. 23

Figure 3.7: Amplification of ground motion on the surface. 23

Figure 3.8: Soil stratification along Zeytinburnu vertical array. 24

Figure 3.9: Robert B. Atwood building in Anchorage of Alaska. 24

Figure 3.10: Intersections of faults in Anchorage. 25

Figure 3.11: Atwood building. 25

Figure 3.12: Plan of Atwood building and six boreholes. 26

Figure 3.13: Different accelerometers at boreholes. 26

Figure 3.14: Shear wave velocity profile obtained in Anchorage. 27

Figure 3.15: Recorded earthquake with ID tag of A.1. 27

Figure 3.16: Recorded earthquake with ID tag of A.2. 28

Figure 3.17: Recorded earthquake with ID tag of A.3. 28

Figure 3.18: Recorded earthquake with ID tag of A.4. 28

Figure 3.19: Recorded earthquake with ID tag of A.5. 29

Figure 3.20: Recorded earthquake with ID tag of A.6. 29

Figure 3.21: Recorded earthquake with ID tag of A.7. 29

Figure 3.22: Atwood profile with sensors in longitudinal direction. 30

Figure 4.1: Site response analysis. 31

Figure 4.2: 1D and 3D site response analysis. 32

Figure 4.3: Equivalent linear method. 34

Figure 4.4: Deepsoil program for Zeytinburnu and Alaska. 37

Figure 4.5: Hardening soil model. 44

Figure 4.6: Studied soil profile and FE model of the column of soil. g is the gravity vector. R_v is the static reaction force at the base at the end of stage 1. 53

Figure 4.7: 8 nodal StdBrick elemenet. 54

Figure 4.8: ZeroLength elements. 57

Figure 4.9: EqualDOF XYZ in nodes. 59

Figure 4.10: Applied forces for dynamic analysis. 61

Figure 5.1: Genetic Algorithm framework. 65

Figure 5.2: Incorporation of data processing into 3D SRA. 68

Figure 5.3: Flowchart of the optimization framework. 69

Figure 5.4: Schematic presentation of RMSE concept. 73

Figure 6.1: Sensor with respect to 1D SRA in Zeytinburnu. 75

Figure 6.2: Sensor with respect to 3D SRA in Plaxis3D for Zeytinburnu. 76

Figure 6.3: Sensor with respect to 3D SRA in OpenSeesPy for Zeytinburnu. 77

Figure 6.4: Comparison of 3D SRAs with Sensor in Zeytinburnu. 78

Figure 6.5: Comparison of 3D SRAs and 1D SRA with Sensor for Zeytinburnu. 79

Figure 6.6: 3D SRA with respect to 1D SRA- A.1 (SA). 80

Figure 6.7: 3D SRA with respect to 1D SRA- A.1 (TH). 81

Figure 6.8: 3D SRA with respect to 1D SRA- A.2 (SA). 82

Figure 6.9: 3D SRA with respect to 1D SRA- A.2 (TH). 83

Figure 6.10: 3D SRA with respect to 1D SRA- A.3 (SA). 84

Figure 6.11: 3D SRA with respect to 1D SRA- A.3 (TH). 85

Figure 6.12: 3D SRA with respect to 1D SRA- A.4 (SA)..... 86

Figure 6.13: 3D SRA with respect to 1D SRA- A.4 (TH). 87

Figure 6.14: 3D SRA with respect to 1D SRA- A.5 (SA)..... 88

Figure 6.15: 3D SRA with respect to 1D SRA- A.5 (TH). 89

Figure 6.16: 3D SRA with respect to 1D SRA- A.6 (SA)..... 90

Figure 6.17: 3D SRA with respect to 1D SRA- A.6 (TH). 91

Figure 6.18: 3D SRA with respect to 1D SRA- A.7 (SA)..... 92

Figure 6.19: 3D SRA with respect to 1D SRA- A.7 (TH). 92

Figure 6.20: Düzce earthquake with 1D and 3D models in Alaska profile..... 93

Figure 6.21: Düzce earthquake with 1D and 3D models in Zeytinburnu profile..... 93

Figure 6.22: Using optimized soil profile (Zeytinburnu) for Kütahya earthquake in 3D SRA. 94

Figure 6.23: Using optimized soil profile (Zeytinburnu) for 2013 earthquake in 3D SRA..... 94

LIST OF ACRONYMS AND ABBREVIATIONS

ANSS	Advanced National Seismic System
EW	East-West
FE	Finite Element
GA	Genetic Algorithm
ML	Lacal Magnitude
NAFZ	North Anatolian Fault Zone
NS	North-South
PDMY	Pressure-Dependent Multi-Yield Model
PGA	Peak Ground Acceleration
PIMY	Pressure-Independent Multi-Yield Model
PVC	Polyvinyl Chloride
RMSE	Root Mean Square Error
SCPT	Seismic Cone Penetration Test
SPT	Standard Penetration Test
SSI	Soil-Structure Interaction
TH	Time History Analysis
USGS	United States Geological Survey
UTC	Coordinated Universal Time

1. INTRODUCTION

The impact of earthquakes on the built environment is a subject of significant concern for civil and earthquake engineers, urban planners, and policymakers. Earthquakes pose a serious threat to life and property, and understanding how to mitigate these risks is crucial for enhancing community resilience.

Site conditions play a key role in shaping the intensity and distribution of seismic damage across different regions, as the local geological and geotechnical characteristics can amplify or attenuate seismic waves. This phenomenon, known as site effects, is well-documented in various earthquake events, where buildings located on soft sediments often experience more severe damage compared to those on stiff bedrock [1], [2], [3].

Site-specific response analysis (SRA) is an essential tool in seismic hazard assessment, as it allows engineers to evaluate how local soil conditions influence ground shaking during an earthquake. The analysis typically involves modeling the response of soil layers subjected to incoming seismic waves, characterized by shear wave velocity profiles, shear modulus reduction, and damping ratio curves [4]. By capturing dynamic behavior of soils, SRA helps in determining critical parameters such as peak ground acceleration Peak Ground Acceleration (PGA), spectral accelerations, and other intensity measures that are used in structural design which are crucial in developing building codes and ensuring that structures are designed to withstand the expected levels of seismic forces.

In the context of seismic design, the accurate evaluation of peak ground acceleration and the uniform hazard acceleration spectrum is essential for minimizing structural vulnerability. Several factors influence the outcomes of site-specific response analysis, including soil stratification, material properties, the choice of analytical methods, and, importantly, the selection and scaling of ground motion time histories [5], [6]. Proper selection of representative input motions, compatible with regional seismicity, is critical in capturing the potential variability in ground shaking and achieving reliable design inputs

for earthquake-resistant structures [7], [8].

Earthquakes induce multi-directional ground motions, characterized by complex interactions between the horizontal and vertical components of seismic waves. This multi-directionality poses significant challenges to the resilience and safety of structures, as it affects not only the inertial response of the superstructure but also the dynamic interaction between the structure, foundation, and underlying soil [9], [10], [11], [12].

Ensuring the structural integrity of buildings under multi-directional seismic loading requires a holistic approach to design, where the combined effects of all components of ground motion are accounted for. Ignoring the multi-directional nature of seismic waves can lead to an unreal structural demand, resulting in inadequate assessments of safety and resilience.

1.1 Problem Description

Traditional site response analyses often employ one-dimensional (1D) models only one horizontal component of seismic waves, either East-West (EW) or North-South (NS), with assuming that the soil layers are subjected to vertically propagation of just one component of earthquake waves at a time.

While 1D analysis provides useful information, it does not account for the simultaneous influence of multiple seismic wave components, including the vertical component [13] and both horizontal components at same time, as the earthquake ground motions occur in three dimensions, with significant contributions from both horizontal (EW and NS) and vertical (V) directions, which can influence the dynamic response of soil layers and structures built on such sites.

Three-dimensional (3D) site response analysis represents an advancement in capturing the full behavior of seismic wave propagations through soil. Unlike 1D analysis, 3D site response analysis considers the simultaneous effects of all three components of

an earthquake—East-West (EW), North-South (NS), and Vertical (V) at the same time. This approach allows for a more realistic assessment of ground motion at the site level, particularly when dealing with the combined influence of these components, which can significantly affect the amplitude, duration, and frequency content of the seismic response. The vertical component, often neglected in simplified analyses, can have important implications for both soil behavior and the dynamic response of structures, especially in areas close to fault ruptures where vertical accelerations can be significant [14].

1.2 Scope

The aim of this study is to conduct a comprehensive 3D site response analysis with real captured ground motions in two downhole arrays as deep and short sites to understand how local site and geological characteristics interact with seismic waves originating from an earthquake in multiple directions: East-West (EW), North-South (NS), and Vertical (V).

By considering this multidimensional scope, the study seeks to develop a robust framework for assessing ground surface behavior under seismic loading. This includes analyzing the propagation of seismic waves through different soil layers, accounting for varying stiffness and damping properties, and understanding how these factors contribute to the overall seismic response and their impact on key seismic parameters such as peak ground acceleration, response spectra, and amplification factors. This study aims to bridge the gap between simplified 1D analyses and the complexities inherent in 3D wave propagations.

In conjunction with the comprehensive three-dimensional (3D) site response analysis (SRA), an optimization study was also conducted on the deeper site to address the uncertainties inherent on the shear wave velocity profile (Vs) and the estimated stiffness modulus derived from Vs.

2. LITERATURE REVIEW

2.1 One-Dimensional Site Response Analysis

Site response analysis (SRA) is a fundamental component of geotechnical earthquake engineering, aiming to evaluate how local soil condition affects ground motion during seismic events and understanding the influence of local site conditions on seismic response is crucial for accurately predicting building damage during earthquakes.

Numerous factors influence the outcomes of SRA, including site conditions, the utilized input motions, and the type of analysis conducted. For instance, soil heterogeneity, layering, and nonlinearity can significantly affect seismic wave propagation and amplification [15]. Additionally, the selection of input motions, particularly their amplitude, frequency content, and duration, plays a critical role in accurately predicting site response [7], [8].

While some studies suggest that fault type may not significantly impact the results of SRA at the ground surface [16], the overall complexity of seismic wave propagation necessitates more advanced analytical approaches. In the context of seismic hazard analysis and earthquake engineering, emphasizing the importance of local site response analysis is particularly crucial in regions susceptible to significant seismic activities. Recent substantial seismic events in Türkiye, such as the 2023 Kahramanmaraş earthquake and the 2020 İzmir earthquake, have underscored the critical necessity of this analytical approach ([17], [18]. These powerful earthquakes have heightened awareness of the vulnerability of structures and infrastructure in Türkiye, serving as stark reminders of the need for a comprehensive understanding of local geological and geotechnical conditions.

The extensive damage and loss of life experienced during these events highlights the urgent need for improved methods to predict and mitigate seismic risks. The most common approach in SRA has traditionally been the one-dimensional (1D) site response

analysis, which simplifies the problem by applying one horizontal earthquake motion which vertically propagating through horizontal soil layers [13].

This method is commonly used by geotechnical engineers to estimate ground shaking levels and assess seismic hazards at specific locations [1], which estimates of response spectra and intensity measures like peak ground acceleration (PGA) to help characterize site amplification factors [19]. However, 1D SRA considers only a single horizontal component of ground motion, either East-West (EW) or North-South (NS) and assumes vertical propagation of seismic waves, potentially oversimplifying the complex nature of seismic ground motions.

2.2 Limitations of One-Dimensional Site Response Analysis

One-Dimensional Site Response Analysis (1D SRA) is widely used in geotechnical earthquake engineering due to its computational efficiency and simplicity. However, it has notable limitations arising from its simplifying assumptions and not considering the multidirectional nature of earthquake ground motions.

Primarily, 1D SRA assumes that soil layers are infinite and homogeneous in the horizontal directions, neglecting lateral heterogeneity, variations in soil properties, topography, and complex geological conditions [1], [20]. This assumption often does not hold true in real-world scenarios where lateral variations can significantly influence seismic wave propagation. In other hand, earthquakes generate seismic waves that propagate in all directions, comprising two horizontal components (EW and NS) and a vertical component (V).

The simultaneous occurrence of these components can lead to complex soil responses at ground surface that are not adequately addressed by 1D analysis, which typically considers only one horizontal component at a time [13]. This simplification can result in the underestimation of seismic hazards and insufficient structural designs, as

multi-directional ground motions, including the vertical component, can significantly affect soil response and structural demands [21] [22]. Moreover, the inclusion of the vertical component (V) in site response analysis is essential, as vertical accelerations can have significant effects on structures, especially can increase the axial force on columns by about 50 percent [23] making its consideration crucial for comprehensive seismic design.

Numerous studies have highlighted the inadequacies of 1D SRA in capturing the spatial variability of soil profiles and ground motions. Madiai [24] demonstrated that 1D analyses could not account for complex wave propagation effects observed in sites with significant lateral heterogeneity. McGann et al. [25] emphasized that 1D SRA might underestimate ground motion amplification in basins and valleys where 3D effects are significant. Similarly, Makra et al. [26] and Pretell et al[27].

observed discrepancies between recorded ground motions and 1D SRA predictions in areas with complex geology, indicating the need for more sophisticated analysis methods. Smerzini compared one-dimensional, two-dimensional, and three-dimensional effects of site geometry on SRAs and found that one-dimensional analyses often fail to capture critical features of seismic response, particularly in near-field regions [14]. The dynamic behavior of the soil is significantly influenced by both the characteristics of the applied earthquake and the three-dimensional nature of the soil model. In situations where 1D analysis is inadequate, such as regions with pronounced lateral variations in soil properties, topographic irregularities, or complex seismic wave fields, a more comprehensive approach is necessary.

This ensures accurate predictions of ground motion characteristics like amplitude, frequency content, and duration, which are critical for seismic design and hazard assessment [28]. Three-dimensional SRA accounts for the simultaneous consideration of all

three components of earthquake motion—East-West (EW), North-South (NS), and vertical— thereby capturing the multi-directional nature of seismic loading [29]. It incorporates lateral variations in soil properties by modeling the spatial variability in soil stiffness, density, and damping characteristics, allowing for a more accurate representation of heterogeneous subsurface conditions [22].

Additionally, three-dimensional consideration of site can strongly affect ground amplifications at ground [30]. Advancements in computational capabilities and numerical methods have facilitated the implementation of 3D SRA, with high-performance computing and sophisticated software tools enabling the simulation of large-scale models that capture essential features of complex sites.

This progress has made 3D SRA a practical and more precise tool for seismic hazard assessment and engineering design. Some recent studies have explored 3D SRA over the traditional 1D method focusing mostly on geometry of site in three directions (3di) rather than using multidirectional input motions (3D). Pretell et al. conducted 3di ground motion analyses incorporating 3di soil simulations, highlighting the importance of accounting for source, path, and site effects comprehensively [27]. McGann et al. demonstrated that 3di SRA could capture basin-induced amplification effects that 1D analyses miss[31].

Lopez-Caballero and Modaressi-Farahmand Razavi emphasized the Neglecting the vertical component can lead to underestimation of seismic demands on structures[32]. Akinci et al. and Douglas et al. used synthetic ground motions to study 1di seismic responses in Istanbul. While valuable, these studies may not fully capture the complexities of inputting actual earthquake components (EW, NS and V) at same time and instead they are focusing on multi-dimensional geometry of site [33], [34].

In other studies, Seylabi et al. used computed physics-based generated 3D ground motion simulations for a valley in California to conduct SRAs for soil stations. Their

results showed that for used sites 3D analysis revealed lower PGA than 1D analysis, indicating differences in seismic demand predictions [35]. Besides, Zhang et al. used simulated ground motions from different physics-based broadband ground motion simulations in Istanbul with high PGAs, applying linear material models for comparison of 1D and 3D SRAs. They found that 90 percent of sites had larger responses in 3D analysis compared to 1D, concluding that the 1D approach cannot accurately capture variations in soil properties [36]. However, these studies using 3D ground motions have relied on simulated, physics-based generation of ground motions rather than real earthquake records.

Recently Ansal et al. (2024) investigated the impact of utilizing all three recorded components (EW, NS, Vertical) of the Silivri earthquake (Lacal Magnitude (ML)=5.7, 26/09/2019) on the Atakoy soil profile in Istanbul using PLAXIS3D for site response analysis and DEEPSOIL for 1D analysis. Their results highlighted the benefits of incorporating three components of earthquake at same time for modeling compared to 1D analysis, showing better agreement with recorded acceleration response spectra.

Smerzini and Pitilakis conducted a 3D model using a 3D physics-based kinematic representation of an extended seismic source with a simplified homogeneous velocity profile , employing the spectral element code GeoELSE. They concluded that 1D and 2D methods underestimate ground motions at the surface, while 3D simulations provide better predictions [37]. Similarly, Özcebe et al. compared different numerical approaches as one, two and three dimensional for predicting near-fault physics based simulated ground motions in alluvial basins by using FLAC2D, STRATA for 1D, and the SPEED code for 3D simulations, they found that the 3D geometric model revealed responses closer to recorded data at the ground surface [38].

From the reviewed literature, several gaps were identified. Most studies referred to 3D site response analysis as multi geometry and dimension of the site rather than using multi directional input ground motions. Besides, other studies have used simplified shear

wave velocity profiles, potentially overlooking spatial variations and uncertainties in soil properties. A few studies as Ansal et al. (2024) have directly compared 3D and 1D SRAs using both real earthquake components and detailed real soil profiles, especially in regions with high seismic risk like Türkiye [39], [40].

In other hand there is no study for accounting uncertainties inherent in soil properties and optimization of shear wave velocity to use in 3D SRA as they used just average shear wave velocity profiles, potentially overlooking uncertainties inherent in the data [25], [36]. Given that Türkiye is predominantly in high seismic zones and has experienced recent devastating earthquakes, there is growing concern about the ability of models to predict future real seismic events accurately [28].

In conclusion, this research addresses a critical gap in seismic response analysis by highlighting the importance of multi-directional input motions and using real data for a deep (Zeytinburnu) and a shallow site (Alaska) with using real soil profile (Zeytinburnu) for considering uncertainties in shear wave velocity, possibly through optimization studies, to capture inherent variability in soil properties and showing improvement of 3D SRA results on ground surface by using optimized shear wave velocity through soil profile.

3. CHARACTERIZATION OF DOWNHOLE ARRAYS

3.1 Zeytinburnu Downhole Array

Istanbul's proximity to the North Anatolian Fault Zone (NAFZ) makes it particularly vulnerable to significant seismic events, posing a serious threat to both human life and infrastructure. The NAFZ, a major right-lateral strike-slip fault system, runs parallel to the northern coast of Turkey, with its western segment extending beneath the Marmara Sea, approximately 20-30 km south of Istanbul.

This proximity increases the likelihood of the city experiencing a large-magnitude earthquake, as seismic energy continues to accumulate along the fault. Historical earthquakes, such as the 1999 İzmit earthquake (Mw 7.4), demonstrate the devastating impact that seismic activity along the NAFZ can have on the region. Evaluating the site response in Istanbul is essential, as the city's complex geology—ranging from soft alluvial deposits to limestone bedrock—can amplify seismic waves, especially in low-lying areas.

The choice of the Zeytinburnu vertical array for this study is particularly relevant due to the district's historical significance, dense population, and known exposure to complex geological conditions and high seismic risk (Günay et al., 2011). Zeytinburnu contains a mix of old and new buildings, many of which were constructed without adherence to modern seismic standards, making the area particularly vulnerable to seismic hazards.

This research focuses on analyzing the site response within this critical area to provide valuable insights for local authorities and stakeholders. The findings aim to highlight the importance of doing 3D SRA rather than 1D SRA in high seismic zones. Incorporating site-specific studies such as these into seismic microzonation efforts and urban planning will be essential for enhancing the city's resilience. With Istanbul's population density and economic significance, developing effective mitigation strategies is

imperative to minimize losses, protect lives, and ensure the sustainability of the built environment.

3.1.1 Location

Zeytinburnu is a densely populated district located on the European side of Istanbul, Turkey, along the coast of the Marmara Sea (Figure 3.1). It lies between 40.9939° N latitude and 28.9010° E longitude, covering an area of approximately 12 square kilometers. The district is situated within the western segment of the North Anatolian Fault Zone (NAFZ), with a straight-line distance of about 20-25 km from the fault line beneath the Marmara Sea, making it highly susceptible to seismic events. Zeytinburnu's proximity to the coast also exposes it to secondary seismic hazards, such as liquefaction and tsunami risks, which need to be considered in seismic hazard assessments.

Figure 3.1: *Zeytinburnu district in Türkiye*

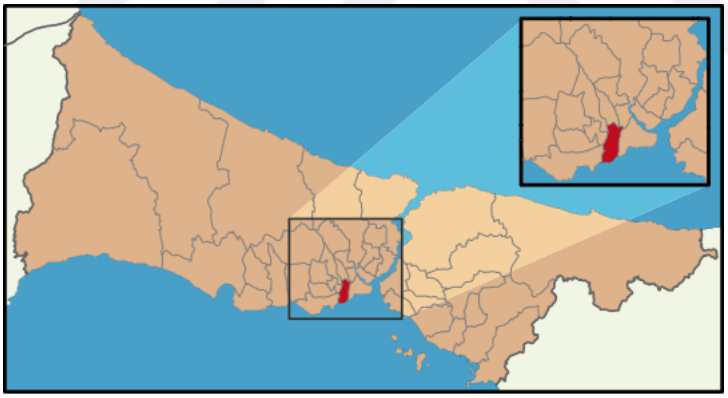

3.1.2 Instrumentation

The instrumentation for the Zeytinburnu vertical array site consists of accelerometers installed at multiple depths to capture detailed seismic response data (See Figure 3.2). These sensors are part of the Istanbul Rapid Response Network and are strategically placed to monitor ground motion at different levels, providing critical information about

how seismic waves propagate through the soil layers. The array includes sensors located at the surface, $-30\,\mathrm{m}$, $-57\,\mathrm{m}$, and bedrock levels, allowing for a comprehensive analysis of the site's behavior during seismic events.

The accelerometers record ground motion in three orthogonal directions: East-West (EW), North-South (NS), and Vertical (V), ensuring that all components of seismic activity are measured. These sensors captured important seismic data from several events, including the 2011 Kütahya earthquake, with the site located approximately 196 km from the epicenter.

Figure 3.2: *Accelerometers along Zeytinburnu vertical array.*

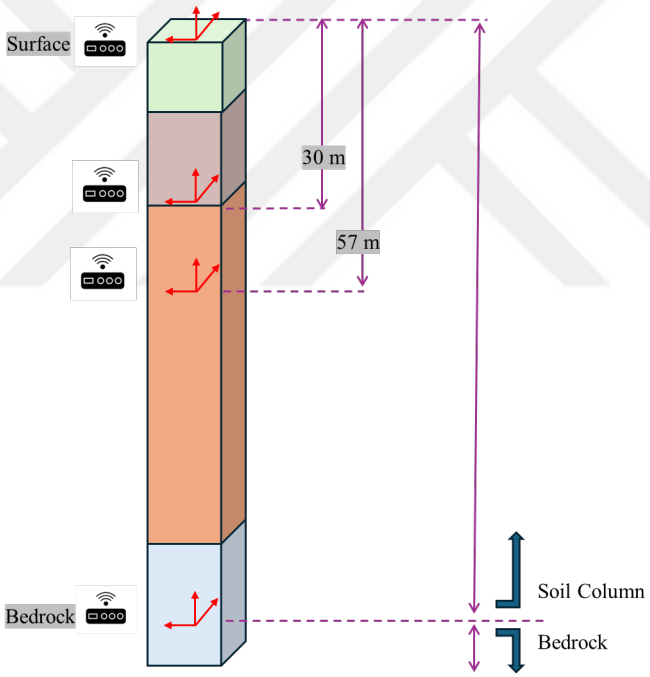

3.1.3 In-situ Tests

Shear wave velocity is a critical parameter in seismic response analysis, as it directly relates to the stiffness and dynamic behavior of soil layers during seismic events. It can be measured using field techniques such as the PS Suspension Logging Test. This

in-situ test is widely used due to its reliability in capturing the stiff modulus of soils. At the Zeytinburnu vertical array site, the PS Suspension Logging Test was employed to determine the shear wave velocity (Vs) profile (see Figure 3.3). A fluid-filled borehole was created using the rotary mud drilling technique, allowing precise measurements at various depths. The investigated soil profile extended to a total depth of 260 meters, and the site exhibited a natural frequency of 0.37 Hz. The average shear wave velocity across the entire profile was found to be 382 m/s.

Figure 3.3: *Shear wave velocity profile obtained by PS logging test in Zeytinburnu.*

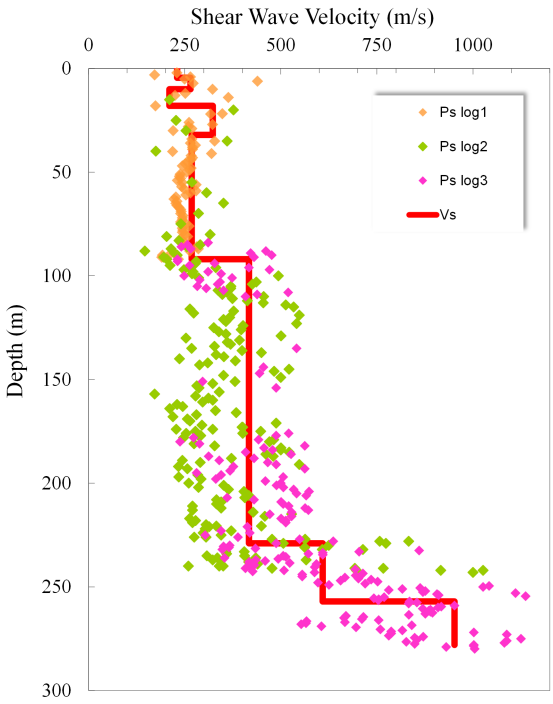

As illustrated in Figure 3.3, the shear wave velocity generally increases with depth, a common trend in geotechnical profiles due to increasing confining pressure and soil density. In the upper layers (0–30 m), lower velocities were observed, reflecting the presence of soft, unconsolidated soils such as clay and silt. This depth range is particularly significant, as in-situ tests like the PS Suspension Logging Test and Seismic Cone Penetration

Test (SCPT) are most reliable in capturing soil stiffness within this zone. Between 30 and 100 meters, the velocities increase as the soil becomes more compact and consolidated. Beyond 100 meters, the trend continues, with a notable increase in velocity around 250 meters, indicating the transition to bedrock.

3.1.4 Selected Earthquakes

The available earthquake, which was selected for Zeytinburnu occurred in Kütahya, Türkiye, on May 19, 2011, at 20:15 local time (17:15 Coordinated Universal Time (UTC)). The epicenter was located at approximately 39.60° N latitude and 29.92° E longitude. This seismic event had a magnitude of Mw=5.8 and lasted for 134 seconds (Figure 3.4). Accelerometers installed at various soil levels in the Zeytinburnu vertical array captured this earthquake, recording ground motions in the East-West (EW), North-South (NS), and Vertical (V) directions.

Figure 3.4: *Distance of Zeytinburnu to Kütahya Earthquake.*

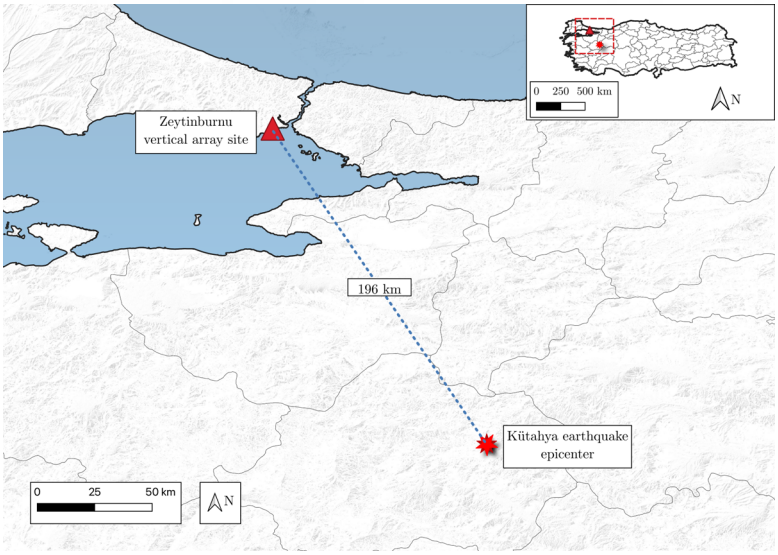

Figure 3.5 shows the recorded accelerations, while Figure 3.6 presents the acceleration response spectra for a 5 percent damping ratio in all three directions at the specified

levels. Table 3.1 provides detailed key ground motion parameters for the bedrock in each direction.

Table 3.1: *Summary of Kütahya earthquake in EW, NS and V directions*

Parameter	**(EW)**	**(NS)**	**(V)**
Max. Acceleration $[g]$	*0.00062*	*0.00115*	*0.0015*
Time of Max. Acceleration $[s]$	*35.86*	*35.655*	*0.015*
Max. Velocity $[\frac{cm}{s}]$	*0.12798*	*0.18761*	*0.17437*
Time of Max. Velocity $[s]$	*38.96*	*36.805*	*43.995*
Max. Displacement $[cm]$	*0.09583*	*0.16544*	*1.34386*
Time of Max. Displacement $[s]$	*42.14*	*47.52*	*133.995*
Vmax / Amax $[s]$	*0.21137*	*0.1663*	*0.1185*
Acceleration RMS $[g]$	*0.00008*	*0.00012*	*0.00009*
Arias Intensity $[\frac{m}{s}]$	*0.00001*	*0.00003*	*0.00002*
Acceleration Spectrum Intensity $[g.s]$	*0.0006*	*0.00105*	*0.00057*
A95 parameter $[g]$	*0.0004*	*0.00085*	*0.00046*

The analysis of the recorded seismic data revealed significant amplifications of seismic motions at the surface (see Figure 3.7). These findings highlight the seismic response of the Zeytinburnu soil profile and emphasize the necessity of understanding these amplifications for seismic hazard assessment and structural design. The increased ground motions at the surface underscore the importance of site-specific studies to inform building codes and develop effective mitigation strategies, particularly in areas with complex soil conditions like Zeytinburnu.

3.1.5 Soil Property

The soil profile of the Zeytinburnu site exhibits significant heterogeneity with distinct layers varying in composition and stiffness, as reflected by the shear wave velocity values. At the surface, a Fill layer is present, characterized by relatively low shear wave velocity, indicative of loosely compacted or artificial material. Below the fill, weathered

limestone with clay interlayers extends to approximately 50 meters, exhibiting slightly higher shear wave velocities, though the presence of weathering and clay reduces its stiffness (see Figure 3.8).

Between 50- and 100-meters depth, the profile consists of clay-silty sand-silt layers, showing further reduction in stiffness due to their fine-grained texture. As the depth increases to around 150 meters, clay-silt dominates, further decreasing the shear wave velocity, which reflects the material's low resistance to seismic wave propagation. This layer continues until approximately 250 meters, where the profile transitions into weathered greywacke, which is denser and has a moderate increase in shear wave velocity. Below 270 meters, an unweather greywacke is encountered, exhibiting the highest shear wave velocity, indicating the presence of intact, hard rock with high stiffness and low deformability.

3.2 Alaska Downhole Array

3.2.1 Location

Alaska, renowned for its natural beauty and harsh landscapes, is also one of the most seismically active regions on Earth (see Figure 3.10), with a long history of powerful earthquakes. The 1964 Great Alaska Earthquake, a pivotal event in seismic history, struck on March 27 (Good Friday) with a magnitude of 9.2, making it the largest earthquake ever recorded in the Northern Hemisphere. This catastrophic quake, which lasted over four minutes, affected an area of approximately 130,000 square kilometers (50,000 square miles). It caused 131 fatalities and inflicted property damage amounting to 500 million dollars in 1964 currency—its impact remains visible across Alaska's landscape today.[41]

Anchorage, the state's largest city, plays a key role in seismic research due to its historical vulnerability to earthquakes. A prime example is the Robert B. Atwood Building, located at 550 West 7th Avenue in the heart of downtown Anchorage (61.2175° N,

149.8902° W) (Figure 3.9). This 20-story, 81-meter-tall (265 ft) office building, constructed in 1980 following the 1979 Uniform Building Code, houses government offices for the State of Alaska.

3.2.2 Instrumentation

The Atwood Building's seismic monitoring system (Figure 3.11)[41], part of the Advanced National Seismic System Advanced National Seismic System (ANSS) is one of the most advanced structural monitoring setups in the United States. In 2003, the United States Geological Survey (USGS) installed a network of accelerometers throughout the Atwood Building to monitor and analyze its response to seismic events. Given the region's seismic history, such as the 1964 earthquake, the building was selected to provide critical data on the behavior of tall structures during earthquakes.

This 20-story building features a comprehensive array of sensors strategically installed to capture detailed seismic data. Accelerometers are distributed across multiple key levels, including the parking and street levels, the electrical and mechanical floors, the roof, and the 2nd, 7th, 8th, 13th, 14th, and 19th floors. This arrangement enables precise monitoring of the building's dynamic behavior during seismic events, allowing engineers to evaluate how different parts of the structure respond to ground shaking.[42]

In addition to the internal instrumentation, six instrumented boreholes (see Figure 3.12 and Figure 3.13) and a seventh surface sensor are located approximately one city block away from the building. These boreholes, with depths of 6.1 meters, 13.7–15.2 meters, 21.3 meters, 42.7 meters, 50.3 meters, and 61 meters, are positioned over an area of 7.6 meters by 4.6 meters, with 1.8-meter spacing in both the east-west (EW) and north-south (NS) directions. Each borehole has a diameter of 0.2 meters (8 inches), cased with Polyvinyl Chloride (PVC) pipes, and grouted to ensure stability and accuracy in the readings. A surface sensor, along with these boreholes, provides critical data on free-field

ground motions, capturing seismic waves before they interact with the building.

The placement of the boreholes—sufficiently distant from the building—ensures their recordings are unaffected by the building's movements. The fiberglass enclosure near the site, located 0.6 meters from the northern and western boundaries, houses two boreholes at depths of 6.1 meters and 13.7–15.2 meters, positioned 1.8 meters from the enclosure's centerline. This configuration allows for accurate seismic readings, free from disturbances caused by nearby structural vibrations.[42]

Since their deployment in 2003, these sensors have recorded numerous small and medium-sized earthquakes from both local and distant sources. Monitoring seismic wave propagation from the subsurface to the building's structure enables detailed studies of Soil-Structure Interaction (SSI). All data from the boreholes and building sensors are transmitted to the United States Geological Survey (USGS) facility in Menlo Park, California, where it is processed, analyzed, and made available to the engineering community.

This real-time data sharing enhances the understanding of the Atwood Building's seismic performance and contributes to the development of improved seismic design practices and mitigation strategies for similar structures in high-risk seismic regions.

3.2.3 In-situ Tests

The presented shear wave velocity profile for Anchorage obtained by In-situ tests (Figure 3.14) reveals the variation in stiffness of subsurface materials with depth, which is crucial for understanding the site's seismic response [41]. The profile shows that near the surface, the shear wave velocity starts relatively low, suggesting the presence of soft or loose sediments. As the depth increases, the Vs values gradually rise in discrete steps, indicating the transition through different soil or geological layers with varying stiffness.

3.2.4 Selected Earthquakes

The seismic monitoring system at the Atwood Building has captured records from several significant earthquakes in Alaska, providing valuable data on how seismic waves interact with the soil and structure (Table 3.2) with different PGA values (Table 3.3). The selected events include a range of magnitudes, hypocenter depths, and durations, highlighting the diverse seismic activity in the region. These earthquakes, recorded at various points in time, allow for a detailed analysis of soil-structure interaction (SSI) and site response.

One of the notable events is the Point MacKenzie Earthquake of November 30, 2018, with a magnitude of Mw 7.0 and a hypocenter depth of 46 km, which lasted for approximately 210 seconds. This earthquake provided crucial insights into how large-magnitude events impacted the Bootlegger Cove Formation and surrounding areas. Similarly, other earthquakes with magnitudes ranging from Ml 5.0 to 6.0 were recorded, each contributing unique data for seismic assessment.

The events include the Big Lake Earthquake, also on November 30, 2018, with a magnitude of Mw=5.2, as well as subsequent earthquakes such as the Sukkozero Earthquake (Ml=5.5) and the Suoyarvi Earthquake (Ml=6.0), which lasted 165 seconds and 180 seconds, respectively. These events were recorded across multiple depths, ranging from 40 km to 111 km, reflecting the complex seismic behavior of the region. The durations of ground shaking varied between 150 and 210 seconds, providing diverse datasets for studying how seismic waves propagate through different soil layers and how the structure responds to varying levels of seismic excitation. Collectively, the data collected from these earthquakes are essential for refining seismic hazard assessments and guiding the design and retrofit of structures in Anchorage and other seismically active areas.

Among the earthquakes listed in Table 3.3, A.6 has the highest Peak Ground Acceleration (PGA) value across all components, with a PGA of 0.253194 in the East-West

Table 3.2: *Recorded Earthquakes at Atwood Building*

ID tag	Event	Date	Latitude	Longitude	90Depth (km)	90Magnitude	90Duration (sec)	90Recorded Directions
A.1	Point MacKenzie	Feb 27, 2021	61.3	149.9	42	MI 5.3	159	EW, NS, V
A.2	Sukkozero	Apr 08, 2021	63.2	148.5	77	MI 5.5	165	EW, NS, V
A.3	Suoyarvi	May 31, 2021	62.4	148.1	48	MI 6.0	180	EW, NS, V
A.4	Lemi	Feb 02, 2023	61.0	152.2	111	MI 5.0	150	EW, NS, V
A.5	Ust-Luga	Mar 19, 2023	59.6	151.9	65	MI 5.4	162	EW, NS, V
A.6	Point MacKenzie	Nov 30, 2018	61.3	149.9	46	Mw 7.0	210	EW, NS, V
A.7	Big Lake, AK	Nov 30, 2018	61.4	149.9	40	Mw 5.2	156	EW, NS, V

(EW) direction, 0.251212 in the North-South (NS) direction, and 0.300744 in the Vertical (V) direction. These values are significantly higher than those for the other earthquakes, indicating a stronger ground motion for A.6. On the other hand, the minimum PGA values are observed in A.5, with a PGA of 0.001117 in the EW direction, 0.001303 in the NS direction, and 0.00095 in the V direction, showing that this earthquake had the least ground motion among those recorded. This range highlights the variability in seismic impact across different events.

Table 3.3: *Recorded PGAs at three directions*

ID Tag	PGA (EW)(g)	PGA (NS)(g)	PGA (V)(g)
A.1	0.037834	0.03458	0.015136
A.2	0.006404	0.004917	0.002098
A.3	0.029906	0.033447	0.013276
A.4	0.00181	0.001785	0.007149
A.5	0.001117	0.001303	0.00095
A.6	0.253194	0.251212	0.300744
A.7	0.007195	0.009437	0.00612

The provided figures (from Figure 3.15 to Figure 3.21) display the recorded acceleration time histories by accelerometers for different recorded earthquake events at Atwood building (including those with ID tags of A.1 to A.7). The data are presented for various layers of the site, namely for the surface, two mid-depth levels (z = -4.6 m and z = -10.7 m), and the bedrock. The time histories are shown for three components

(East-West, North-South, and Vertical), providing a comprehensive understanding of the seismic response at each depth level. Additionally, corresponding spectral accelerations to these time histories are also shown to evaluate better earthquake content across the site layers.

3.2.5 Soil Property

The Atwood Building in downtown Anchorage is founded on the Bootlegger Cove Formation, a complex geological unit that plays a crucial role in seismic response studies. This formation, approximately 30.5 to 45.7 meters (100 to 150 feet) thick, is characterized by a diverse range of soil types, each with distinct properties that influence how seismic waves propagate through the subsurface. The formation's susceptibility to failure was dramatically demonstrated during the 1964 Great Alaska Earthquake, which caused landslides and widespread ground deformation.

Understanding the Atwood Building's seismic response is essential for enhancing the safety and resilience of future structures, particularly in geologically active regions like Anchorage.

Figure 3.5: *Recorded acceleration time histories at various depths and three directions.*

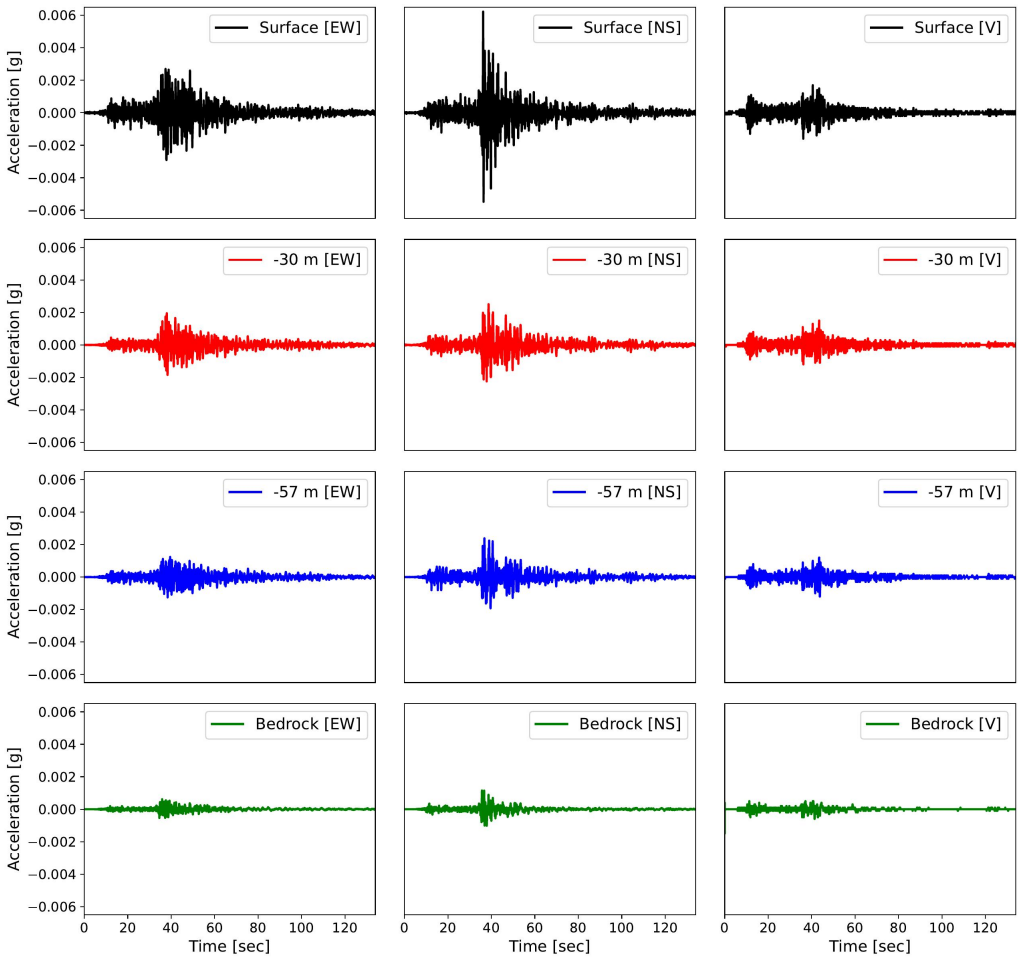

Figure 3.6: *Corresponding recorded spectra accelerations at various depths and three directions.*

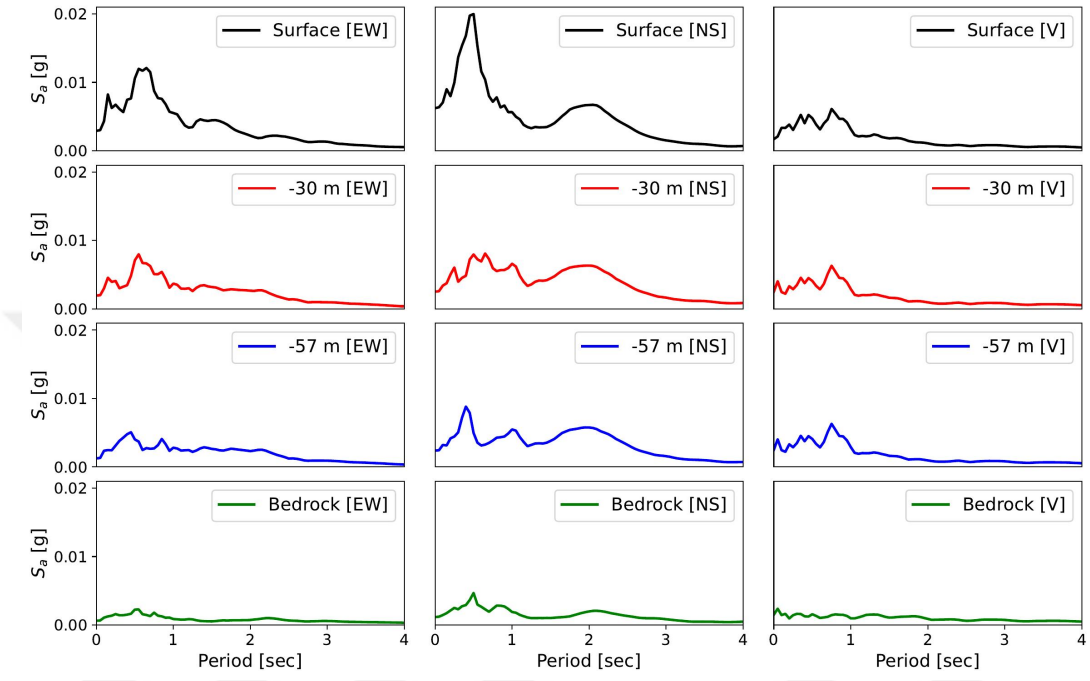

Figure 3.7: *Amplification of ground motion on the surface.*

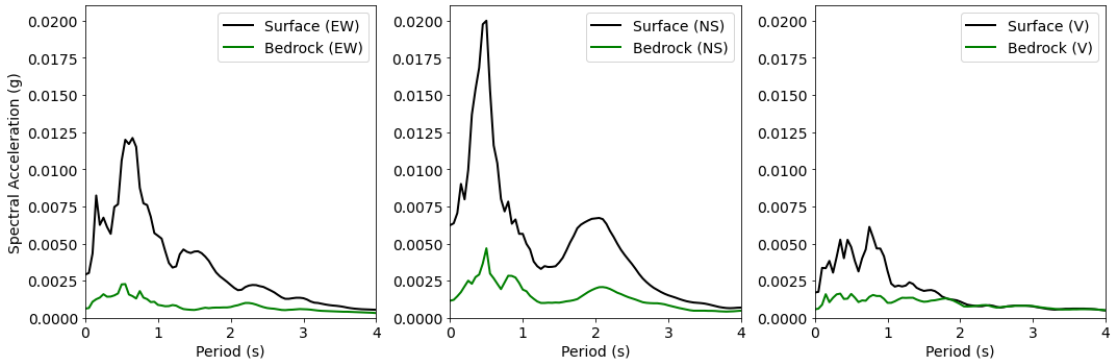

Figure 3.8: *Soil stratification along Zeytinburnu vertical array.*

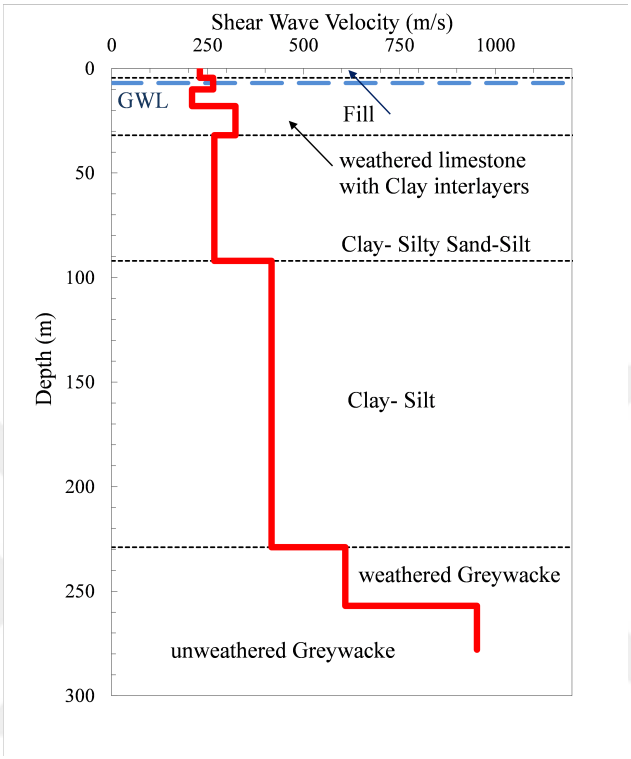

Figure 3.9: *Robert B. Atwood building in Anchorage of Alaska.*

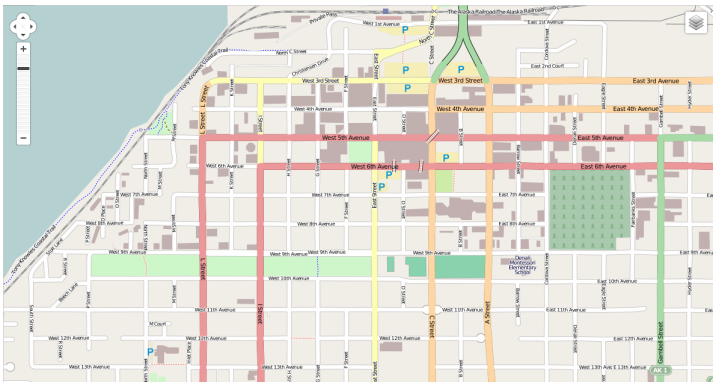

Figure 3.10: *Intersections of faults in Anchorage.*

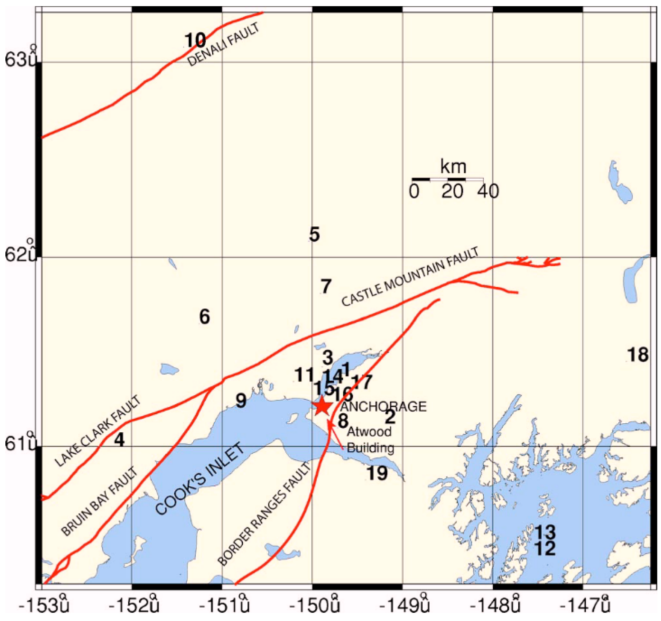

Figure 3.11: *Atwood building.*

Figure 3.12: *Plan of Atwood building and six boreholes.*

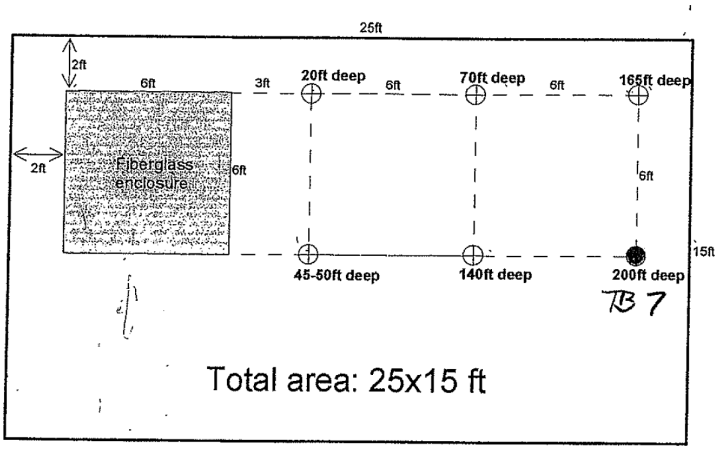

Figure 3.13: *Different accelerometers at boreholes.*

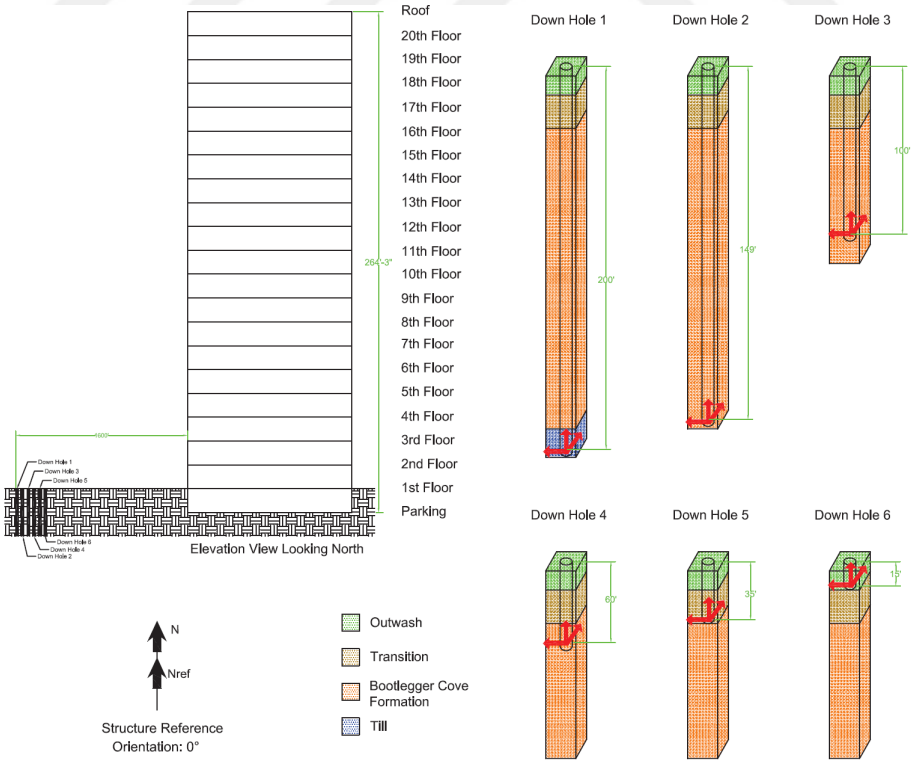

Figure 3.14: *Shear wave velocity profile obtained in Anchorage.*

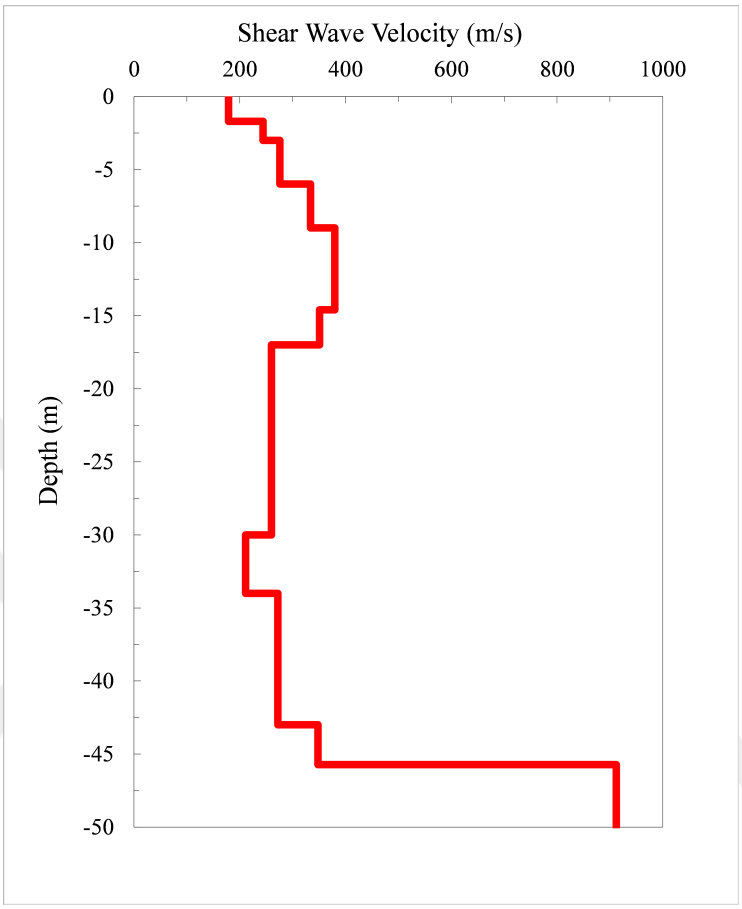

Figure 3.15: *Recorded earthquake with ID tag of A.1.*

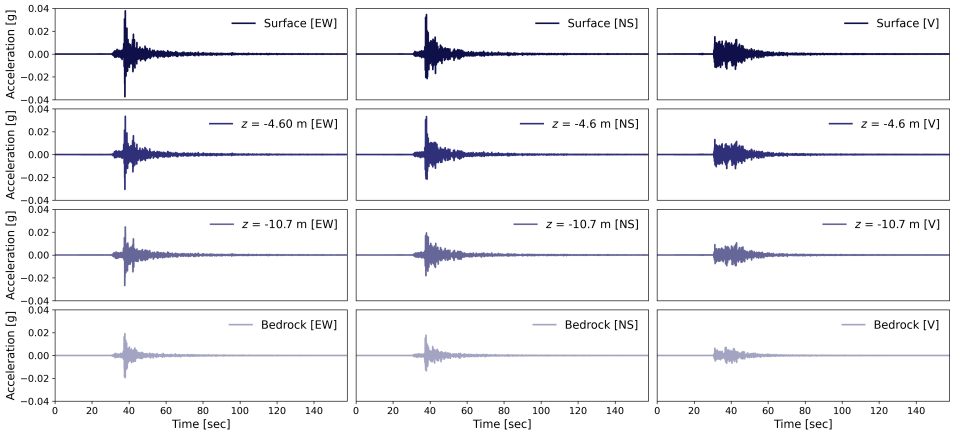

Figure 3.16: *Recorded earthquake with ID tag of A.2.*

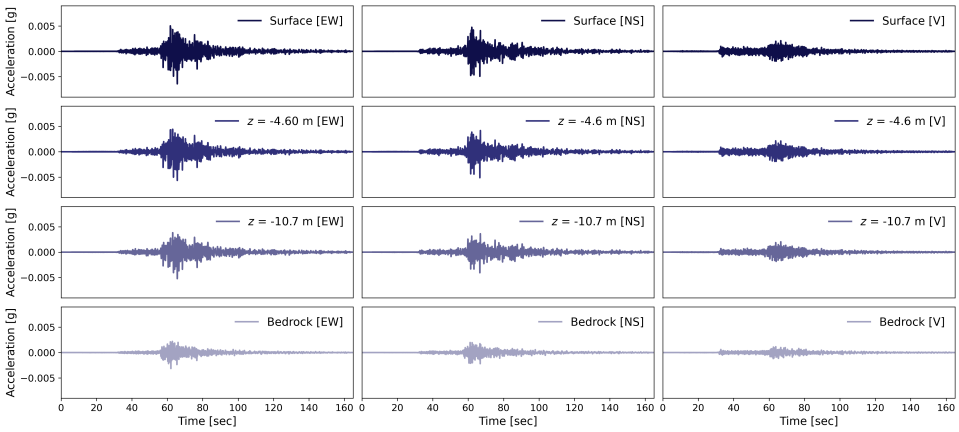

Figure 3.17: *Recorded earthquake with ID tag of A.3.*

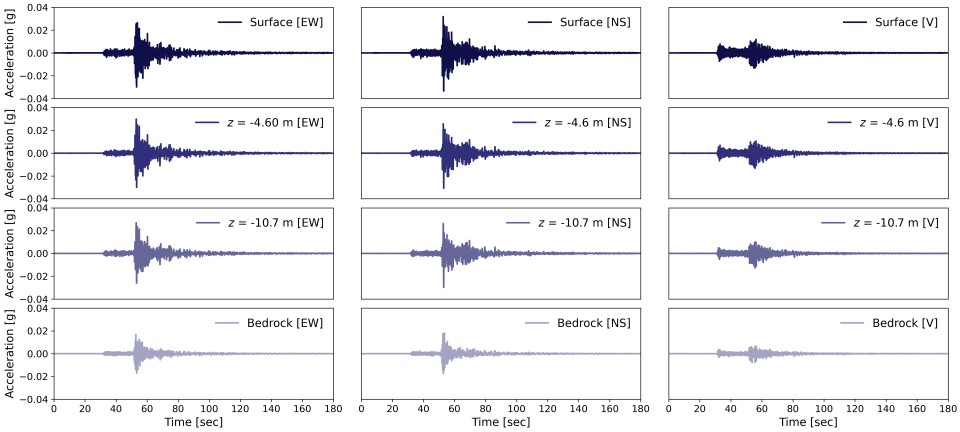

Figure 3.18: *Recorded earthquake with ID tag of A.4.*

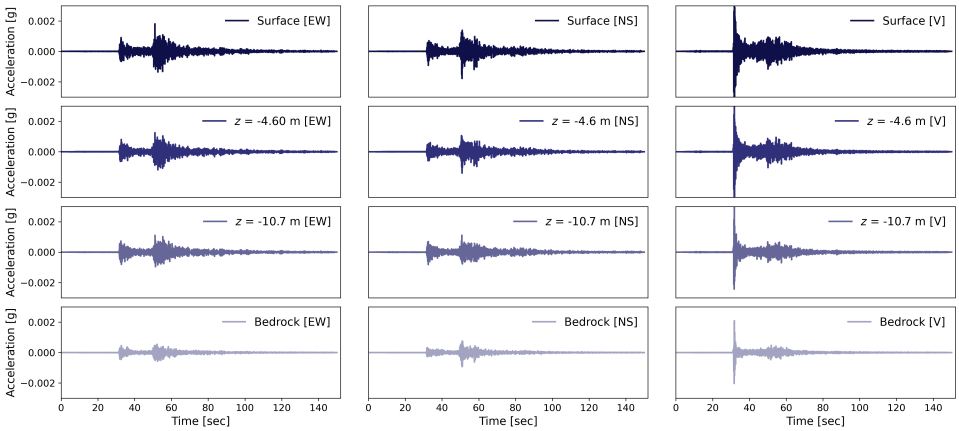

Figure 3.19: *Recorded earthquake with ID tag of A.5.*

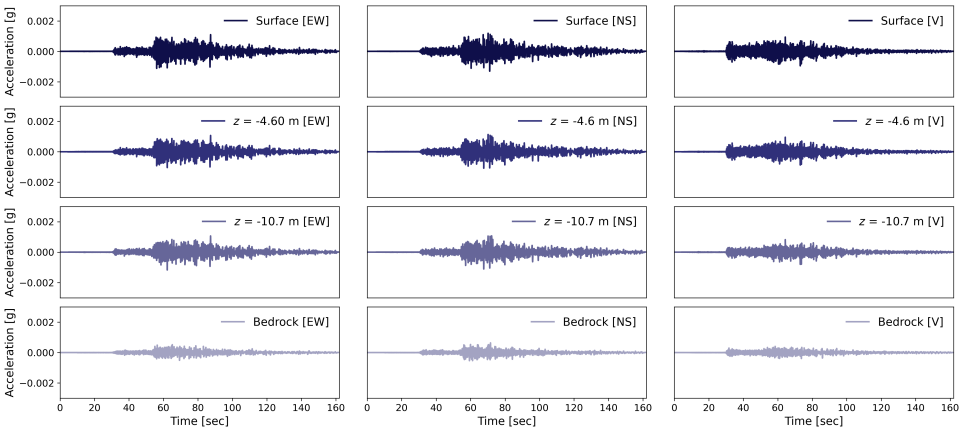

Figure 3.20: *Recorded earthquake with ID tag of A.6.*

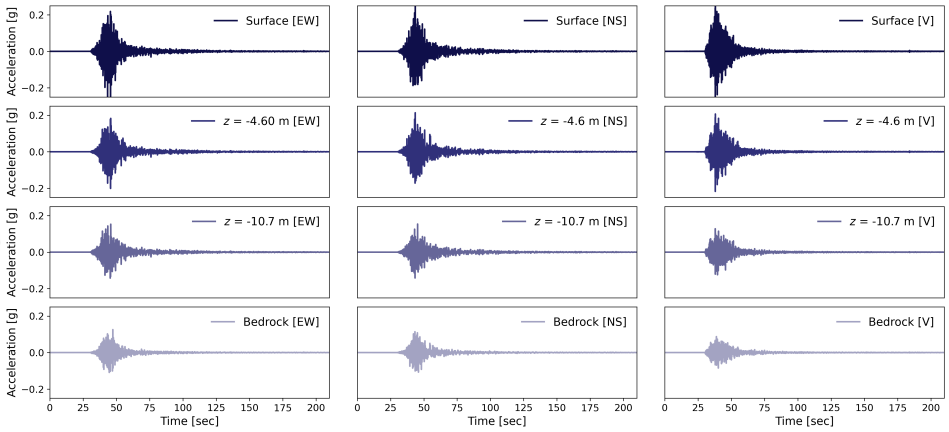

Figure 3.21: *Recorded earthquake with ID tag of A.7.*

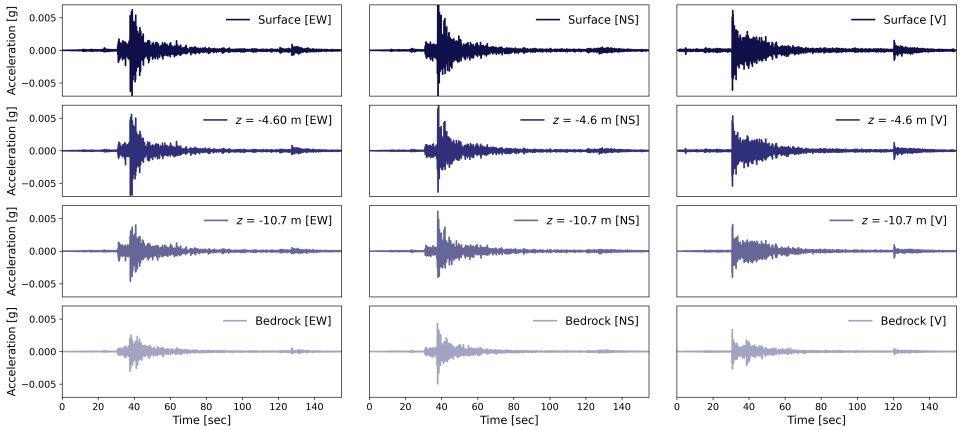

Figure 3.22: *Atwood profile with sensors in longitudinal direction.*

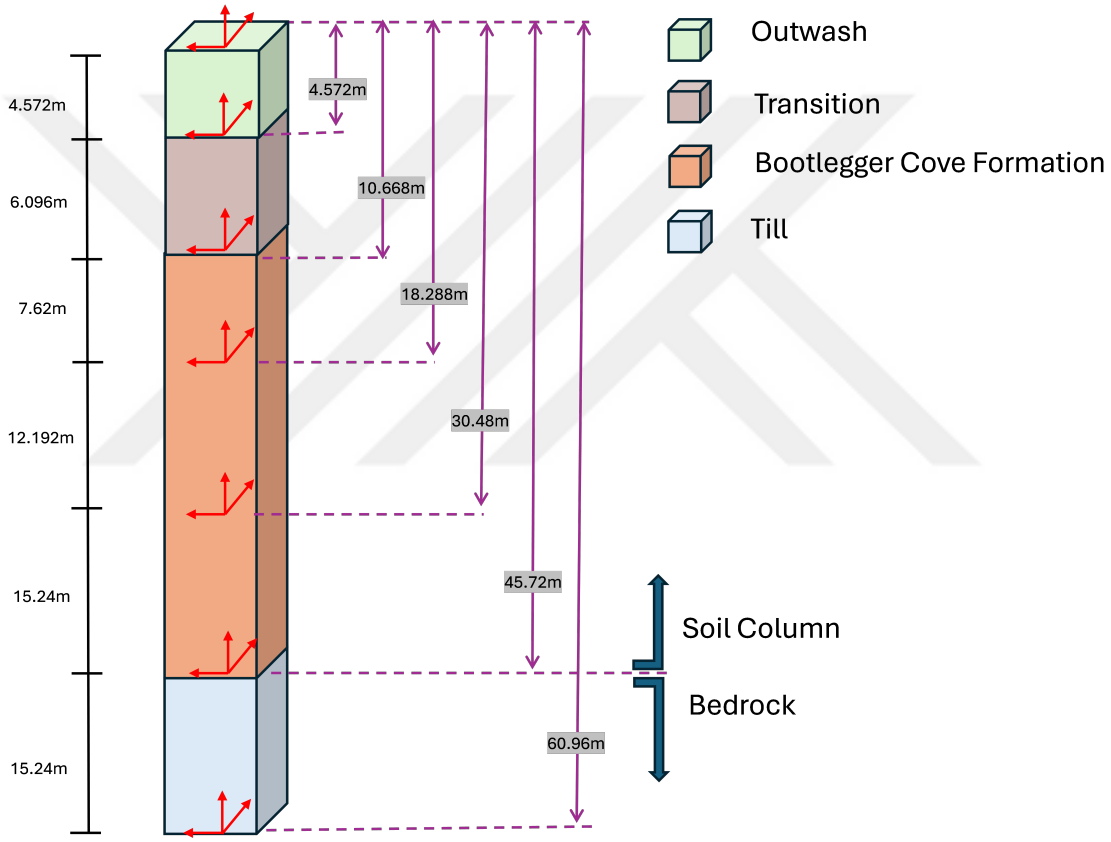

4. SITE RESPONSE ANALYSIS MODELING

Site response analysis is a geotechnical engineering procedure used to evaluate how a specific site will respond to seismic ground shaking, accounting for the local soil and rock conditions (Figure 4.1). This analysis assesses the amplification, damping, and resonance of seismic waves as they travel from bedrock to the ground surface, influenced by the site's geological and geotechnical properties, such as soil layers, material stiffness, and damping characteristics. By simulating the propagation of seismic waves through soil layers, site response analysis helps predict surface ground motions, which are essential for designing earthquake-resistant structures and assessing seismic hazards in a given area.

Figure 4.1: *Site response analysis.*

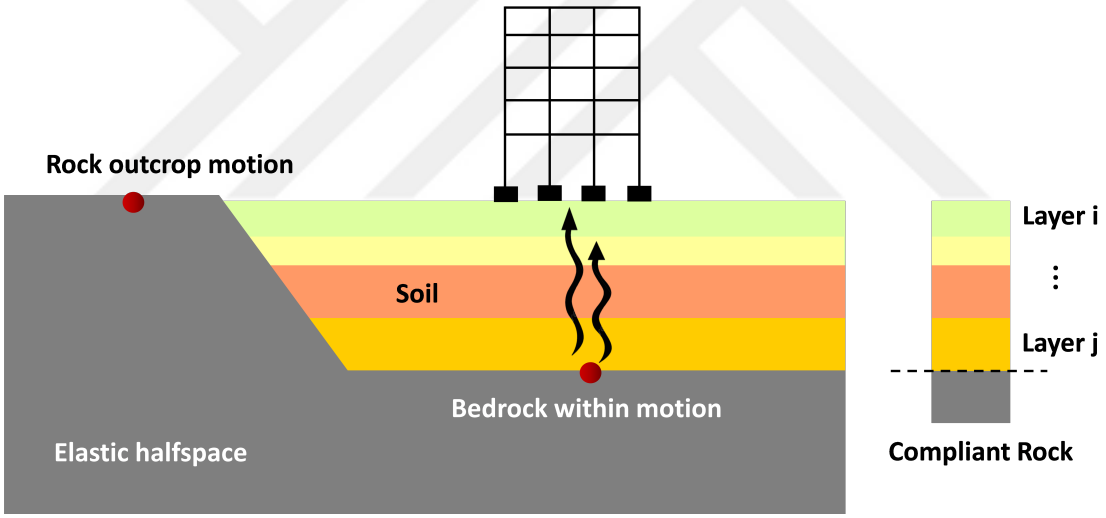

This research focuses on conducting both 1D and 3D site response analyses using advanced computational tools, specifically PLAXIS3D [43], [44], OpenSees [45], and DEEPSOIL [46]. These tools enable comprehensive modeling of soil behavior under seismic loading conditions, allowing for a nuanced analysis of the soil's response to multidirectional seismic excitations and providing insights into the differences between 1D and 3D site response analyses (Figure 4.2).

The methodology involves simulating seismic wave propagation through the Zeytinburnu and Atwood soil profiles. In the 3D analysis, simultaneous application of East-West (EW), North-South (NS), and Vertical (V) ground motion components is considered, capturing the complex interactions in the soil layers under multidirectional loading. In contrast, the 1D analysis follows traditional practices by applying only one horizontal component at a time, representing a simplified approach to seismic response. Each computational tool provides unique capabilities that enhance analysis.

PLAXIS3D, for instance, supports modeling complex geometries and soil-structure interactions, critical for accurate 3D site response analysis [43]. OpenSees offers a flexible framework for nonlinear dynamic analysis with a variety of material models and boundary conditions, facilitating a more adaptable modeling approach. DEEPSOIL, which specializes in deep soil deposits, offers linear, equivalent linear and nonlinear analysis options, making it particularly valuable for comparative studies between 1D and 3D models.

Figure 4.2: *1D and 3D site response analysis.*

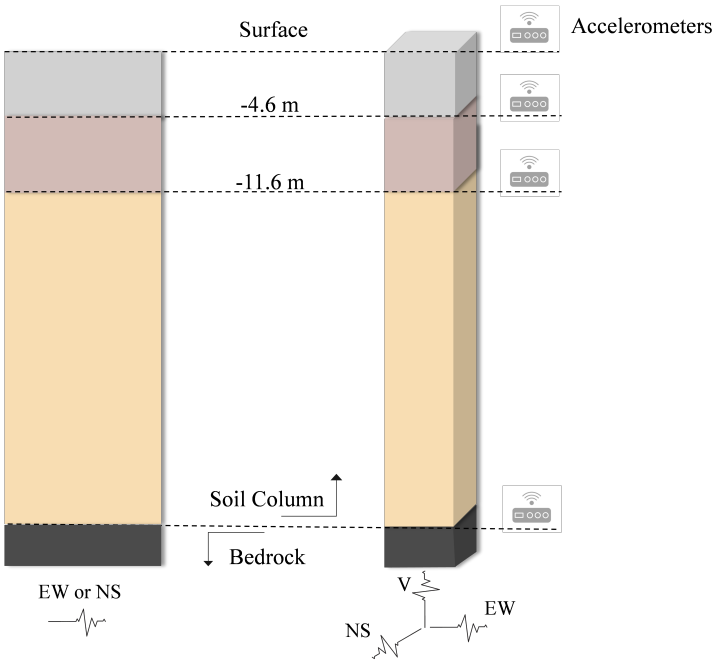

By comparing results across these tools and methods, this study aims to highlight the importance of each approach, offering guidance on selecting the most appropriate analysis method based on specific site conditions and project requirements. This comparative analysis contributes to geotechnical earthquake engineering by validating numerical models against real-world data and presenting case studies that can inform future site response analysis practices.

4.1 Deepsoil

4.1.1 Introduction to DEEPSOIL

DEEPSOIL is a widely used software for seismic site response analysis, employing the finite difference method to model soil behavior under seismic loading. It offers linear (L), equivalent linear (EL), and nonlinear analysis (NL) modes, making it adaptable to various geotechnical engineering challenges. Linear and equivalent linear methods of program are the most famous ones among researchers due to ease of use and good results to some extent. In addition to the EL method in Deepsoil, the program offers nonlinear (NL) analysis to model strain-dependent behavior. Unlike linear models, which assume a constant stress-strain relationship, NL models account for changes in stiffness and damping with increasing strain [47], [48].

While NL analysis provides a sophisticated framework, it is not without limitations. Research by Phillips and Hashash [49] indicates that DEEPSOIL's NL method may underestimate nonlinear responses under extreme loading conditions. This underestimation could impact the reliability of seismic performance predictions, underscoring the need for complementary models or additional verification to ensure comprehensive analysis.

A key advantage of DEEPSOIL is its ability to accommodate numerous ground motions without restrictions on motion length, the number of soil layers, or material

property variability. This flexibility makes it suitable for both simple and complex site response projects.

4.1.2 Equivalent Linear Analysis in DEEPSOIL

The equivalent linear method, originally proposed by Seed and Idriss, balances computational efficiency with detailed soil behavior modeling which is a widely used approach in geotechnical engineering for analyzing site response during seismic events [15]. This method leverages degradation curves, which depict the reduction in soil stiffness and strength with increasing strain, to model the non-linear behavior of soil.

The Equivalent Linear (EL) model employs an iterative process to accurately determine the shear modulus and damping ratio of soil properties which can be specified either at discrete points, representing specific values of strain, or by defining parameters that describe the backbone curve of a nonlinear soil model. This backbone curve effectively captures the relationship between shear stress and strain, allowing for a more precise simulation of soil response during seismic events. By iteratively refining these properties, the EL model ensures that the soil's dynamic behavior is accurately represented, leading to more reliable predictions of ground motion and structural performance.

Figure 4.3: *Equivalent linear method.*

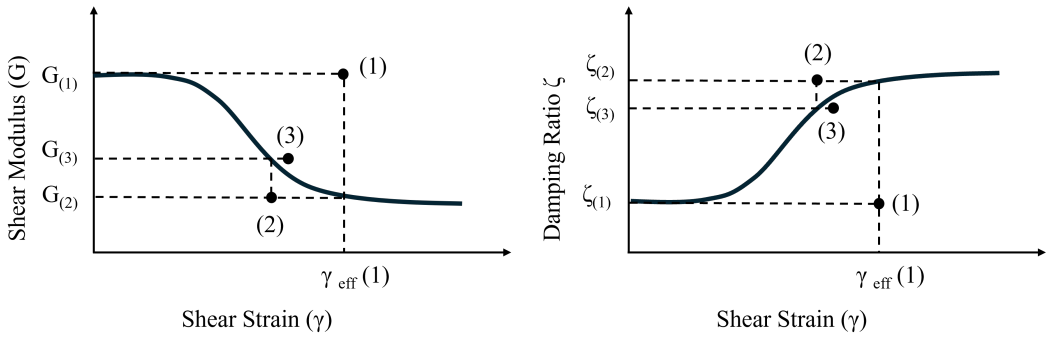

To do so, this method initially assumes the soil characterized by the maximum shear modulus $G^{(1)}$ and minimum damping ratio $\zeta^{(1)}$. It predicts the effective strain γ_{eff}

through linear analysis and then estimates the shear modulus $G^{(2)}$ and damping ratio $\zeta^{(2)}$ for this effective strain (see Figure 4.3).

Defining the effective strain is a crucial step when performing an equivalent linear analysis. This effective shear strain, calculated as a percentage of the maximum strain, is used to update the estimates of the soil's shear modulus and damping ratio. The recommended and default value for this effective shear strain is 0.65%.

This value is significant because it represents the strain level at which soil properties are reassessed to more accurately reflect the soil's behavior under seismic loading conditions. An equation that describes the relationship between effective shear strain and earthquake magnitude (Equation 4.1) ensures that the modeled soil response aligns accurately with the expected seismic activity:

$$\gamma_{\text{eff}} = f(M_{\text{w}}) \tag{4.1}$$

where γ_{eff} is the effective shear strain, and M_{w} is the earthquake magnitude.

$$\gamma^{i}_{\text{eff}} = R_{\gamma}\gamma^{i}_{\text{max}} \tag{4.2}$$

in which:

$$R_{\gamma} = \frac{M-1}{10} \tag{4.3}$$

where Equation (4.3) is the ratio of the effective shear strain over maximum shear strain, which depends on earthquake magnitude [50].

The use of equivalent linear methods is realistic for low and medium cyclic strains [47]. In current research Equivalent linear method was used for doing 1D site response analysis in Deepsoil Program.

4.1.3 Input Parameters and Configuration in DEEPSOIL

The first step in the DEEPSOIL analysis process is to select the type of analysis. In the introductory tab (Analysis Definition), the user must choose the Analysis Method (such as Equivalent Linear, Linear, or Nonlinear), the Solution Type (Frequency Domain or Time Domain), and the Default Soil Model for all newly generated layers.

Additionally, the user needs to select the Default Hysteretic Re/Unloading Formulation for cyclic loading analysis. Optional settings include enabling Automatic Profile Generation based on input data, selecting the Unit System (English or Metric), and specifying Complementary Analyses (Equivalent Linear-Frequency Domain, Linear-Frequency Domain, or Linear-Time Domain). By carefully configuring these settings, users can tailor the analysis to their specific needs, ensuring more accurate and reliable seismic site response assessments.

In the first step of our study, we carefully selected specific settings in DEEPSOIL to ensure precise and reliable seismic site response assessments. We chose the Equivalent Linear method for the analysis, conducted in the Frequency Domain to effectively capture frequency-dependent soil behavior. The General Quadratic/Hyperbolic Model (GQ/H) was selected as the default soil model for all newly generated layers, providing a robust representation of the soil's stress-strain relationship. To accurately simulate energy dissipation during cyclic loading, we used the Non-Masing Re/Unloading formulation as the default selection for the program. Additionally, we included Equivalent Linear-Frequency Domain as the complementary analysis type, tagged under Analysis ID DS-EL4, to gain further insights into the soil's frequency-dependent behavior.

These carefully chosen settings aligned with the objectives of our study, allowing for a comprehensive and nuanced understanding of the site's seismic response. As the second step (Figure 4.4) when using DEEPSOIL, the user must specify the typical soil properties for each layer in the model. The selection of these properties is crucial as they

Figure 4.4: *Deepsoil program for Zeytinburnu and Alaska.*

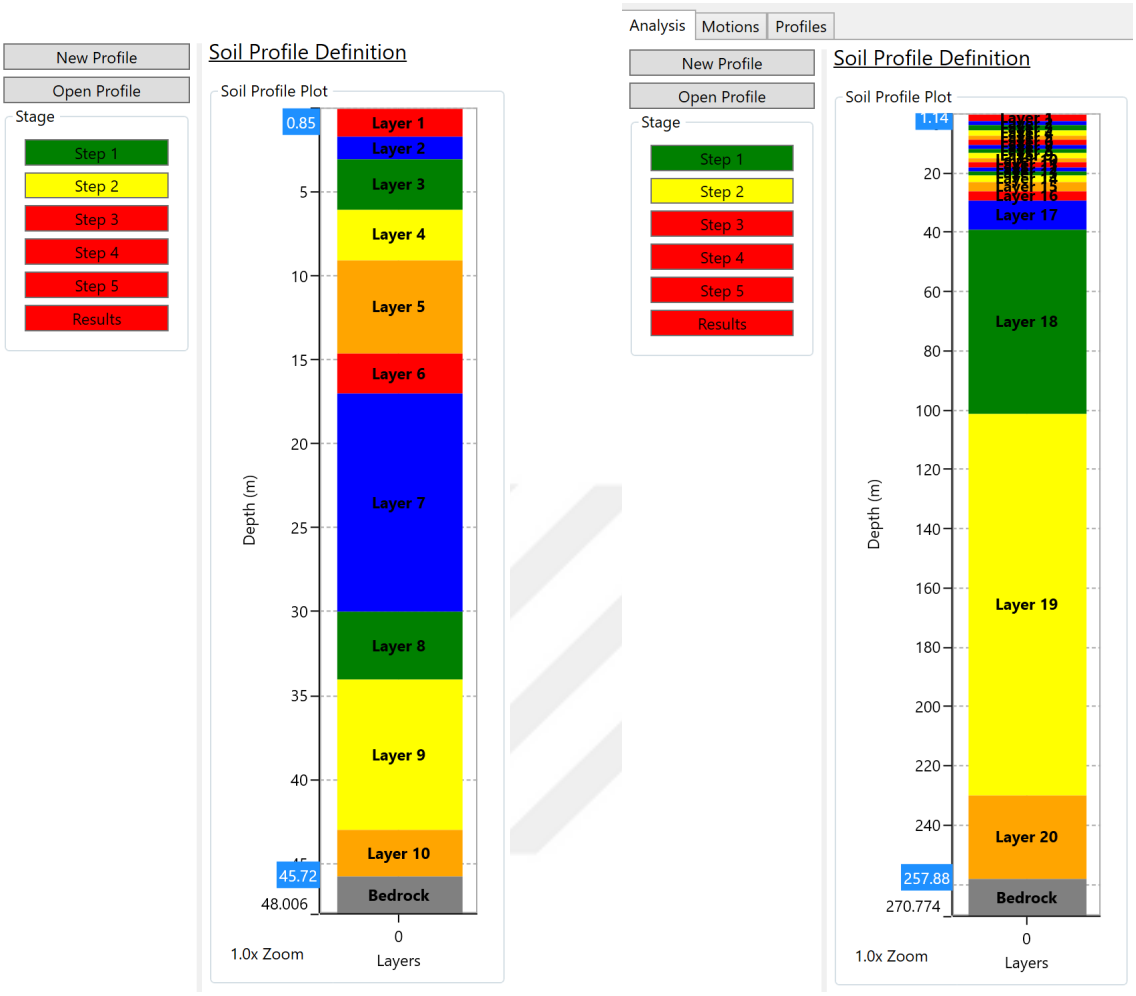

directly influence the accuracy and reliability of the analysis results.

For each soil layer, essential properties such as thickness, unit weight, shear wave velocity, effective vertical stress, and shear strength are defined to ensure accurate modeling (Table 4.1,Table 4.2). Reference degradation curves were selected according to soil type: the Vucetic and Dobry (1991) [51] curves for clay layers and the Seed and Idriss (1970) [15] curves for sand layers.

To minimize artificial damping, In the next step of using DEEPSOIL, it uses a

viscous damping formulation to model small strain damping, which results in frequency-dependent damping.

DEEPSOIL offers three types of Rayleigh damping formulations, but it is generally recommended to use the frequency-independent damping formulation for most analyses to avoid the pitfalls of artificial damping (Equation 4.4). This recommendation ensures that damping effects are accurately represented without introducing unnecessary numerical artifacts.

$$G^* = G\left(1 + 2i\zeta\right) \tag{4.4}$$

where:

- G^* is the complex shear modulus,
- G is the shear modulus,
- i is the imaginary unit,
- ζ is the damping ratio.

This formulation ensures that damping remains uniform across all frequencies, which is essential for accurate seismic analysis. The frequency-independent shear modulus results in frequency-independent damping, making it the recommended choice for analysis in **DEEPSOIL**. This modulus ensures that the damping remains consistent across different frequencies, enhancing the accuracy and reliability of seismic response analysis. Notably, this is the same modulus used in **SHAKE91**, which has been widely accepted and validated in geotechnical earthquake engineering practice.

Table 4.1: *Alaska soil profile details.*

Col No	***depth [m]***	$\mathbf{V_s}$ **[m/s]**	γ **[kN/m^3]**	**E [kN/m^2]**	**G [kN/m^2]**	**K [kN/m^2]**
1	45.72	348	20	702403	242208	2341344
2	43	272	20	429107	147968	1430357
3	34	211	20	258221	89042	860739
4	30	260	20	392080	135200	1306933
5	17	351	20	714565	246402	2381886
6	14.6	380	20	837520	288800	2791733
7	9	334	20	647024	223112	2156749
8	6	276	20	441820	152352	1472736
9	3	244	20	345308	119072	1151029
10	1.7	179	20	185837	64082	619459

Table 4.2: *Zeytinburnu soil profile details 1.*

Col No	***Soil***	***depth [m]***	***thickness [m]***	$\mathbf{V_s}$ **[m/s]**	γ **[kN/m^3]**
1	Clay	2.3	2.28	230	17.3
2	Clay	3.8	1.52	230	17.3
3	Clay	5.5	1.55	265	17.3
4	Clay	6.90	1.56	265	17.3
5	Clay	8.5	1.59	265	17.3
6	Clay	10.1	1.56	210	17.3
7	Clay	11.4	1.37	210	17.3
8	Clay	12.9	1.50	210	17.3
9	Clay	14.4	1.52	210	17.3
10	Clay	15.9	1.50	210	17.3
11	Clay	17.5	1.62	210	17.3
12	Clay	19.1	1.50	323	17.3
13	Clay	20.5	1.42	323	17.3
14	Sand	22.8	2.25	323	17.3
15	Sand	25.7	2.99	323	17.3
16	Clay	28.7	3.00	323	17.3
17	Clay	38.7	10.03	268	17.3
18	Clay	100	62.00	417	17.3
19	Clay	229	129.0	417	17.3
20	Clay	257.8	28.00	417	17.3

4.2 Plaxis3D

4.2.1 Introduction to Plaxis3D

PLAXIS 3D is a robust Finite Element (FE) software specifically designed for geotechnical engineering applications. This program provides advanced computational tools to simulate the complex interactions between soil, structures, and external loads under static and dynamic conditions. PLAXIS3D is particularly suited for three-dimensional modeling, offering a range of features tailored to address challenges in geotechnical analysis, including soil-structure interaction, deep foundations, slope stability, and seismic response analysis.

In the context of 3D site response analysis, PLAXIS3D stands out for its ability to model the heterogeneous and anisotropic nature of soil layers, incorporating realistic boundary conditions and non-linear material behavior. The program's dynamic analysis module enables the simulation of earthquake loading, considering both ground motion time histories and frequency-dependent soil behavior. Through advanced constitutive soil models, such as the Hardening Soil model and the Mohr-Coulomb model, PLAXIS3D accurately captures the stress-strain behavior of soils under cyclic and transient loading conditions.

One of the program's key strengths lies in its ability to accommodate complex geometries and stratigraphy, allowing for the detailed representation of subsurface conditions in three dimensions. Additionally, PLAXIS3D provides comprehensive tools for pre-processing, mesh generation, and post-processing, enabling the efficient visualization of results such as displacement fields, stress distributions, and acceleration time histories. This makes it a powerful tool for analyzing seismic site response and evaluating the impact of dynamic loads on geotechnical systems, contributing to the development of safe and reliable engineering designs.

4.2.2 Why Plaxis3D program?

PLAXIS3D was utilized in this study to ensure the reliability and accuracy of the implemented and written code for 3D site response analysis (SRA) developed in OpenSeesPy. As OpenSeesPy is an open-source framework requiring custom coding for the specific problem, it was essential to validate the results generated by this code. To achieve this, a widely recognized commercial software like PLAXIS3D was selected as a benchmark tool for comparison, as it was the only available software with the ability to implementation of 3D SRA inside.

By employing PLAXIS3D, which is specifically designed for geotechnical analysis and dynamic site response studies, we aimed to verify that the results obtained from our OpenSeesPy simulations align with those generated by a proven 3D finite element software. This comparative approach provides a critical layer of validation for the custom-developed code, allowing us to test the accuracy of the 3D SRA results under similar input conditions. Using PLAXIS3D alongside OpenSeesPy ensures that the reliability of the OpenSeesPy-based results can be confidently assessed, as any discrepancies or deviations can be carefully analyzed. This validation process not only enhances confidence in the implemented model but also serves to demonstrate the robustness of OpenSeesPy as a tool for 3D SRA when compared to established commercial software.

For the validation process, we focused on the Zeytinburnu soil profile to compare the results obtained from OpenSeesPy with those generated by PLAXIS3D. This site was selected as a representative case for validation due to its well-defined soil properties and the availability of reliable input data. By using PLAXIS3D as a benchmark, we ensured that the implemented 3D site response analysis (SRA) in OpenSeesPy produced accurate and credible results for this specific case.

Once the validation for the Zeytinburnu soil profile was completed and the results from OpenSeesPy were found to be in good agreement with those from PLAXIS 3D,

we were confident in the reliability and robustness of the OpenSeesPy model. This approach allowed us to streamline the analysis process while maintaining confidence in the results generated by OpenSeesPy for other sites, based on the demonstrated accuracy in the Zeytinburnu validation.

4.2.3 Hardening Soil Model in Plaxis3D

In selecting the appropriate soil model for this analysis, we initially employed the Mohr-Coulomb model based on available soil properties, due to its simplicity, and widespread use in geotechnical engineering. However, this model resulted in significant overestimation, particularly under dynamic loading conditions, which led to unrealistic predictions of soil behavior. Recognizing the limitations of the Mohr-Coulomb model, we explored alternative models.

Based on insights from previous research and studies, the Hardening Soil (HS) model emerged as the next logical choice as the HS model was compatible with the soil data available for this study in Zeytinburnu, including the necessary parameters to simulate the model. So, the Hardening Soil (HS) mo del which Initially designed by Schanz [52] was chosen for this analysis due to its ability to represent the behavior of soil under varying load levels compared to the Mohr-Coulomb model.

As mentioned, the decision to transition to the HS model was based on the availability of specific data for the soil profile (Zeytinburnu) like Nspt tests and the parameters required by advanced soil models. The HS model incorporates features such as stress-dependent stiffness, unloading-reloading stiffness, and a more realistic representation of elasto-plastic behavior, which are essential for accurately simulating site response under seismic loads. Additionally, the HS model has been validated in numerous studies by researchers in the field, demonstrating its reliability and suitability for applications involving complex geotechnical conditions and dynamic analyses.

The Hardening Soil model is an advanced tool for simulating soil behavior under dynamic loading conditions, such as those experienced during earthquakes. In PLAXIS3D, the Hardening Soil model effectively captures the complex soil behavior during seismic events [53]. This model provides a more accurate prediction of soil behavior than the Mohr-Coulomb model, primarily because it includes different stiffness definitions for loading and unloading cases [54].

This model is a sophisticated tool designed to simulate the behavior of various soil types, including both soft and stiff soils, under a wide range of loading conditions. When soil is subjected to primary deviatoric loading, it demonstrates decreasing stiffness along with the development of irreversible plastic strains. In a drained triaxial test, the relationship between axial strain and deviatoric stress can be effectively approximated by a hyperbolic curve. This concept was initially formulated by Kondner [55] and later incorporated into the widely recognized hyperbolic model by Duncan and Chang [56].

However, the Hardening Soil model significantly enhances and surpasses the traditional hyperbolic model in several key aspects. Firstly, it employs the theory of plasticity instead of elasticity, allowing for a more accurate representation of soil behavior under stress. Secondly, it accounts for soil dilatancy, which is the tendency of soil to change in volume under shear stress. Finally, it introduces a yield cap, which helps in modeling the ultimate state of soil yielding more accurately. These improvements make this soil model a reliable tool for predicting soil behavior under complex loading conditions, particularly in dynamic environments such as earthquakes.

The Hardening Soil model (Figure 4.5) uses three types of stiffness parameters as soil input: E_{50} (secant stiffness in a standard drained triaxial test), E_{ur} (unloading/reloading stiffness), and E_{oed} (tangent stiffness for primary oedometer loading) (Table 4.3). These parameters lead to high accuracy in predicting the magnitude of soil deformations. PLAXIS3D recommends default values of $E_{50} = E_{oed}$ and $E_{ur} = 3E_{50}$ as average values

for different soil types. Based on the available data (Standard Penetration Test (SPT)) data for the Zeytinburnu site, E_{50} was estimated.

Unlike simpler models that use a single modulus for all stress states, the Hardening Soil model differentiates between primary loading, unloading/reloading, and confined compression. This differentiation is crucial for accurately predicting how soils will behave under various types of loading, particularly in cyclic or dynamic scenarios such as earthquakes.

Figure 4.5: *Hardening soil model.*

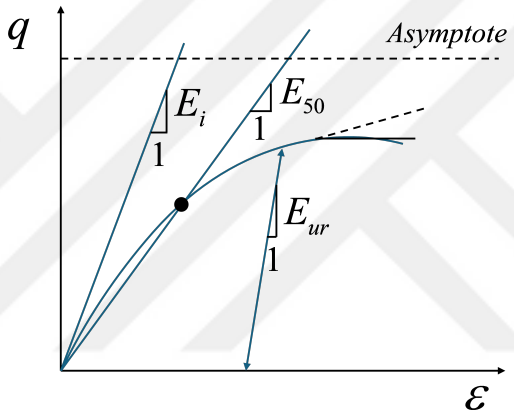

The model also incorporates an advanced yield criterion that accounts for both shear and volumetric hardening. This dual hardening mechanism allows the model to simulate more complex soil behaviors, including the effects of over consolidation and preloading, which are common in natural soils. The Hardening Soil model's capability to simulate these behaviors makes it a powerful tool for geotechnical engineers who need to predict soil responses accurately under a wide range of loading conditions. Moreover, the model's parameters, such as the stiffness moduli E50, Eur, and Eoed, are derived from standard laboratory tests, making it relatively straightforward to calibrate.

These parameters can be adjusted based on specific site conditions, providing a tailored approach to modeling soil behavior. The use of these specific stiffness parameters

ensures that the model can capture the non-linear and hysteretic behavior of soils, which is essential for realistic seismic response analysis.

By implementing the Hardening Soil model in our study, we aim to provide a comprehensive understanding of soil behavior under seismic loading. This model accounts for the soil's history of stress and plastic yielding, offering a detailed representation of how soil layers respond to dynamic forces. By comparing the results from the Nonlinear Hardening Soil model with those from the Equivalent Linear method, the study aims to highlight the strengths and limitations of each approach, thereby enhancing the reliability and accuracy of seismic site response assessments. Required parameters of Hardening Soil model which were defined for Zeytinburnu profile:

Table 4.3: *Hardening Soil model Required Parameters.*

Parameter	**Definition**	**unit**
E_{50}	Secant stiffness in standard drained triaxial test	$[kN/m^2]$
E_{oed}	Tangent stiffness for primary oedometer loading	$[kN/m^2]$
E_{ur}	Unloading / reloading stiffness	$[kN/m^2]$
c	Cohesion	$[kN/m^2]$
Φ	Friction angle	$[^\circ]$
ψ	Dilatancy angle	$[^\circ]$
ν	Poisson's ratio	$[-]$
p_{ref}	Reference stress for stiffnesses (default $p_{ref} = 100\,kN/m^2$)	$[kN/m^2]$
k_0	K value for normal consolidation (default $k_0 = 1 - \sin\Phi$)	$[-]$

Suggested Correlations for different soil types of Hardening soil model parameters [57] Based on Zeytinburnu soil profile type, Clayey Sand and Silty/Sandy Clay correlation was chosen. (Table 4.4)

Poison's ratio was assumed as 0.45. The dilatancy angle measures the volumetric change a soil undergoes when sheared and calculated from Dilatancy angle. Positive dilatancy indicates volume expansion, while negative indicates compression. In many

Table 4.4: *Suggested Correlations for different soil types of HS model.*

Soil Type	$\mathbf{E_{50}}$	$\mathbf{E_{ur}}$	$\mathbf{m}$
Dark Grey Clay	*2500N*	$10E_{50}$	*0.8*
Hard Clay	*1100N*	$10E_{50}$	*0.8*
Dense to Very Dense Sand	*1000N*	$3E_{50}$	*0.5*
Medium to Dense Sand	*750N*	$3E_{50}$	*0.8*
Clayey Sand and Silty/Sandy Clay	*900N*	$3E_{50}$	*0.85*
Stiff Clay	*700N*	$3E_{50}$	*0.85*
Soft and Medium Clay	*250Su*	8 to $10E_{50}$	*1*
Filling Ground	*5000-7000*	$5E_{50}$	*0.5*

practical applications, especially for normally consolidated clays and silty soils, the dilatancy angle is often assumed to be neglectable and very small so setting it to zero can provide a reasonable approximation [58].

This is because these soils typically exhibit little to no volume change during shear, making the zero assumption a simplification that aligns with observed behavior. Table 4.4 outlines the parameters applied in the hardening soil (HS) model within Plaxis3D for the Zeytinburnu soil profile, reflecting the unique geotechnical characteristics of the area.

Estimation of friction angle (ϕ), cohesion (c) and void ratio (e) were done based on corrected value of N_{spt} test with raw data which was done in the field.

N_{spt} values were calculated as below (Equation 4.5):

The estimation of the friction angle (ϕ) which is critical for determining shear strength, cohesion (c) representing the soil's ability to stick together and resist shear stress, and void ratio (e) was based on corrected N_{spt} values from field tests.

$$N_{1,60} = NC_N C_R C_S C_B C_E \tag{4.5}$$

Table 4.5: *Used parameters for HS model in Plaxis3D for Zeytinburnu soil profile.*

No	$\mathbf{E_{50}}$ $[\mathbf{kN/m^2}]$	$\mathbf{E_{oed}}$ $[\mathbf{kN/m^2}]$	$\mathbf{E_{ur}}$ $[\mathbf{kN/m^2}]$	$\mathbf{G_{0ref}}$ $[\mathbf{kN/m^2}]$	$\mathbf{m}$	$\mathbf{w_n}$	$\mathbf{c_c}$
1	2872	2872	22982	61181	1	20	0.15
2	6032.7	6032	48262	76674	1	31	0.26
3	13501	13501	108015	95711	1	31	0.26
4	6320	6320	50560	77823	1	31	0.26
5	11491	11491	91928	91576	1	31	0.26
6	14220	14220	113761	95711	1	31	0.26
7	237002	237002	1896015	158029	1	19	0.14
8	25136	25136	201093	109240	1	19	0.14
9	47740	47740	477400	138245	0.85	19	0.14
10	7000	7000	35000	95711	0.5	19	0.14
11	23987	23987	191900	107648	1	19	0.14
12	19250	19250	192500	119303	0.85	37	0.32
13	32340	32340	323400	130317	0.85	37	0.32
14	18000	18000	54000	115848	0.8	37	0.32
15	262500	262500	787500	167796	0.5	37	0.32
16	21689	21689	173514	106079	1	37	0.32
17	18960	18960	151681	103009	1	37	0.32
18	15400	15400	154000	114159	0.85	37	0.32
19	15400	15400	154000	114159	0.85	37	0.32
20	15400	15400	154000	114159	0.85	37	0.32

$N =$ measured standard penetration resistance in the field

$C_N =$ factor to normalize N to a common reference effective overburden stress

$C_R =$ correction for rod length

$C_S =$ correction for non-standardized sampler configuration

$C_B =$ correction for borehole diameter

$C_E =$ correction for hammer energy ratio

C_N was calculated from Kayen et al. (1992), which limits its max value to 1.7

$$C_N = \frac{2.2}{\left(1.2 + \frac{\sigma'_v}{P_a}\right)} \tag{4.6}$$

$$P_a = 101.3 \quad [kPa] \tag{4.7}$$

Corrected Nspt values are presented in Table 4.6.

for calculating the cohesion of each soil layer (Equations 4.8 and 4.9), experimental correlations were used based on Puri's correlation [59]:

$$\textit{for} \quad 1 < N_{\text{SPT}} < 25 \quad c = 0.0464 N_{\text{SPT}} + 0.0075 \quad \left[\frac{kg}{cm^2}\right] \tag{4.8}$$

$$\textit{for} \quad 25 < N_{\text{SPT}} < 52 \quad c = 0.0702 N_{\text{SPT}} - 0.5453 \quad \left[\frac{kg}{cm^2}\right] \tag{4.9}$$

for friction angle and void ratio (Equation 4.10 and 4.11) of corresponding soil layers a correlation based on a study from Anbazhagan was used [60] :

$$\phi = 0.3125 N_{\text{SPT}} + 26.1261 \quad [^\circ] \tag{4.10}$$

Table 4.6: *Corrected Nspt test data for Zeytinburnu soil profile.*

N **(corrected)**	N_{SPT} **(model)**	**Layer depth (m)**	**Thickness Layer (m)**	**Shear strength (kPa)**	**Unit weight** $(\mathbf{kN/m^2})$	σ'_v (kN/m^2)	**CN**	**CE**	**CB**	**CR**	**CS**
2	3	2.3	2.3	79	17.3	16.6	1.6	0.5	1	0.8	1
4.2	7	3.8	1.5	87	17.3	27.7	1.5	0.5	1	0.8	1
9.4	14	5.3	1.6	117	17.3	39	1.4	0.5	1	0.95	1
4.4	7	6.9	1.6	124	17.3	50.4	1.3	0.5	1	0.95	1
8	14	8.5	1.6	130	17.3	62	1.2	0.5	1	0.95	1
9.9	18	10.1	1.6	99	17.3	73.4	1.1	0.5	1	1	1
165	300	11.4	1.4	517	17.3	83.3	1.1	0.5	1	1	1
17.5	35	12.9	1.5	123	17.3	94.3	1	0.5	1	1	1
68.2	136	14.4	1.5	165	17.3	105.4	1	0.5	1	1	1
9.6	24	15.9	1.5	129	17.3	141.8	0.8	0.5	1	1	1
16.7	37	17.6	1.6	143	17.3	128.1	0.9	0.5	1	1	1
27.5	61	19.1	1.5	239	17.3	139.1	0.9	0.5	1	1	1
46.2	115	20.5	1.4	269	17.3	149.4	0.8	0.5	1	1	1
24	60	22.7	2.3	255	17.3	165.8	0.8	0.5	1	1	1
262.5	750	25.7	3.0	371	17.3	187.7	0.7	0.5	1	1	1
15.1	43	28.7	3.0	256	17.3	209.6	0.7	0.5	1	1	1
13.2	44	38.7	10.0	236	17.3	282.8	0.6	0.5	1	1	1
22	44	100.0	62.0	598	17.3	730	1	0.5	1	1	1
22	44	229.0	129.0	1076	17.3	1671.7	1	0.5	1	1	1
22	44	257.0	28.0	1461	17.3	1876.1	1	0.5	1	1	1

$$e = 1.202 N_{\text{SPT}}^{-0.217} \tag{4.11}$$

The level of Rayleigh damping is controlled by the damping ratio and the circular frequencies of two modes of vibration f_1 and f_2 (Equation 4.12). This type of approach is discussed in most dynamic analysis texts like Chopra[9]. Hardening soil models also require Rayleigh damping parameters, which were calculated for the Kütahya earthquake.

$$f_1 = \frac{v_{\text{avg}}}{4H}; \quad f_2 = n \cdot f_1 \tag{4.12}$$

in which n (Equation 4.13):

$$n = \frac{\textit{fundamental frequency of the input signal at bedrock}}{\textit{fundamental frequency of the whole soil layer}} \tag{4.13}$$

Based on the PLAXIS Library documents, in hardening soil model, hysteretic damping of the soil depends on the input soil properties which can simulate damping at strains larger than 10^{-4} to $10^{-2}\%$, so to do dynamic analysis with mentioned model and simulating soil damping during application, using small amount of Rayleigh damping was suggested for damping of lower strains in PLAXIS3D [53]. To do so, the target damping ratio of ζ_1, ζ_2 and related frequencies of f_1 and f_2 should be selected. Based on suggestions, for energy dissipation at low strains it's recommended to keep magnitude of ζ_1 and ζ_2.

equally and in a range of 0.5 to 2% [15],[51], so for the scope of this study $\zeta_1 = \zeta_2 = 1\%$ were selected respectively. f_1 as the fundamental frequency of the whole soil profile for Zeytinburnu site was calculated as 0.3703 Hz by Deepsoil program, and f_2 estimated as $f_2 = nf_1$ based on Hudson research, which n refers to the closest odd number of ratios of fundamental frequency of ground motion to the fundamental frequency of the whole soil profile, so in this way f_2 was calculated and introduced to the program respectively[61].

The geometry of Zeytinburnu profile was simulated down to engineering bedrock. For studied site, size of mesh as very fine was selected with check meter size in dimensions which met the requirements of mesh guidelines (element size should be less than $\frac{1}{8}$ *wave Length*) recommended by Kuhlemeyer & Lysmer and appropriate absorbing boundary conditions due to wave transfers during application was also chosen [62].

In PLAXIS 3D, specific boundary conditions are utilized to effectively model dynamic soil-structure interactions while minimizing artificial wave reflections at the model boundaries, ensuring the accuracy of seismic simulations. The first one is Compliant Base Boundary Condition which this condition is applied at the base of the model (end of column) and integrates a combination of prescribed displacement history and a viscous damping mechanism. This configuration allows for the realistic input of seismic motion at the base while dissipating incoming waves, making it an optimal choice for earthquake simulations.

The second one is Free Field Boundary Condition which is used for the lateral boundaries (column sides), this condition incorporates a combination of load history and viscous damping. The load history replicates the motion in the free field at the boundary level, while the viscous component absorbs seismic waves, effectively reducing reflections and replicating the behavior of an infinitely extended ground domain. The application of these boundary conditions within PLAXIS3D significantly enhances the fidelity of seismic site response simulations by accurately capturing wave propagation and energy dissipation, thereby improving the robustness of the numerical analysis [43], [44].

After preparing the 3D finite element model in Plaxis3D and applying appropriate boundary conditions and defining the acceleration time histories at the three directions, the site response analysis was conducted into two steps.

In the first step an initial gravitation was applied including the weight of the soil column and the second step was dynamic excitation phase. During the application of

gravity load, material behavior was linear elastic and in the dynamic loading phase, the stress-strain response was elastic-plastic. In dynamic phase, earthquake ground motions were applied to the base of the soil column in desired directions with different nodal recorders at surface and mid-layers and the results were shown in terms of acceleration time histories and spectra acceleration.

4.3 OpenSeesPy

4.3.1 Proposed framework

To achieve a realistic simulation of the seismic response at specific sites, it is crucial to understand the impact of local soil characteristics on the amplitude and frequency attributes of seismic waves. This approach involves developing a three-dimensional finite element (FE) model of a soil column within the OpenSeesPy framework, employing isotropic elastic soil material constitutive models (Figure 4.6).

In this configuration, three-dimensional input acceleration time histories—east-west, north-south, and vertical—are applied at the base of the model, representing the bedrock level. Radiation damping is represented using Lysmer-Kuhlemeyer dashpots [62], which simulate the dissipation of seismic wave energy. In addition to the mentioned framework for predicting 3D SRA with respect to 1D SRA, a model refinement process utilized for considering deterministic genetic algorithms for parameter updating like shear wave velocity and elastic modulus of soil profile.

This refinement process involves Zeytinburnu down-hole array data with help of available Nspt test data for this borehole, enhancing the accuracy in characterizing soil properties by minimizing the differences between observed (by accelerometers) and simulated spectral responses (by numerical model). The objective is to predict 3D SRA behavior with actual site-specific responses as captured in the down-hole array data. This methodological framework combines sophisticated modeling and data-driven calibration

to enhance the predictive capacity of seismic site response models. By integrating these advanced techniques, the framework provides essential insights into 3D local soil dynamics, contributing to improved seismic risk assessment and management for civil engineering applications.

4.3.2 Proposed FE model for predicting 3D SRA

This FE model uses OpenSeesPy with Python language to predict 3D response In OpenSeespy [63], the Site Response Analysis (SRA) is conducted by modeling the subsurface profile as a vertically layered column of soil, underlain by an elastic half-space that simulates the stiffness and rigidity of the bedrock. This model configuration assumes a level ground surface without any slope, ensuring that the soil column's response to seismic loading reflects solely the local stratigraphy and soil properties rather than topographic effects.

Figure 4.6: *Studied soil profile and FE model of the column of soil. g is the gravity vector. R_v is the static reaction force at the base at the end of stage 1.*

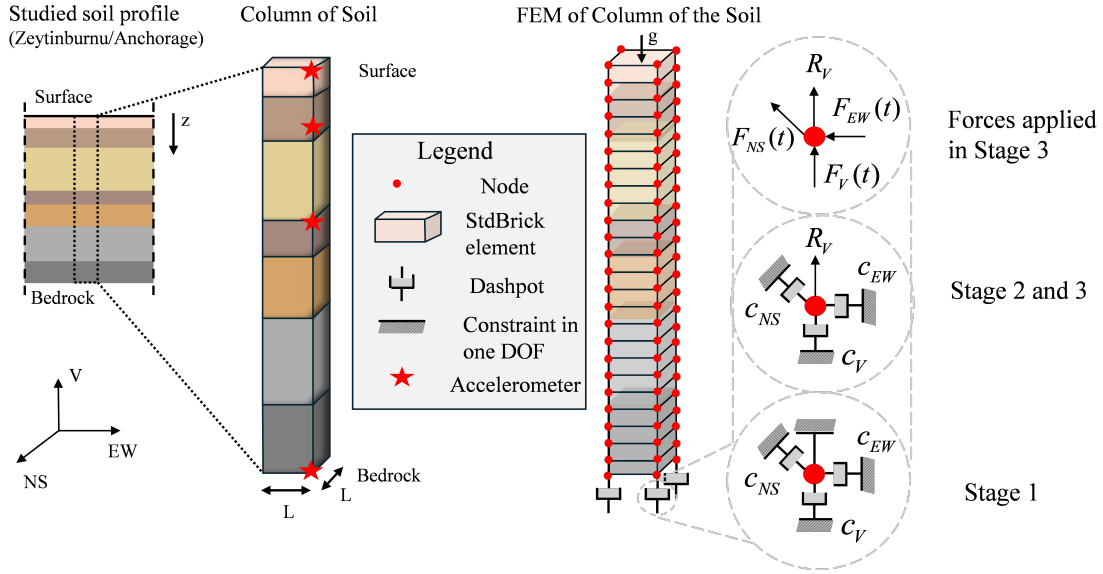

The model structure is schematically illustrated in Figure 4.6. Each soil layer

within the model is discretized using StdBrick elements (see Figure 4.7), which facilitate the construction of an eight-node brick element based on a trilinear isoparametric formulation [64]. The dimensions of these elements, denoted as L, are kept consistent in the global x (east-west) and y (north-south) directions, allowing for uniform lateral resolution, while adjustments are made in the z (vertical) direction to account for variations in soil layer thickness and depth.

Figure 4.7: *8 nodal StdBrick elemenet.*

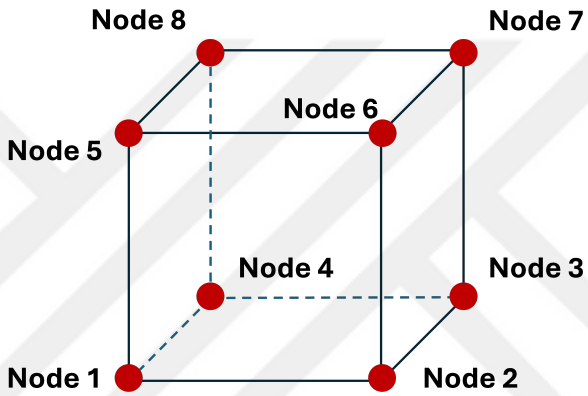

This model was used for two soil profiles: Zeytinburnu and Anchorage site To effectively capture the complex nonlinear behavior of soils, in this study, two nonlinear constitutive models from the OpenSeesPy library, namely Pressure Depend Multi Yield (PDMY) and Pressure-Independent Multi-Yield Model (PIMY), were employed to simulate soil behavior. These models were chosen due to their established capability to represent the essential mechanical responses of soils under varied loading conditions[65], [66], [67].

The PIMY material model is specifically designed for materials whose deviatoric stress-strain behavior dominates and is largely insensitive to confinement changes, such as organic soils or clays. During gravity or static loading, the material exhibits linear elastic behavior. However, under dynamic or cyclic loading, the material transitions to an

elastic-plastic response, formulated using the multi-surface concept with associative flow rules. The yield surfaces adhere to the VonMises criterion.

This model has been widely applied in scenarios involving monotonic or cyclic loading of soils with minimal confinement sensitivity [66]. Conversely, the Pressure-Dependent Multi-Yield Model (PDMY) model is an elastic-plastic material that is particularly suitable for sands and silts subjected to monotonic or cyclic loading conditions. When implemented in solid elements such as FourNodeQuad or Brick elements, it effectively simulates the response of soil. The plasticity in this model is also based on the multi-surface concept, with yield surfaces following the Drucker-Prager criterion. This model has been extensively used in finite element analyses due to its robust representation of pressure-sensitive behaviors in granular materials [66].

In addition to elastic, shear and bulk modulus, these models require more soil parameters as initial void ratio e_0, atmospheric pressure (P_{atm}) as a reference stress, friction angle (ϕ), number of yield surfaces and cohesion (c) and besides proper calibration of these parameters based on soil testing data is crucial for accurate simulations. All these parameters were chosen. based on available information about soil profiles and proposed calibrated input parameters [65], [68].

To accurately represent seismic energy dissipation within the model, Lysmer-Kuhlemeyer dashpots [62] are implemented using Viscous Uniaxial materials coupled with ZeroLength elements. These dashpots simulate radiation damping by absorbing outgoing seismic waves as they traverse the soil column, effectively preventing wave reflections at the boundaries of the model and thus replicating an infinite domain which are essential for achieving realistic damping effects, are calculated as Equations 4.14, 4.15 and 4.16.

The Viscous Uniaxial material plays a critical role in numerical modeling for accurately simulating the interaction between seismic waves and bedrock. This material,

Table 4.7: *Zeytinburnu soil profile details 2.*

Col No	***depth*** $[\mathrm{m}]$	$\mathbf{E}\,[\mathbf{kN/m^2}]$	$\mathbf{G}\,[\mathbf{kN/m^2}]$	$\mathbf{K}\,[\mathbf{kN/m^2}]$
1	2.3	242553	93289.5	202127
2	3.79	242553	93289.5	202127
3	5.34	321990	123842	268325
4	6.90	321990	123842	268325
5	8.49	321990	123842	268325
6	10.05	202204	77770.6	168503
7	11.41	202204	77770.6	168503
8	12.91	202204	77770.6	168503
9	14.43	202204	77770.6	168503
10	15.93	220905	84963.3	184087
11	17.55	202204	77770.6	168503
12	19.05	478361	183985	398634
13	20.46	478361	183985	398634
14	22.71	478361	183985	398634
15	25.70	478361	183985	398634
16	28.70	478361	183985	398634
17	38.73	329322	126662	274435
18	100	797302	306654	664418
19	229	797302	306654	664418
20	257.8	797302	306654	664418

when coupled with ZeroLength elements (which used to connect nodes at the soil and bedrock interface (Figure 4.8), is particularly effective in representing radiation damping at the bedrock boundary. It replicates the absorption of outgoing seismic waves, thereby preventing artificial reflections that could otherwise distort the results.

Figure 4.8: *ZeroLength elements.*

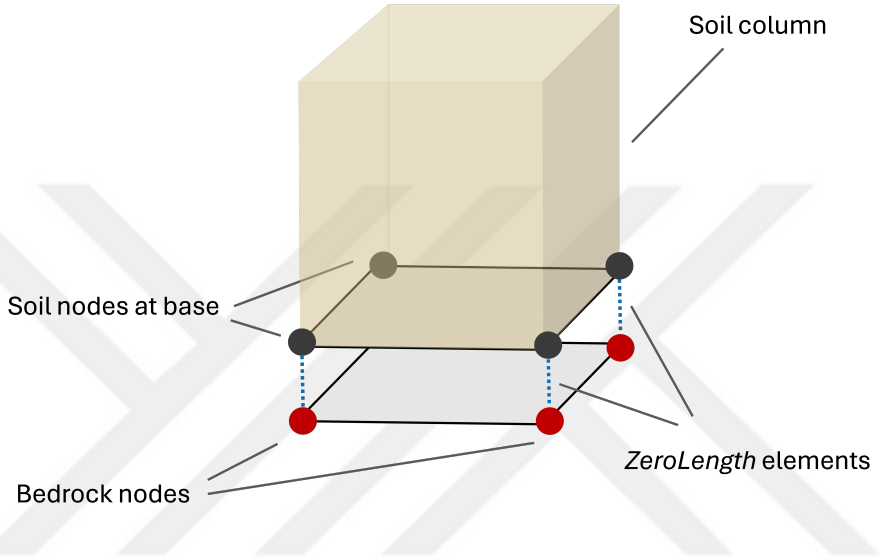

This capability makes it an essential component in dynamic soil-structure interaction and seismic site response analyses, where capturing realistic energy dissipation at the bedrock interface is paramount. In this study, Viscous Uniaxial material is used to model Lysmer-Kuhlemeyer dashpots at the bedrock boundary, ensuring that the seismic waves are absorbed effectively to replicate an infinite domain.

This approach enables the model to accurately represent wave propagation and energy dissipation, critical for achieving reliable results in dynamic analyses involving soil and bedrock interactions. This setup in general ensures that energy is dissipated at the boundaries, enhancing the model's ability to simulate natural seismic wave behavior within the soil profile [69].

For horizontal time histories, dashpot coefficients are calculated based on shear wave velocities (V_{sb}) and for vertical Time History Analysis (TH), dashpot coefficient is

calculated from compression wave (V_{pb}). The east-west (c_{EW}), north-south (c_{NS}), and vertical (c_V) dashpot coefficients are:

$$c_{EW} = \rho_b V_{sb} \cdot A \tag{4.14}$$

$$c_{NS} = \rho_b V_{sb} \cdot A \tag{4.15}$$

$$c_V = \rho_b V_{pb} \cdot A \tag{4.16}$$

where ρ_b is the mass density of the bedrock and $A = L^2$ is the area of elements projected in the horizontal plane. The level of Rayleigh damping is controlled by the damping ratio (ζ) and the circular frequencies of two modes of vibration (ω_1 and ω_2). (Equation 4.17 and 4.18). The model is defined by two target frequencies:

$$\omega_1 = 2\pi \times 0.2 \quad \text{rad/s}, \quad \text{representing the lower frequency} \tag{4.17}$$

$$\omega_2 = 2\pi \times 20 \quad \text{rad/s}, \quad \text{representing the upper frequency} \tag{4.18}$$

These frequencies are selected to cover the range of significant seismic response frequencies [66]. The damping coefficients a_0 and a_1 (Equation 4.19 and 4.20) are calculated to achieve the desired damping ratio across this frequency range:

$$a_0 = \frac{2 \times \zeta \times \omega_1 \times \omega_2}{\omega_1 + \omega_2} \tag{4.19}$$

$$a_1 = \frac{2 \times \zeta}{\omega_1 + \omega_2} \tag{4.20}$$

These coefficients are then used in the Rayleigh damping formulation in OpenSeesPy ensuring that the damping is proportional to both the mass and stiffness matrices of the

system.The model execution process is divided into three sequential stages, as illustrated in the right panel of Figure 4.6. In Stage 1, the base of the soil column is constrained in the vertical direction to establish a stable foundation, while at each level, the upper nodes of elements are linked in three degrees of freedom using the equalDOF command (Figure 4.9).

This command in OpenSeesPy is used to constrain degrees of freedom (DOFs) between two nodes, ensuring that the specified DOFs of one node move identically to those of another. During this initial stage, gravity loading is applied through an extended static analysis. This approach minimizes transient effects, allowing the model to gradually settle and stabilize under gravitational forces, thereby ensuring a robust initial condition for subsequent seismic loading simulations [1].

Figure 4.9: *EqualDOF XYZ in nodes.*

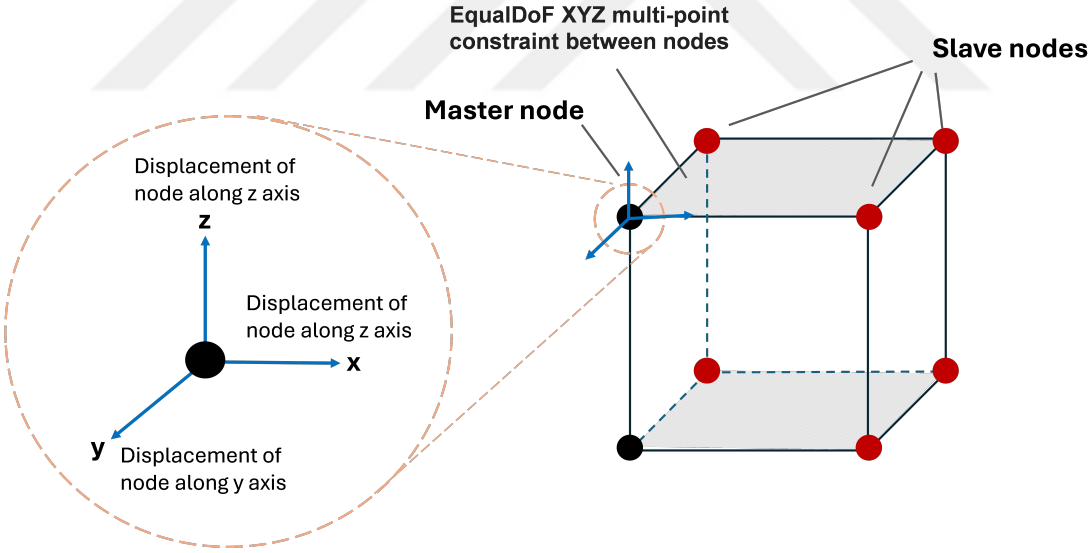

In Stage 2, the vertical constraints applied at the base of the soil column during the initial stage are removed, allowing for a more realistic representation of soil behavior under seismic loading. Following the removal of these constraints, an additional extended

static analysis is conducted to facilitate further stabilization of the model under the adjusted boundary conditions.

To balance the vertical stress and maintain equilibrium, a vertical force (R_v) is applied in the upward direction, with a magnitude equal to the reaction force previously observed at the base. This additional force counteracts any residual imbalances, ensuring that the soil column is in a stable state before the application of dynamic seismic loading in the subsequent stage.

In Stage 3, the model is subjected to a dynamic analysis to assess the soil column's response to seismic excitation. To simulate realistic damping characteristics typical in soil behavior during seismic events, the damping ratio is set to 2% using the Rayleigh damping model. This adjustment aligns with standard practice for simulating energy dissipation within geotechnical models [15].

The earthquake ground motions are introduced at the model's base by applying three-dimensional force time histories. These are implemented through the PathTimeSeries command, with separate time histories assigned for each direction component (east-west, north-south, and vertical). PathTimeSeries command specifies the relationship between the load factor and time as a series of discrete points in a two-dimensional space, where each point is defined by a pair of values representing the load factor and the corresponding time.

This approach allows each base node to receive the complete seismic load in three dimensions, providing an accurate and comprehensive representation of the dynamic forces impacting the soil column. These forces (Equations 4.21, 4.22 and 4.23) are calculated by multiplying the velocity time history of the ground motions with the corresponding dashpot coefficients[62][69](Figure 4.10).

The applied forces in the east-west (F_{EW}), north-south (F_{NS}), and vertical (F_V)

are expressed as:

$$F_{EW}(t) = \frac{c_{EW} \cdot \dot{u}_{EW}(t)}{4} \tag{4.21}$$

$$F_{NS}(t) = \frac{c_{NS} \cdot \dot{u}_{NS}(t)}{4} \tag{4.22}$$

$$F_{V}(t) = \frac{c_{V} \cdot \dot{u}_{V}(t)}{4} \tag{4.23}$$

where c_{EW}, c_{NS}, and c_V are defined in Equation 4.14, 4.15 and 4.16.

$\dot{u}_{EW}(t)$, $\dot{u}_{NS}(t)$, and $\dot{u}_V(t)$ are the three components of the velocity time histories in the east-west, north-south, and vertical directions, respectively. These forces are equally divided among the four base nodes to accurately simulate the distribution of seismic forces across the base of the model, and this is accounted for by dividing by 4 for each of these forces.

Figure 4.10: *Applied forces for dynamic analysis.*

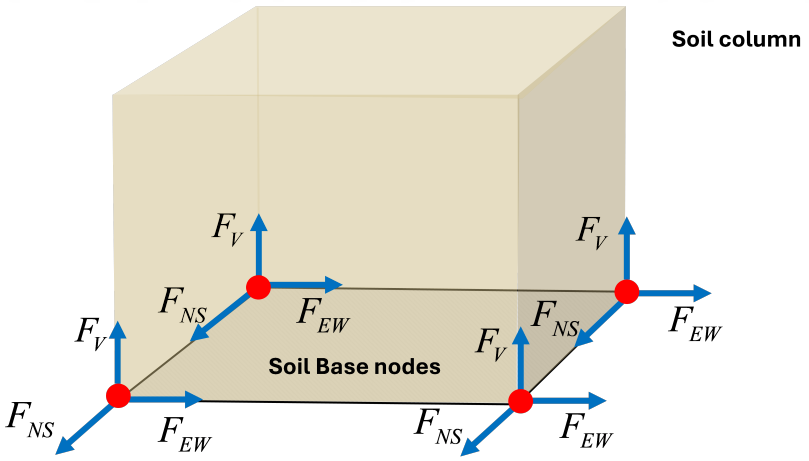

During this stage, displacements, velocities, and accelerations are measured at each node and desired depths. The acceleration response spectra (Sa(T)) is then calculated over a frequency range from 0.005 to 4 Hz with an increment of 0.05 Hz.

5. OPTIMIZATION STUDY

5.1 Background of Optimization study

An optimization study was carried out as a part of study alongside the detailed three-dimensional (3D) site response analysis (SRA) to mitigate uncertainties associated with input data, focusing primarily on the shear wave velocity (V_s and the stiffness modulus derived from it. Shear wave velocity (V_s) is a fundamental parameter that reflects the stiffness and elastic properties of soil, directly influencing its ability to transmit seismic waves, in this case accurate determination of will be crucial for reliable SRA, as it has a significant impact on the computed soil parameters, ground motions and the assessment of seismic site effects [70]. The stiffness modulus, often derived from through empirical relationships, characterizes the soil's resistance to deformation under seismic loading [71].

Evaluating the impact of soil characteristics on site response is essential for predicting ground motion during earthquakes with accuracy. Two parameters substantially affect the outcomes of 3D SRA: the lowest shear wave velocity in the soil profile and the highest frequency that can be effectively captured in the analysis [27]. The dynamic response of soil layers under seismic loading is directly governed by the shear wave velocity, making it a critical factor. In seismic design, the dynamic modulus—comprising both shear and Young's moduli—can be derived through measurements [1]. The PS Suspension Logging test is widely regarded as one of the most effective methods for determining shear wave velocity (V_s) profiles in the field [72], [73].

This method, while useful in seismic investigations, has several inherent limitations influenced by environmental and borehole-specific conditions [74]. One primary issue is its reduced effectiveness in shallow soils, as removing all casing from a borehole

often risks collapse, leaving the uppermost 5 to 10 meters untested. Additionally, in unconsolidated deposits, maintaining borehole wall stability is essential to prevent tool loss, and poor coupling with the soil medium further complicates data collection by degrading wave clarity—especially when drill mud accumulates on the borehole walls. Borehole characteristics themselves also significantly impact the quality of PS logging data. PS logging is sensitive to borehole diameter, wall smoothness, and other irregularities on the wall, which increased rugosity on walls leads to signal distortion, especially affecting S waves. [74]. Smaller boreholes (100 to 200 mm) are ideal for transmitting energy effectively.

besides Environmental noise and adverse weather also pose challenges, particularly in marine settings where vessel noise interferes with signal clarity as the tool nears the surface. Weather interruptions may force testing under time constraints, impacting reliability. Moreover, Structural irregularities such as sidewall cavities and fractures further degrade the seismic signal, with cavities causing diffracted waves and open fractures producing ”multiples “wave reverberations within a layer that amplify S wave distortions, resulting in jagged and unreliable data [74].

In other hand, accurate data is crucial for estimating the mechanical properties of subsurface layers, as unreliable or incomplete profiles can lead to incorrect predictions of ground motion amplification. Such inaccuracies may result in either unsafe designs or overly conservative ones, both of which can have significant consequences. To address this issue, continuous advancements are necessary in both measurement techniques and data interpretation methods to maintain precision in geotechnical analysis and seismic design [75], [76], [77], [78]. While advanced geophysical methods each comes with specific challenges and inherent uncertainties.

Given the probable limitations this study introduces an optimization strategy to enhance the precision of 3D SRA modelings on ground surface. A Genetic Algorithm (GA)

optimization method is applied within the OpenSeesPy framework, an open-source finite element software [79]. Genetic algorithms, inspired by natural selection and genetic processes, are well-suited for addressing complex optimization tasks involving large, nonlinear, and discrete search spaces. These characteristics make them particularly effective for solving challenging problems encountered in geotechnical engineering [80], [81]. Optimization algorithms have become essential tools in recent years for addressing complex problems across diverse fields, including economics, engineering, and environmental sciences [82]. These algorithms often draw inspiration from natural processes such as biological evolution, collective behavior in swarms, and physical principles [83].

They can be broadly divided into two primary categories: single-solution metaheuristics and population-based metaheuristics [84]. Single-solution metaheuristics focus on refining one candidate solution, but this approach carries the risk of being trapped in local optima. On the other hand, population-based metaheuristics, such as genetic algorithms (GAs), explore multiple candidate solutions simultaneously, promoting thorough exploration of the search space and reducing the chances of premature convergence.

One of the key advantages of GAs is their ability to handle optimization tasks without requiring derivative information about the error function, which makes them highly suitable for geotechnical applications where objective functions are often non-differentiable or discontinuous [85], [86]. The adaptability of GAs, achieved through the dynamic adjustment of crossover and mutation probabilities, enables them to avoid local optima and maintain effective global search performance [87].

These crossover and mutation operators are fundamental mechanisms employed to generate offspring individuals, with the primary objective of enhancing the genetic diversity and adaptability of each successive generation. The crossover operator facilitates the exchange of genetic material by recombining the chromosomes of two selected parent individuals, thereby producing offspring with novel genetic configurations. In contrast, the

mutation operator introduces stochastic variations into the genetic sequence of individuals, promoting diversity and preventing premature convergence by exploring a broader solution space (Figure 5.1). [81], [88].

Figure 5.1: *Genetic Algorithm framework.*

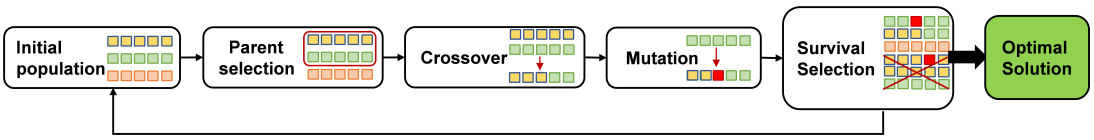

In geotechnical engineering, GAs have proven valuable in identifying key soil parameters necessary for accurate modeling and simulation of soil behavior [89]. This is especially important due to the inherent sensitivity of in-situ geotechnical tests, which may not directly capture essential mechanical properties or adequately reflect the spatial variability of soil layers [52]. By leveraging optimization algorithms, engineers can calibrate numerical models against observational data, leading to more refined estimates of soil properties and enhancing the predictive accuracy of site response analyses. Managing the inherent spatial variability of soil properties presents one of the primary challenges in geotechnical engineering.

This variability introduces significant uncertainty in the behavior of geotechnical structures and influences how superstructures respond to seismic activity [90], [91], [92]. Ignoring such variability can lead to oversimplified assumptions, resulting in either inaccurate predictions of structural response or designs that are overly conservative, potentially compromising both safety and efficiency [93].

Research has shown that about 50% of downhole sites are poorly modeled in one-dimensional (1D) site response analysis (SRA) when only a single shear wave velocity (V_s) profile is used [94], [95], [96]. Furthermore, poorly simulated sites tend to exhibit systematic errors in 1D ground response predictions [97], [98], [99]. Accurate modeling and understanding spatial variability are critical for reliable predictions of soil behavior

under various environmental and loading conditions.

Numerous studies have aimed to integrate spatial variability into 1D ground response analysis by introducing stochastic randomization of , using multiple profiles obtained from surface wave testing, and refining damping techniques [94], [96], [98], [100]. These efforts emphasize the importance of accounting for soil variability to enhance the accuracy of site response analysis. Genetic algorithms (GAs) offer a promising approach for optimizing soil models that incorporate large datasets in spatial analysis. Through the generation of multiple realistic (V_s) profiles based on statistical distributions and optimization criteria, GA enables the development of more representative soil models that better capture the range of possible soil behaviors [101], [102].

This study investigates the impact of uncertainties in the V_s profile on the outcomes of 3D SRA, given the limited research on optimized 3D SRA methods. The GA-based optimization was implemented within the open-source finite element software OpenSees[79]. Integrating GAs with OpenSees allowed for the calibration of soil model parameters by minimizing the discrepancies between recorded and simulated seismic responses. This inverse analysis approach, by generating multiple realistic V_s profiles using a genetic algorithm, adjusts key properties—such as Vs and the stiffness modulus—based on observed ground motion data, enhancing the accuracy of SRA.

The results of this optimization study aim to enhance the precision of 3D SRA predictions contribute to improved seismic design and increased resilience against future seismic events. This incorporation of genetic algorithms into 3D SRA represents a significant advancement in geotechnical earthquake engineering, offering a practical solution to manage uncertainties and enhance the reliability of seismic hazard assessments.

5.2 Benefits of the Optimization Study

The comprehensive framework developed offers several significant benefits. First, refining key input parameters, such as shear wave velocity and stiffness modulus derived from it, reduces uncertainties in SRA, resulting in more accurate predictions of ground motion behavior [93]. This increased reliability ensures that seismic hazard assessments are both precise and practical for engineering applications.

Second, more accurate SRA outcomes lead to well-informed seismic design decisions for foundations and structures, directly contributing to improved safety and performance during earthquakes [103]. Precise modeling of site-specific seismic effects helps engineers design structures that perform optimally under seismic loading, reducing the risk of structural failure. Third, the reduction of excessive conservatism in design parameters lowers construction costs without compromising safety [91].

Optimizing designs allows for efficient use of materials and resources, balancing safety with cost-effectiveness in construction projects. Finally, by enhancing the modeling of soil behavior under seismic loading, the predictive capabilities of site response analyses (SRAs) are substantially improved, leading to more accurate seismic hazard evaluations [104].

5.3 Optimization Framework

5.3.1 Optimization in 3D site response analysis

To improve the accuracy of our 3D site response analysis, a model updating code was implemented, which is informed by experimental accelerometric downhole array data of Zeytinburnu. This data is instrumental in accurately adjusting the shear wave velocity of the different soil layers. The primary goal of updating the model is to minimize the discrepancies between the measured and predicted acceleration response spectra at various depths in EW and NS directions and especially at the ground surface. By doing so,

the model becomes more reflective of the actual ground conditions and the behavior of different soil strata under seismic loading (Figure 5.2).

Figure 5.2: *Incorporation of data processing into 3D SRA.*

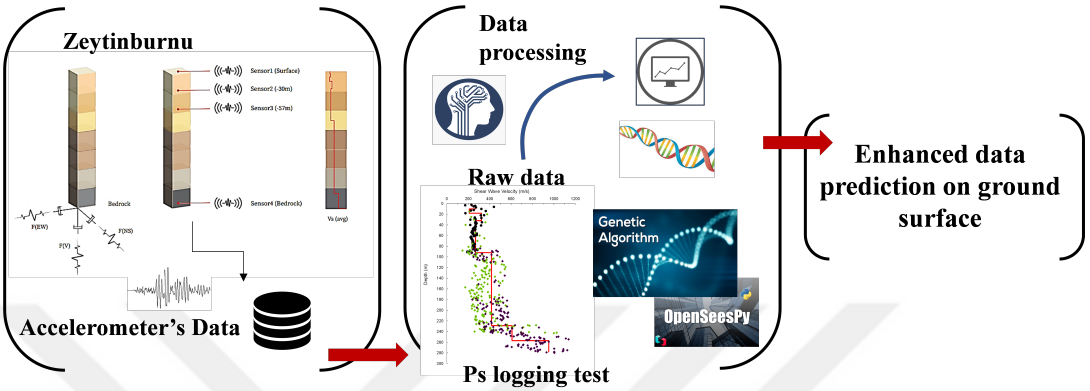

To do so, a genetic algorithm (GA) was employed to optimize soil properties by minimizing the Root Mean Square Error (RMSE) between observed and computed spectral accelerations within a soil profile by using techniques to refine initial seismic models that utilized average shear wave velocity (V_s) values derived from PS Suspension Logging tests. This model established nominal(V_s) parameters for various soil layers based on mean values, with updates expressed as multiples of these initial estimates. The bounds for these multiplication factors were defined by the standard deviation of the initial parameters, facilitating the use of deterministic genetic algorithms for model updating.

5.3.2 Working Principles

The optimization method proposed here utilizes the genetic algorithm metaheuristic approach, a technique often employed in complex problem-solving scenarios. This type of soft-computing algorithm explores the search space by manipulating a set of variables organized into what is known as a design vector (Equation 5.4). Each potential solution signifies a possible shear wave velocity configuration, which aims to improve the performance of ground motion prediction on the ground surface. The process within this

framework is illustrated in Figure 5.3.

The algorithm begins by generating a random initial population of design vectors (potential solutions) within a reliable boundary and assesses the objective function (Equation 5.6) for each one. This objective function serves as a measure of how well each solution meets the desired criteria.

For this study, the objective function calculates the difference between recorded acceleration spectra by accelerometers and calculated ones by the numerical approaches. The most suitable individuals as shear wave velocities which offer the best balance between calculated and recorded spectra on the ground surface, are then chosen using genetic operators. This iterative process of selection and generation continues until an optimal or near-optimal solution is found.

Figure 5.3: *Flowchart of the optimization framework.*

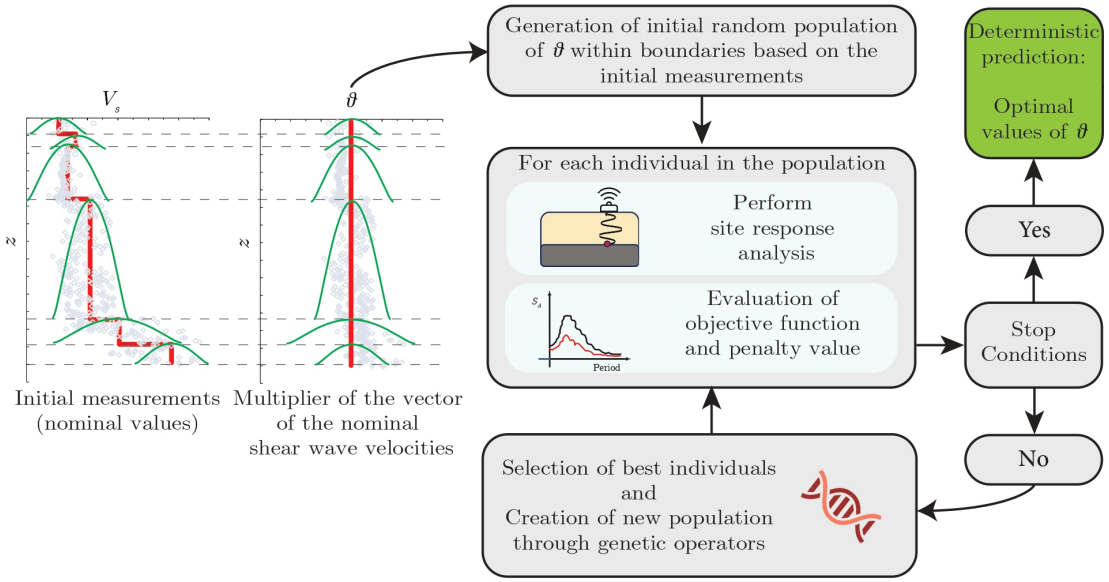

As illustrated in Figure 5.3, the optimization algorithm forms the core of the framework, yet two critical engineering decision phases are left to the designer's discretion. The first phase involves the initial selection of the design variables. This step

allows the designer to define a restricted design space, such as limiting the optimization to a specific portion of the shear wave velocity profile at a specific depth or reducing the number of parameters to be optimized. This targeted approach can make the optimization process more efficient. In the final phase, the designer evaluates a restricted number of optimized solutions with similar fitness levels.

At this stage, the most suitable solution is selected based on technical feasibility and other practical considerations. This decision-making step is crucial as it ensures that the chosen solution is not only optimal in a computational sense but also viable in real-world application. The main features and advantages of this framework, including detailed descriptions of each phase and the underlying principles, are elaborated in the following sections.

5.3.3 Design Vector Encoding

The optimization algorithm aims to identify the optimal shear wave velocity profile obtained by PS logging test that needs to minimize results of 3D site response analysis on the ground surface. This topology optimization is achieved using decision variables (V_s) which each one represents a position of the (V_s) within the boundary. The decision variable of (V_s controls Elastic modulus (Equation 5.1), shear modulus (Equation 5.2) and Bulk modulus (Equation 5.3) of soil materials.

$$E = 2 \cdot \rho \cdot V_s^2(1 + \nu) \tag{5.1}$$

$$G = \rho \cdot V_s^2 \tag{5.2}$$

$$k = E \cdot 3(1 - 2\nu) \tag{5.3}$$

and all decision variables are compiled into design vector b, which is defined as follow:

$$b = [w_{11}, w_{12}, \ldots, w_{ij}]^T \tag{5.4}$$

$$w_{ij} \in [\text{lower boundary}, \text{upper boundary}] \tag{5.5}$$

w_ij are values that includes minimum and maximum values of shear wave velocity obtained by exact PS logging test for the specific depth and shear wave velocities included in the design vector can take values within the boundary. Consequently, the selection of the optimization algorithm relies on genetic algorithms, as this approach is particularly efficient in handling a search space defined by Boolean variables. The implementation of the true boundary condition based on test data, as encoded in the design vector, ensures that the proposed optimized shear wave velocity profile is practical for the prediction of site response analysis on the ground surface. Furthermore, the genetic algorithm's iterative process allows for a comprehensive exploration of the search space and providing optimal results.

5.3.4 Definition of the objective function

The general form of the objective function (OF) to be minimized, also called the fitness function, is designed to evaluate the best solution for prediction of site response analysis within reliable shear wave velocity values. The objective function essentially measures how well a given solution fits the desired criteria, with reliable values indicating a better fit. Mathematically, the objective function can be expressed as:

$$OF(b) = \sum_{j=1}^{m} RMSE_j(b) \tag{5.6}$$

in which:

OF(b): The function we aim to minimize. It evaluates the quality of a solution by calculating the sum of the Root Mean Square Error$RMSE_j(b)$ across multiple evaluations.

b: represents the vector of parameters that we are optimizing. These parameters might include variables that affect ground motion, such as shear wave velocity values and elasticity modulus.

The summation $\sum_{j=1}^{m}$ denotes the summation over m different evaluations or datasets. Each j represents a specific evaluation scenario or dataset where the $RMSE$ is calculated.

$RMSE_j(b)$: The Root Mean Square Error for the j-th evaluation. $RMSE$ is a measure of the differences between the values predicted by a model and the values observed. In this context, it assesses how well the predicted ground motion matches the observed ground motion for a given set of parameters b. The goal is to find the parameter vector b that minimizes this objective function, leading to the best possible solution for predicting ground motion on the ground surface based on reliable shear wave velocity values. Minimizing the $RMSE$ across all evaluations ensures that the solution is robust and performs well across various scenarios.

The general shape of each RMSE (Equation 5.7) is defined as:

$$RMSE = \sqrt{\frac{1}{n}\sum_{i=1}^{n}(y_i - \hat{y}_i(b))^2} \tag{5.7}$$

where:

n is the numerical observations.

y_i is the observed value.

$\hat{y}_i$ is the predicted value.

$RMSE$ is a commonly used metric to measure the differences between values predicted by the numerical model and the recorded ones. By minimizing the RMSE, the optimization algorithm aims to find the predicted ground motion as close to the observed ones (Figure 5.4). Where for site response analysis model calibration the RMSE value for each time step during T period, at the different levels and directions can be conveniently

considered as (Equation 5.8):

$$RMSE = \sqrt{\frac{1}{n}\sum_{i=1}^{n}\left(S_{a,i}(T) - \hat{S}_{a,i}(T)(b)\right)^2} \tag{5.8}$$

The extended form (Equation 5.9) of the objective function provides a more detailed breakdown of the individual components contributing to the overall Root Mean Square Error $RMSE$ in different directions and at various depths.

Figure 5.4: *Schematic presentation of RMSE concept.*

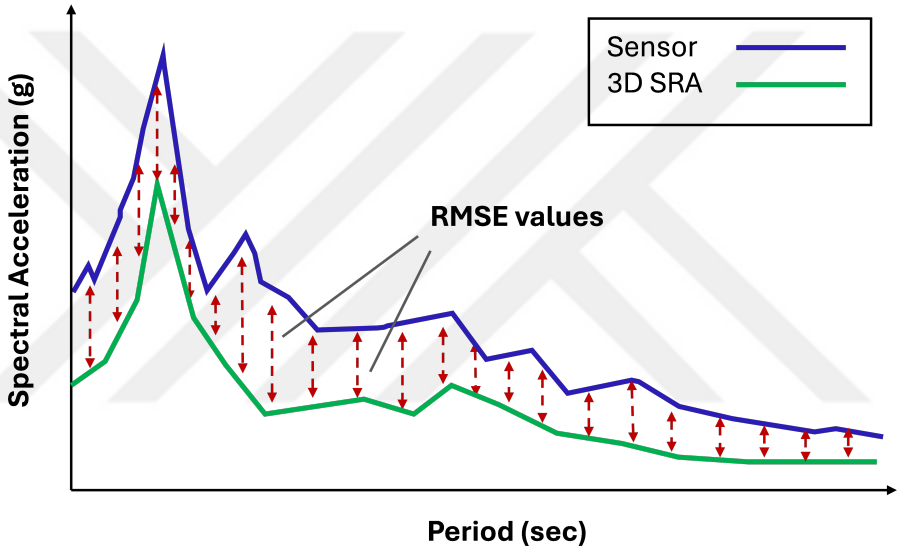

This form allows for a comprehensive evaluation of the ground motion predictions by considering multiple directional and depth-specific errors. For the current study under investigation two ground motions direction and three levels are considered so that the objective function specializes as:

$$OF(b) = RMSE^{S}_{EW} + RMSE^{S}_{NS} + RMSE^{30}_{EW} + RMSE^{30}_{NS} + RMSE^{57}_{EW} + RMSE^{57}_{NS} \tag{5.9}$$

in which:

- $RMSE^{S}_{EW}$ stands for Route Mean Square Error of surface in EW direction. This

component measures the error between predicted and observed values of ground motion on the surface in the EW direction.

- $RMSE^{S}_{NS}$ stands for Route Mean Square Error of surface in NS direction. This component measures the error between predicted and observed values of ground motion on the surface in the NS direction.

- $RMSE^{30}_{EW}$ stands for Route Mean Square Error of -30m in EW direction. This component measures the error 30 meters below the surface in the EW direction.

- $RMSE^{30}_{NS}$ stands for Route Mean Square Error of -30m in NS direction. This component measures the error 30 meters below the surface in the NS direction.

- $RMSE^{57}_{EW}$ stands for Route Mean Square Error of -57m in EW direction. This component measures the error 57 meters below the surface in the EW direction.

- $RMSE^{57}_{NS}$ stands for Route Mean Square Error of -57m in NS direction. This component measures the error 57 meters below the surface in the EW direction.

6. RESULTS

6.1 Zeytinburnu Soil Profile

In this section, the results of the modeling 1D and 3D site response analyses for the Zeytinburnu soil profile under Kütahya earthquakes are presented. The following subsections present and discuss the findings in detail.

6.1.1 1D site response analysis with Deepsoil

The Figure 6.1 displays the results of a 1D site response analysis (1D SRA) with Deepsoil program for the Zeytinburnu soil profile, comparing spectral acceleration (SA) values from sensors (solid black lines) with those from the 1D SRA model (dashed red lines) across periods from 0 to 4 seconds at different levels of surface, -30m and -57m.

Figure 6.1: *Sensor with respect to 1D SRA in Zeytinburnu.*

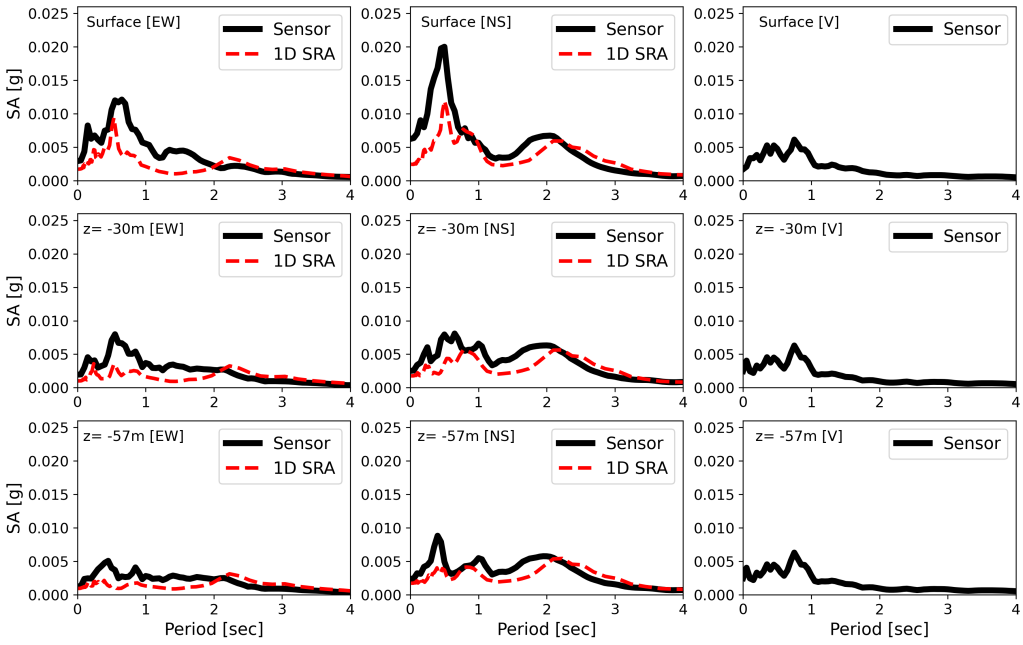

6.1.2 3D site response analysis with Plaxis3D

The Figure 6.2 displays the results of a 3D site response analysis (3D SRA) with Plaxis3D program for the Zeytinburnu soil profile, comparing spectral acceleration (SA) values from sensors (solid black lines) with those from the 3D SRA model (blue lines) across periods from 0 to 4 seconds at different levels of surface, -30m and -57m.

Figure 6.2: *Sensor with respect to 3D SRA in Plaxis3D for Zeytinburnu.*

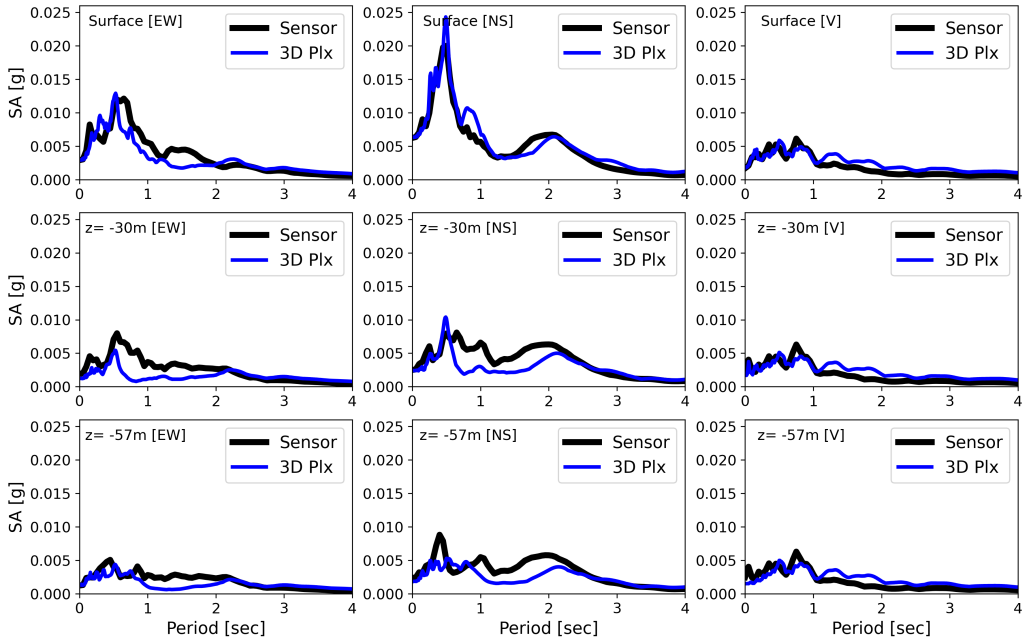

6.1.3 3D site response analysis with OpenSeesPy

The Figure 6.3 displays the results of a 3D site response analysis (3D SRA) with OpenSeesPy code for the Zeytinburnu soil profile, comparing spectral acceleration (SA) values from sensors (solid black lines) with those from the 3D SRA model (green lines) across periods from 0 to 4 seconds at different levels of surface, -30m and -57m.

Figure 6.3: *Sensor with respect to 3D SRA in OpenSeesPy for Zeytinburnu.*

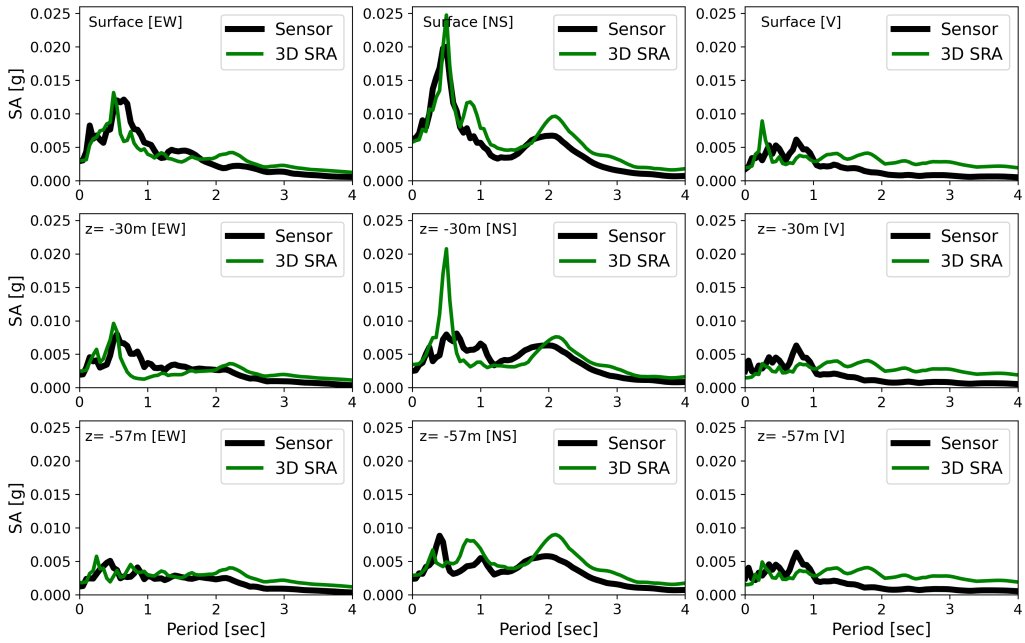

6.1.4 Comparison of three methods

The Figure 6.4 displays the comparison results of a 3D site response analysis (3D SRA) with OpenSeesPy code and Plaxis3D program for the Zeytinburnu soil profile, comparing spectral acceleration (SA) values from sensors (solid black lines) with those from the 3D SRA model (green and blue lines) across periods from 0 to 4 seconds at different levels of surface, -30m and -57m.

The Figure 6.5 displays the comparison results of a 3D site response analysis (3D SRA) with OpenSeesPy code and Plaxis3D program for the Zeytinburnu soil profile, comparing spectral acceleration (SA) values from sensors (solid black lines) with those from the 3D SRA model (green and blue lines) across periods from 0 to 4 seconds at different levels of surface, -30m and -57m.

Figure 6.4: *Comparison of 3D SRAs with Sensor in Zeytinburnu.*

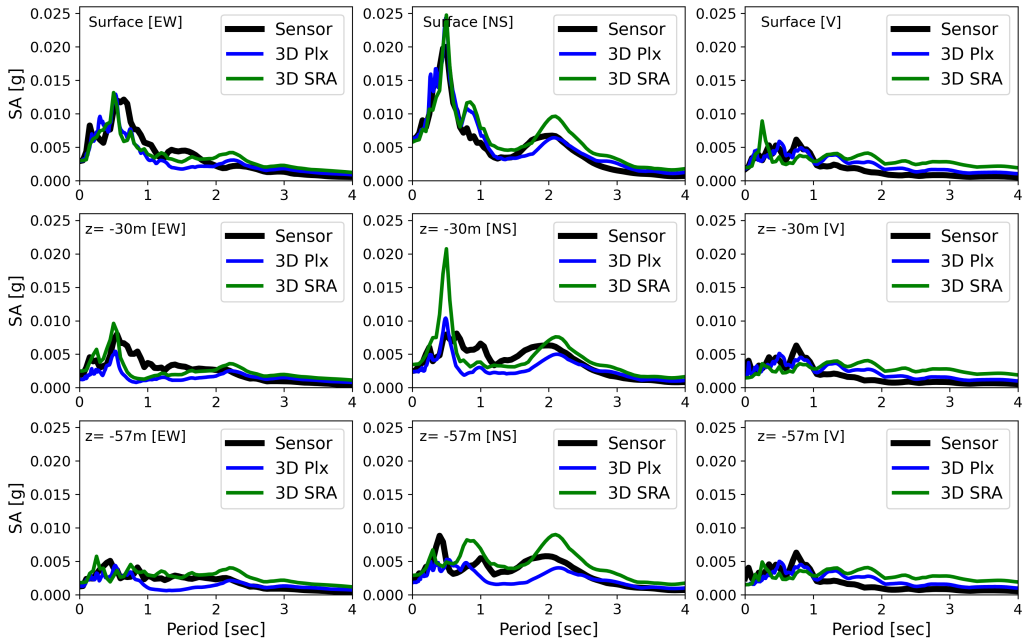

6.2 Alaska Soil profile

In this section, the results of the 1D and 3D site response analyses (SRA) for the Alaska soil profile under six different high-magnitude earthquakes are analyzed. The following subsections present and discuss the findings in detail.

6.2.1 1D and 3D site response analysis

Figure 6.6 illustrates the spectral acceleration (SA) comparisons for the earthquake with ID tag of A.1 between three datasets: 3D site response analysis (3D SRA) results (green lines) modeled using the OpenSeesPy framework, 1D site response analysis (1D SRA) results (red dashed lines) obtained using the Deepsoil program, and recorded sensor data (black lines). The comparisons span three orthogonal directions: East-West (EW), North-South (NS), and Vertical (V), and are presented for three depths: the surface, -4.6 m, and -11.6 m.

Figure 6.5: *Comparison of 3D SRAs and 1D SRA with Sensor for Zeytinburnu.*

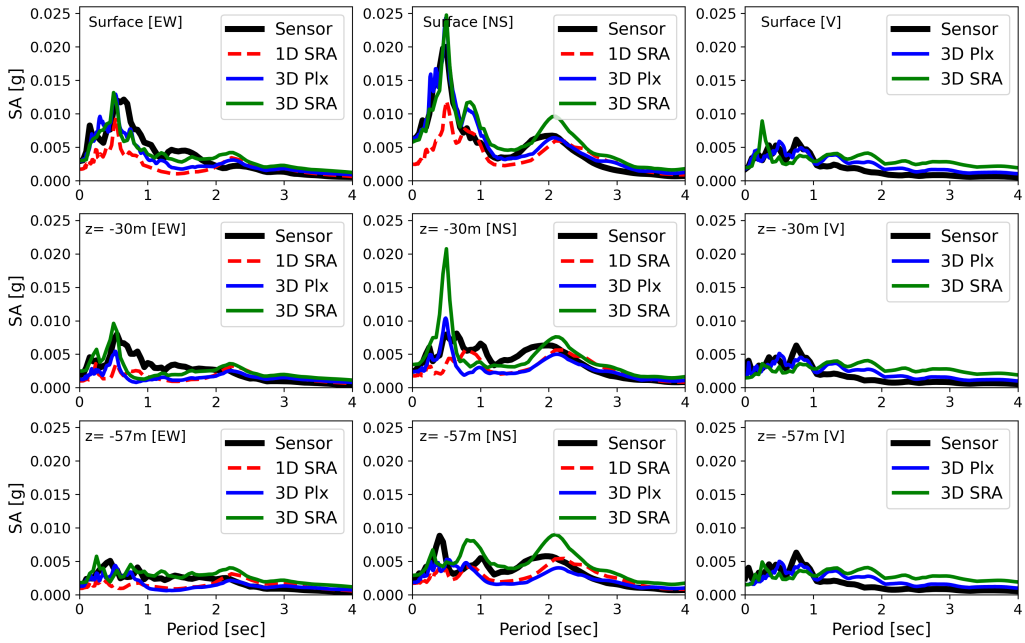

The SA values are plotted against periods ranging from 0 to 2.5 seconds to evaluate the accuracy of the simulations at capturing the dynamic response of the soil layers. The results demonstrate that 3D SRA predictions show a closer alignment with the sensor measurements compared to 1D SRA, particularly for periods above 1 second in the horizontal directions (EW and NS). However, in the vertical component (V), both 3D SRA and 1D SRA exhibit some discrepancies relative to the sensor data, reflecting the challenges in accurately modeling vertical motion. These observations underscore the advantages of 3D SRA in providing a more realistic representation of site dynamics for the Alaska soil profile, particularly for complex ground motions.

Figure 6.7 shows the corresponding Acceleration time histories of the graphs mentioned. In this section, the results of the 1D and 3D site response analyses (SRA) for the Alaska soil profile under seven different high-magnitude earthquakes are analyzed. The following subsections present and discuss the findings in detail.

Figure 6.8 presents the spectral acceleration (SA) comparisons for the for the

Figure 6.6: *3D SRA with respect to 1D SRA- A.1 (SA).*

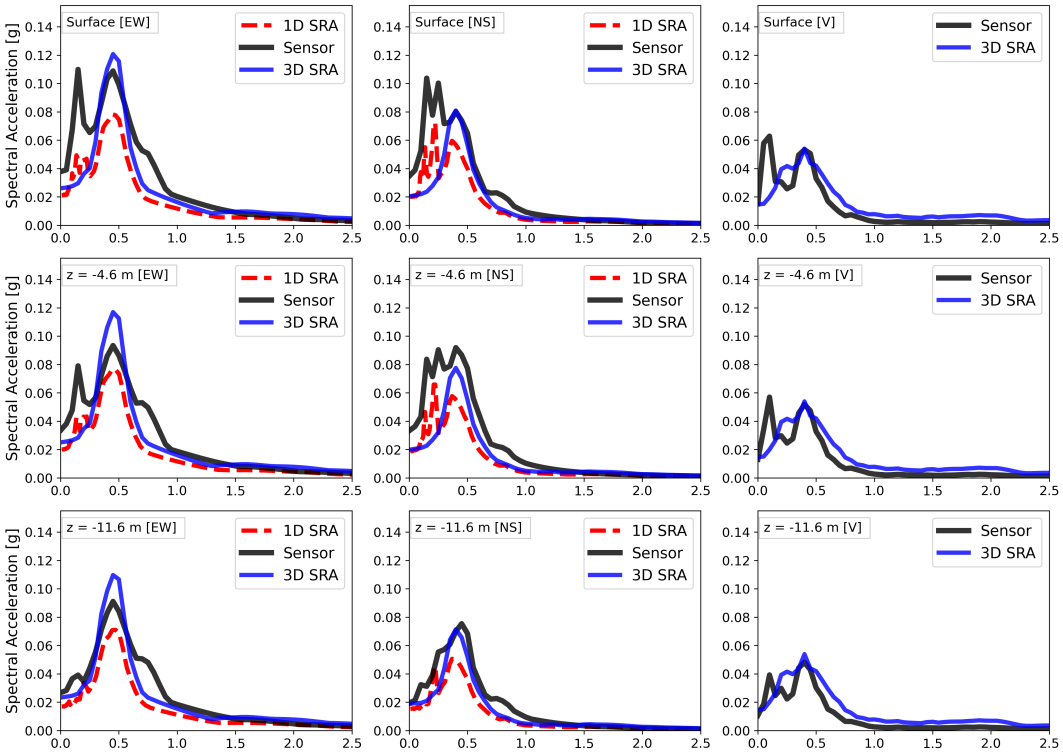

earthquake with ID tag of A.2, showcasing results from 3D site response analysis (3D SRA) performed using the OpenSeesPy code (green lines), 1D site response analysis (1D SRA) using the Deepsoil program (red dashed lines), and recorded sensor data (black lines). The analysis spans three orthogonal directions (East-West (EW), North-South (NS), and Vertical (V)) at the surface, -4.6 m, and -11.6 m depths, with SA values plotted against periods ranging from 0 to 2.5 seconds. At the surface level in the EW direction, the sensor data shows a peak SA of approximately 0.025 g around 0.6 seconds, closely matched by the 3D SRA with a peak of about 0.016 g, while the 1D SRA underestimates the response at around 0.018 g.

These comparisons demonstrate that the 3D SRA consistently provides better alignment with the sensor data across all depths and directions, particularly for horizontal

Figure 6.7: *3D SRA with respect to 1D SRA- A.1 (TH).*

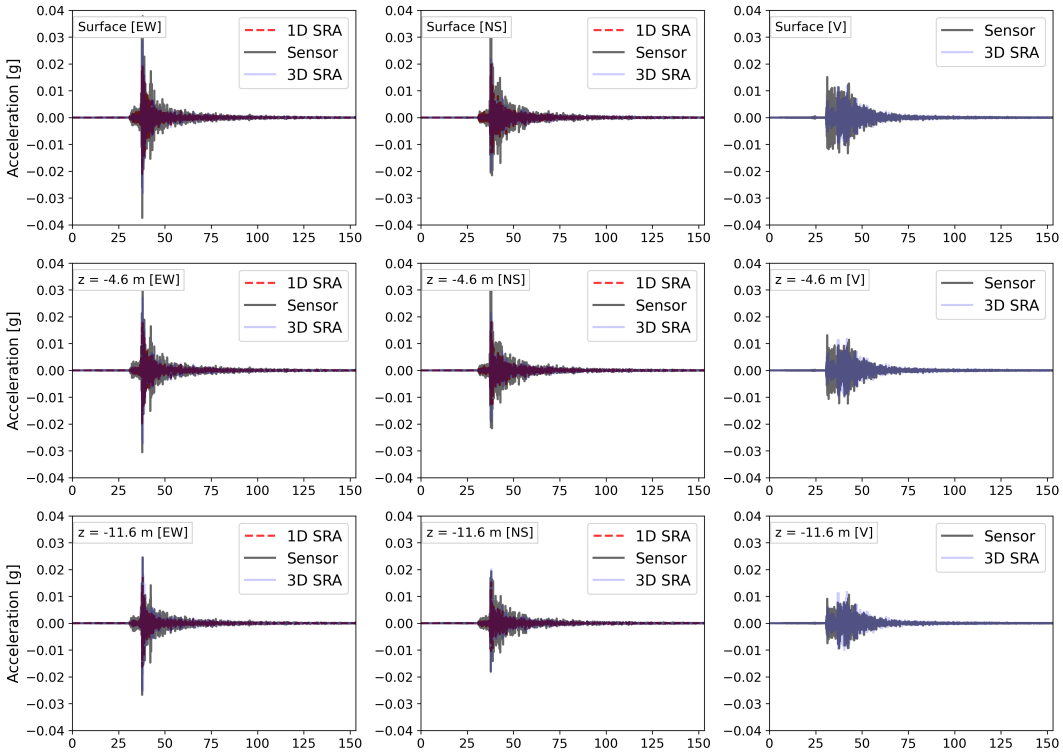

components and longer periods exceeding 1 second. The 1D SRA, in contrast, underestimates the SA values across most cases, with larger deviations observed for deeper layers and vertical components. This highlights the superiority of 3D SRA in capturing the complex dynamic behavior of the A.2 soil profile, especially for horizontal motion and extended periods, providing greater predictive accuracy for site response analysis. Figure 6.9 shows the corresponding Acceleration time histories of the graphs mentioned.

Figure 6.10 presents the spectral acceleration (SA) comparison for the A.3 earthquake, analyzing results from 3D site response analysis (3D SRA) using the OpenSeesPy code (green lines), 1D site response analysis (1D SRA) conducted with the Deepsoil program (red dashed lines), and recorded sensor data (black lines). The analysis spans three depths—surface, -4.6 m, and -11.6 m—and covers periods ranging from 0 to 4 seconds in three orthogonal directions: East-West (EW), North-South (NS), and Vertical (V). In the

Figure 6.8: *3D SRA with respect to 1D SRA- A.2 (SA).*

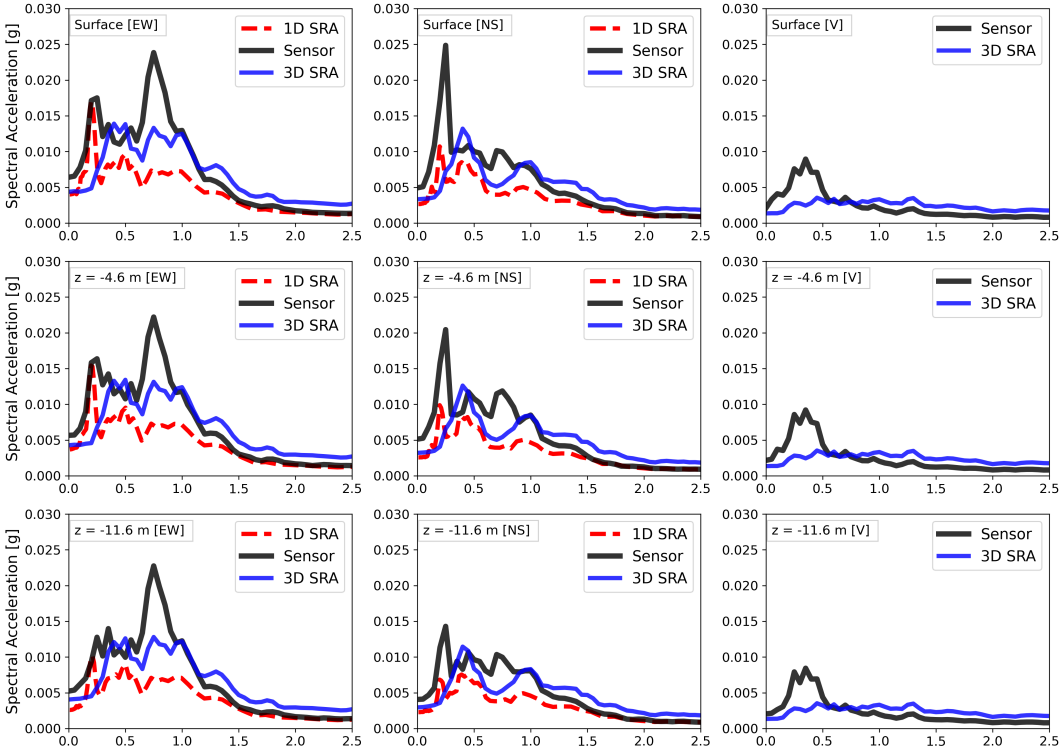

EW direction, the 3D SRA predictions show good alignment with the sensor data across all depths, capturing both the peak values and trends effectively.

However, in the NS direction, the 3D SRA slightly overestimates the SA values, particularly for shorter periods around 0.5 seconds, while the 1D SRA underestimates the response for the same range. These differences become more pronounced at deeper layers (-4.6 m and -11.6 m), where the 3D SRA remains closer to the sensor data but exhibits a tendency for overestimation. In contrast, the 1D SRA predictions fall consistently below than 3D SRA results, reflecting its higher limitations to capture the site response accurately in this direction. Figure 6.11 shows the corresponding Acceleration time histories of the graphs mentioned.

The Figure 6.12 displays the comparison results of the A.4 tag earthquake for a 3D site response analysis (3D SRA) with OpenseesPy code and 1D site response analysis (1D

Figure 6.9: *3D SRA with respect to 1D SRA- A.2 (TH).*

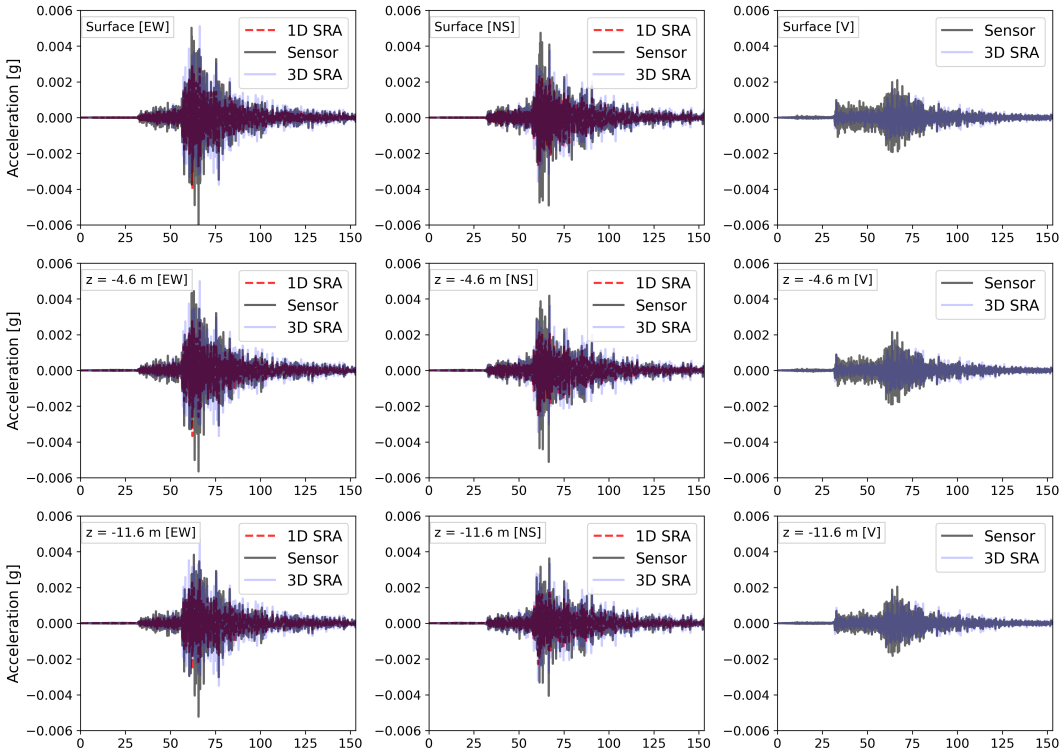

SRA) using Deepsoil program for the Alaska soil profile, comparing spectral acceleration (SA) values from sensors (black lines) , 1D SRA (dashed red lines) with those from the 3D SRA models (green lines) across periods from 0 to 4 seconds at different levels of surface, -4.6m and -11.6m.

Fo the East-West (EW) Direction, at all depths, the 3D SRA shows good alignment with the sensor data, particularly for periods between 0.5 and 1.5 seconds. The peak SA values of the 3D SRA closely match the recorded data, reflecting its accuracy in this direction. The 1D SRA underestimates the SA consistently across the surface and deeper layers, particularly at shorter periods (¡1.5 seconds).

For North-South (NS) Direction, the 3D SRA overestimates the SA values slightly across all depths, with the overestimation being most pronounced at shorter periods around 0.4–0.5 seconds and the 1D SRA significantly underestimates the SA compared to both

Figure 6.10: *3D SRA with respect to 1D SRA- A.3 (SA).*

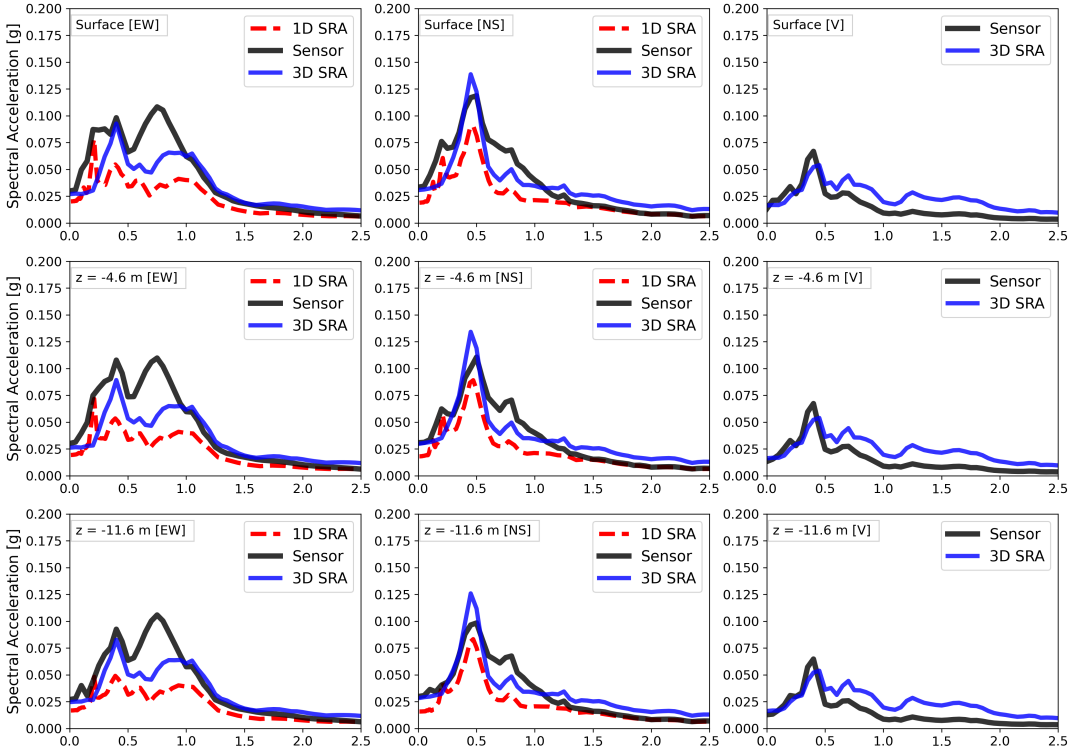

the sensor data and the 3D SRA, especially at the surface and -4.6 m depths. For Vertical (V) Direction, the 3D SRA aligns reasonably well with the sensor data, though some deviations are observed at shorter periods (¡0.5 seconds). Figure 6.13 shows the corresponding Acceleration time histories of the graphs mentioned.

The Figure 6.14 displays the comparison results of the A.5 tag earthquake for a 3D site response analysis (3D SRA) with OpenseesPy code and 1D site response analysis (1D SRA) using Deepsoil program for the Alaska soil profile, comparing spectral acceleration (SA) values from sensors (black lines) , 1D SRA (dashed red lines) with those from the 3D SRA models (green lines) across periods from 0 to 4 seconds at different levels of surface, -4.6m and -11.6m.

The A.6 earthquake, being the highest-magnitude event analyzed, exhibits larger

Figure 6.11: *3D SRA with respect to 1D SRA- A.3 (TH).*

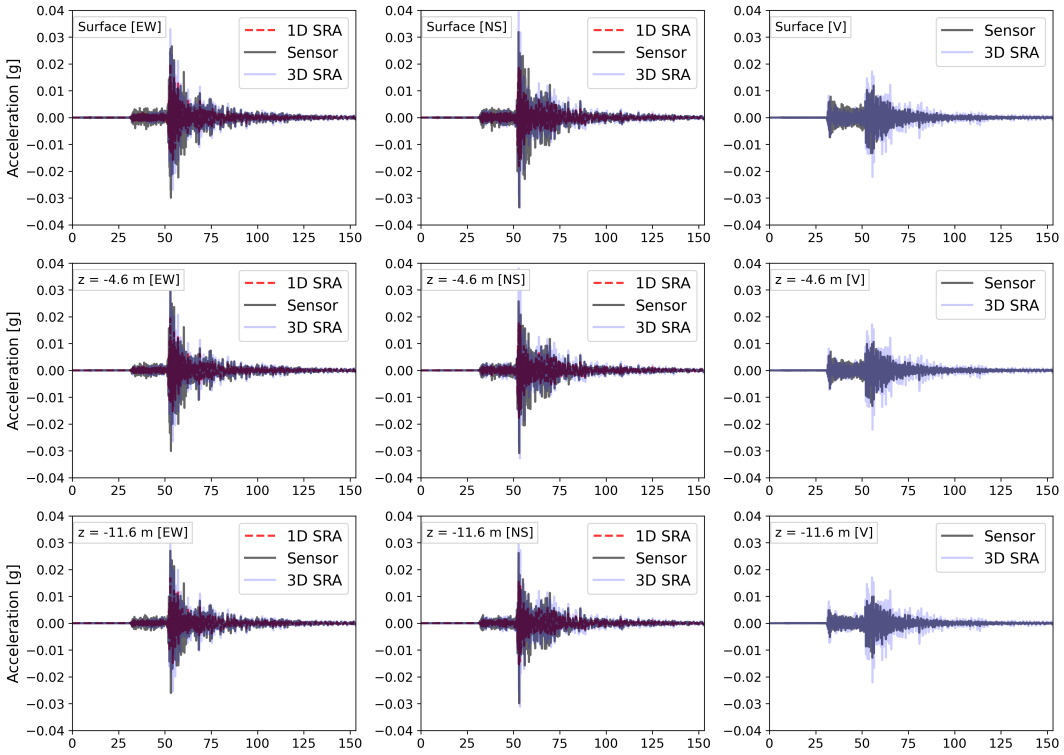

spectral accelerations compared to other earthquakes in this study. The 3D SRA captures the site response accurately in the EW direction and reasonably in the NS and V directions, though slight overestimations are observed in the latter two. The 1D SRA consistently underestimates the SA across all components and depths, highlighting its limitations in accurately modeling high-magnitude events.

These results emphasize the importance of 3D SRA in capturing the complexities of site response during high-magnitude earthquakes, particularly in horizontal components and at deeper layers. The robust performance of the 3D SRA further validates its use for dynamic site response analyses involving significant seismic events. Figure 6.15 shows the corresponding Acceleration time histories of the graphs mentioned.

Figure 6.16 displays the comparison results of the A.6 tag earthquake for a 3D site response analysis (3D SRA) with OpenSeesPy code and 1D site response analysis (1D

Figure 6.12: *3D SRA with respect to 1D SRA- A.4 (SA).*

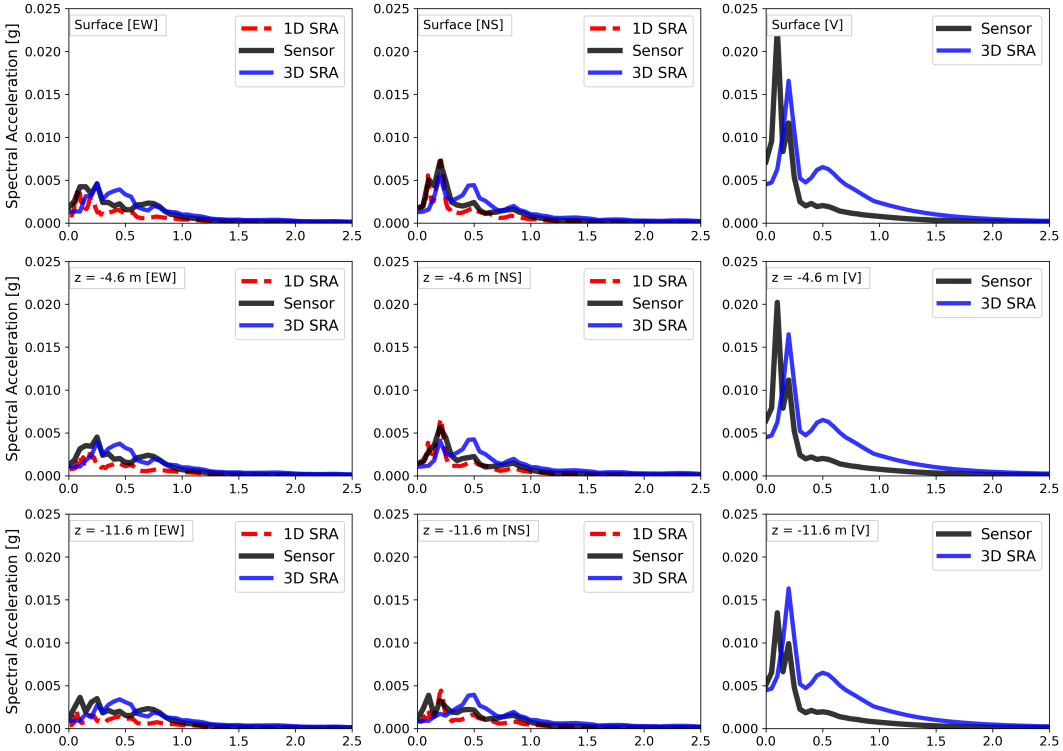

SRA) using Deepsoil program for the Alaska soil profile, comparing spectral acceleration (SA) values from sensors (black lines) , 1D SRA (dashed red lines) with those from the 3D SRA models (green lines) across periods from 0 to 4 seconds at different levels of surface, -4.6m and -11.6m.

While the 3D SRA does not perfectly capture the surface behavior for this event, its predictions are notably closer to the sensor data compared to the 1D SRA. Predicting soil behavior, particularly at the surface, is inherently challenging due to the complexity of soil interactions and nonlinear dynamic effects. However, the near alignment achieved by the 3D SRA, especially at deeper layers, demonstrates its capability to provide reliable predictions. Considering the limitations of soil behavior modeling and the complexity of site-specific dynamics, the 3D SRA's performance is satisfactory and represents a significant improvement over 1D SRA predictions. Figure 6.17 shows the corresponding

Figure 6.13: *3D SRA with respect to 1D SRA- A.4 (TH).*

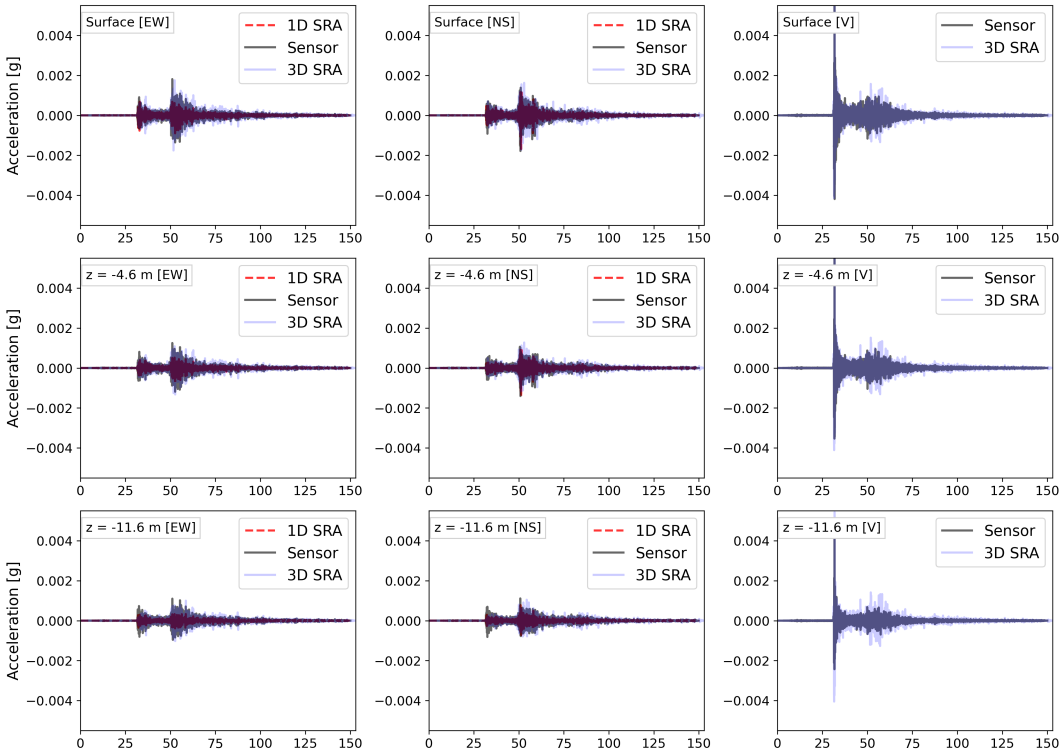

Acceleration time histories of the graphs mentioned.

The Figure 6.18 displays the comparison results of the A.7 tag earthquake for a 3D site response analysis (3D SRA) with OpenSeesPy code and 1D site response analysis (1D SRA) using Deepsoil program for the Alaska soil profile, comparing spectral acceleration (SA) values from sensors (black lines) , 1D SRA (dashed red lines) with those from the 3D SRA models (green lines) across periods from 0 to 4 seconds at different levels of surface, -4.6m and -11.6m. Figure 6.19 shows the corresponding Acceleration time histories of the graphs mentioned.

Building upon the previous analysis of the Alaska soil profile subjected to seven distinct earthquakes and compare results with respect to sensor, this study extends the modeling of 3D SRA to include the Düzce earthquake, a significant seismic event happened in 1999.

Figure 6.14: *3D SRA with respect to 1D SRA- A.5 (SA).*

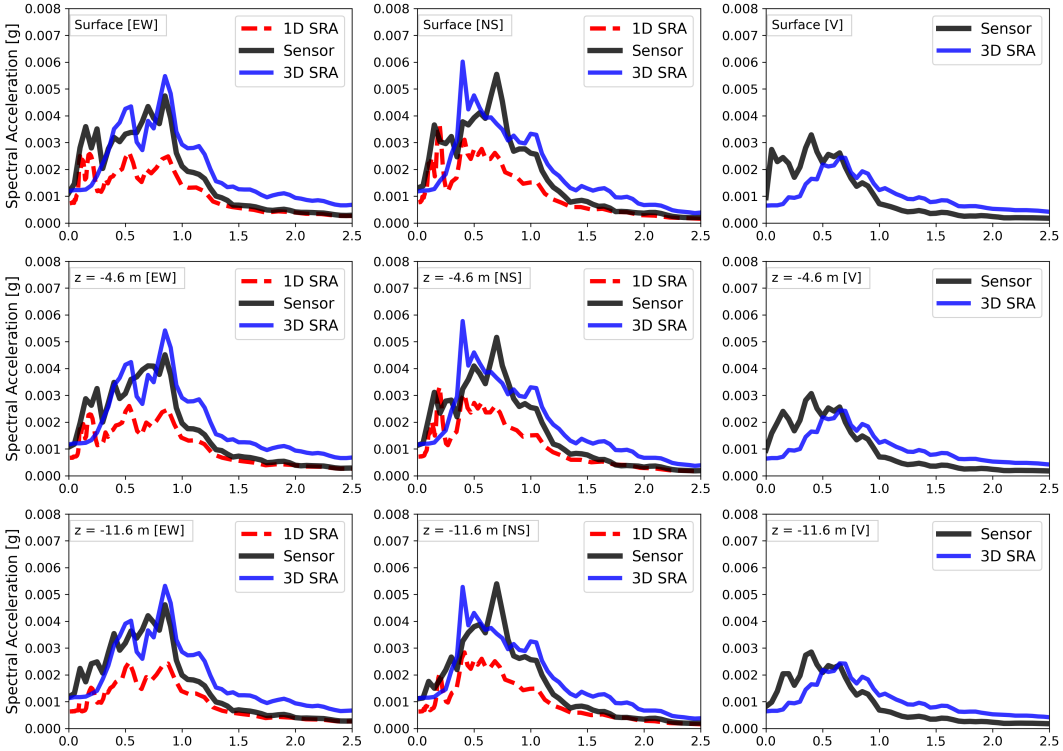

The analysis compares the ground surface responses of two soil profiles, Alaska and Zeytinburnu, using both 1D and 3D site response models. Results in Figure.6.20 and Figure.6.21 reveal notable differences between the two models. These findings underscore the importance of 3D site response modeling for accurate seismic hazard assessment in urban environments.

6.3 Results of Optimization study

To evaluate the effectiveness and reliability of the proposed framework for optimization of soil profile, 3D site response analyses were conducted using data from an additional seismic event: the January 8, 2013, Ege Denizli (Aegean Sea) earthquake. The sensor layout employed for this event was identical to the configuration described earlier for Zeytinburnu.

Figure 6.15: *3D SRA with respect to 1D SRA- A.5 (TH).*

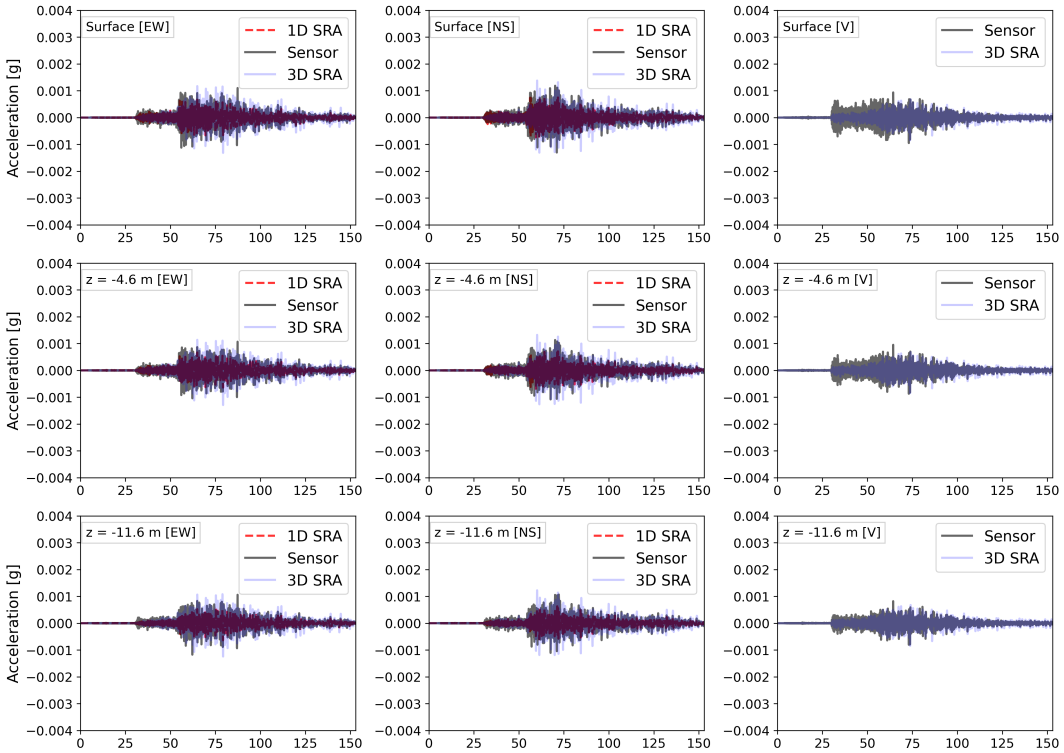

These results provided an additional validation signal to assess the framework's ability to refine soil models and improve site response predictions. Comparisons between the not optimized and optimized models reveal that the optimized profile aligns more closely with the recorded ground motions, particularly for the horizontal components (EW and NS). This improvement demonstrates the framework's ability to refine key soil properties such as shear wave velocity, leading to enhanced predictive accuracy. The error between the measured and not optimized results, as defined by Equation 5.7, was reduced from 0.178g to 0.150g when using the optimized parameters. This reduction underscores the framework's capacity to generalize parameter adjustments effectively, even when optimized for a different seismic event, confirming its broader applicability.

Figure 6.22 illustrates the deterministic evaluation for a comparison of the results of a 3D SRA for original soil profile against the optimized one in Zeytinburnu soil profile

Figure 6.16: *3D SRA with respect to 1D SRA- A.6 (SA).*

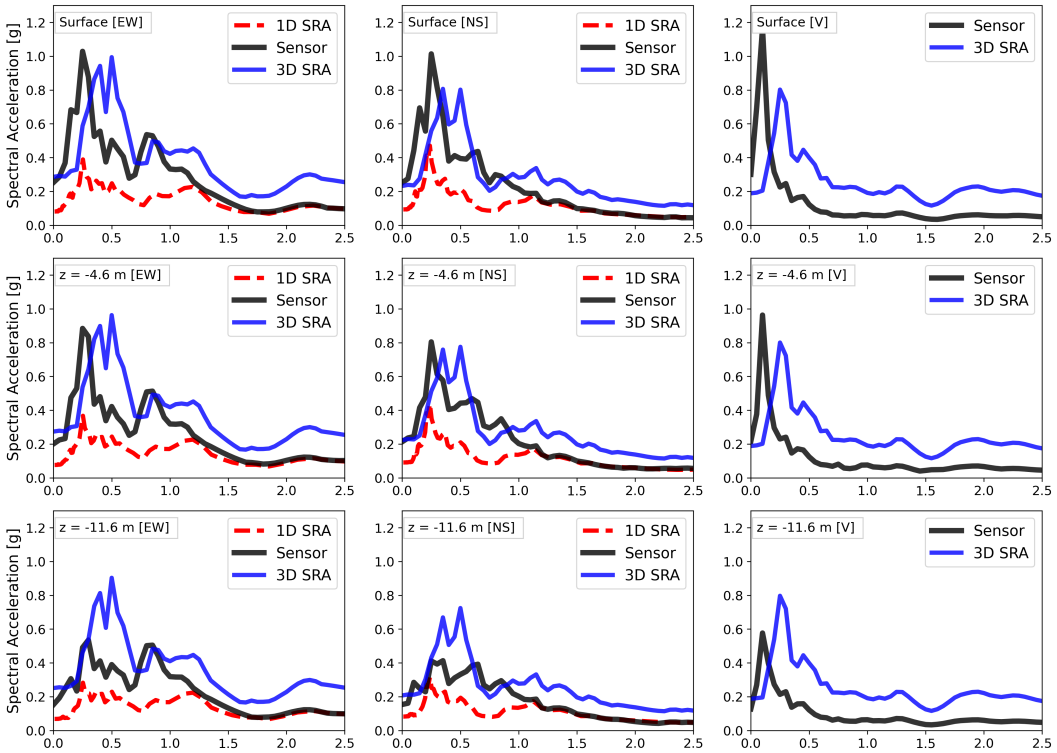

using Kütahya earthquake, illustrating the framework's potential to adjust key parameters effectively.

Figure 6.23 illustrates the deterministic evaluation, comparing the results of a 3D site response analysis (SRA) for the original soil profile against the optimized one in the Zeytinburnu soil profile, using the 2013 Ege Denizli earthquake as input. This comparison highlights the framework's ability to effectively adjust key soil parameters, such as shear wave velocity, even when applied to a seismic event different from the one used for optimization. The results demonstrate the robustness of the framework in refining soil models to enhance predictive accuracy across multiple earthquake scenarios.

Even though the predictions from the provided code for 3D site response analysis (SRA) exhibit good alignment with sensor measurements, the use of the optimized soil

Figure 6.17: *3D SRA with respect to 1D SRA- A.6 (TH).*

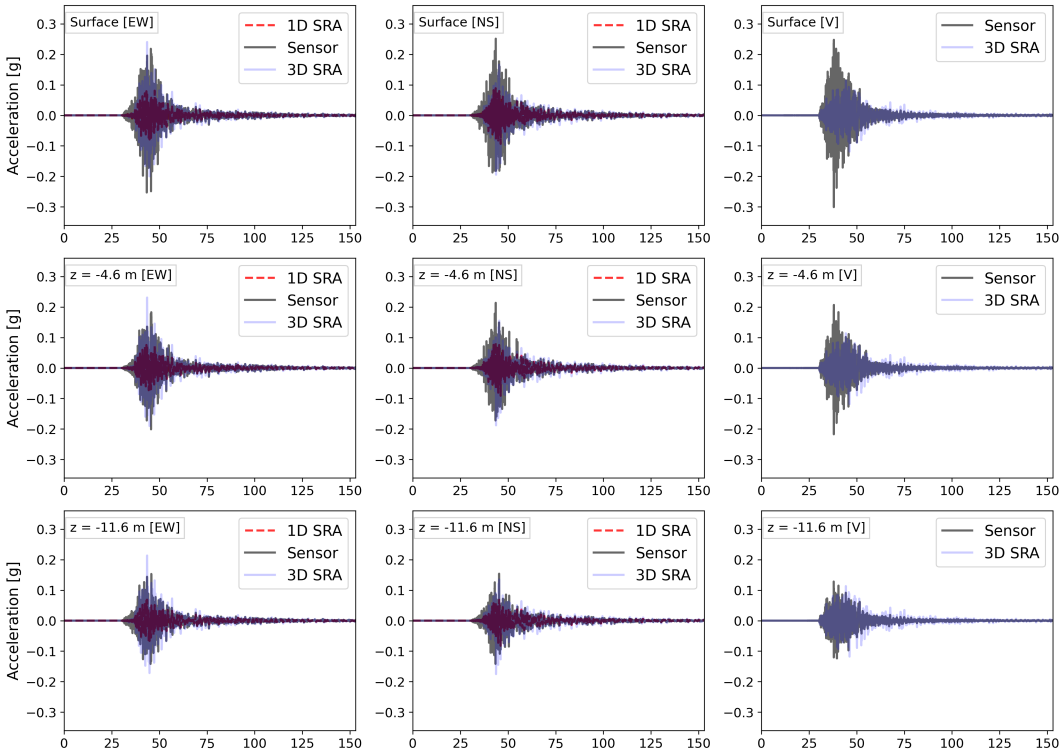

profile significantly enhances the accuracy of the results, particularly for periods exceeding 1.5 seconds. This improvement demonstrates the framework's capability to refine soil parameters effectively, leading to a better representation of 3D site-specific dynamic behavior at longer periods.

Figure 6.18: *3D SRA with respect to 1D SRA- A.7 (SA).*

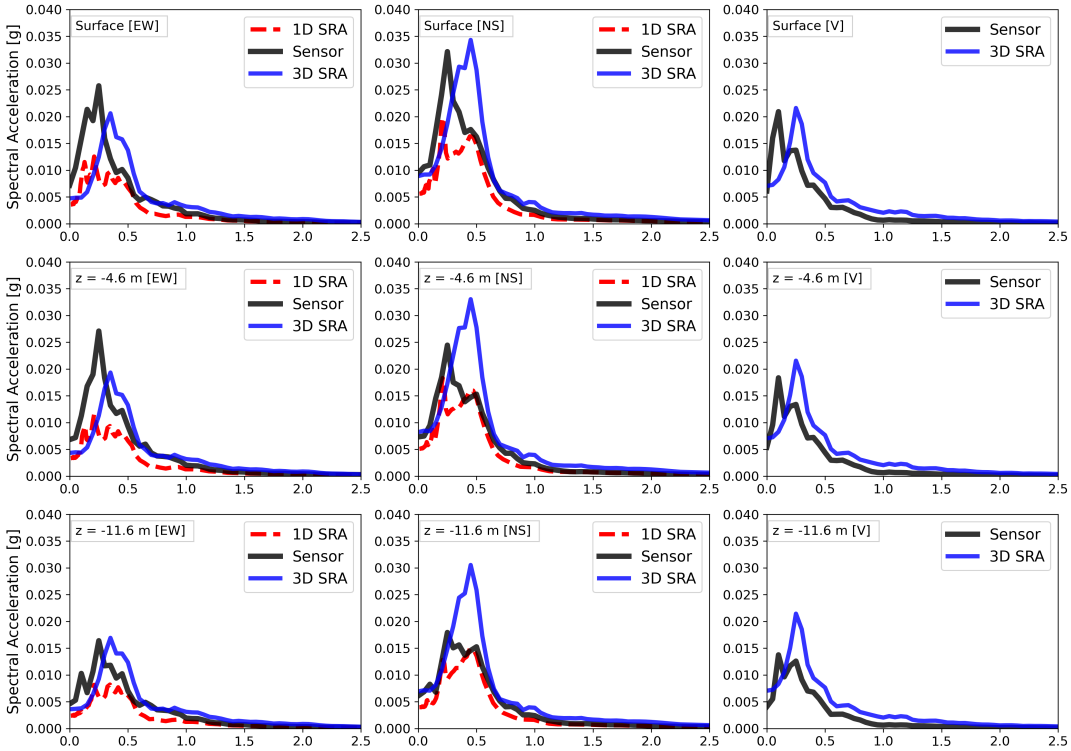

Figure 6.19: *3D SRA with respect to 1D SRA- A.7 (TH).*

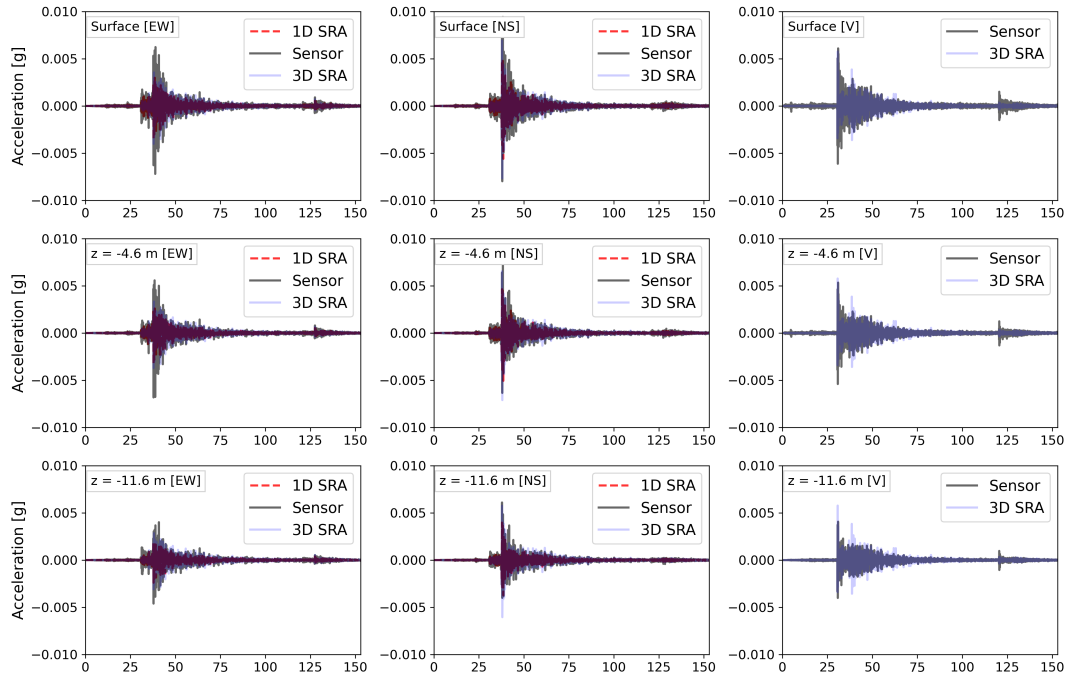

Figure 6.20: *Düzce earthquake with 1D and 3D models in Alaska profile.*

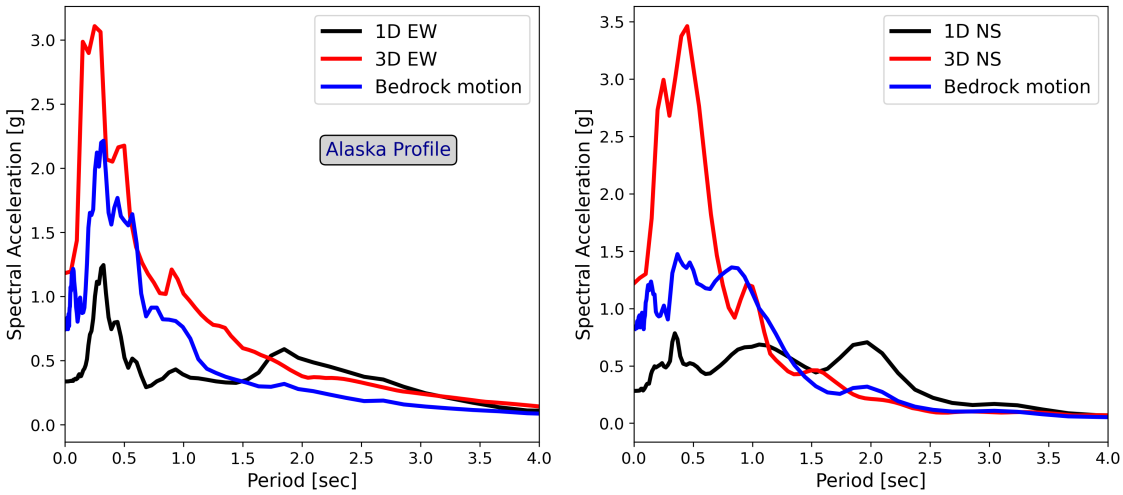

Figure 6.21: *Düzce earthquake with 1D and 3D models in Zeytinburnu profile.*

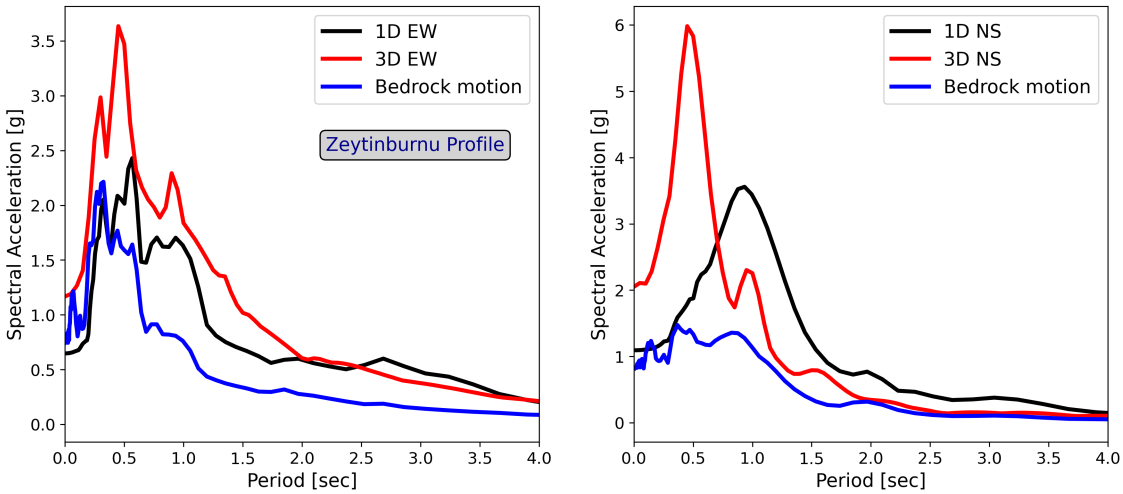

Figure 6.22: *Using optimized soil profile (Zeytinburnu) for Kütahya earthquake in 3D SRA.*

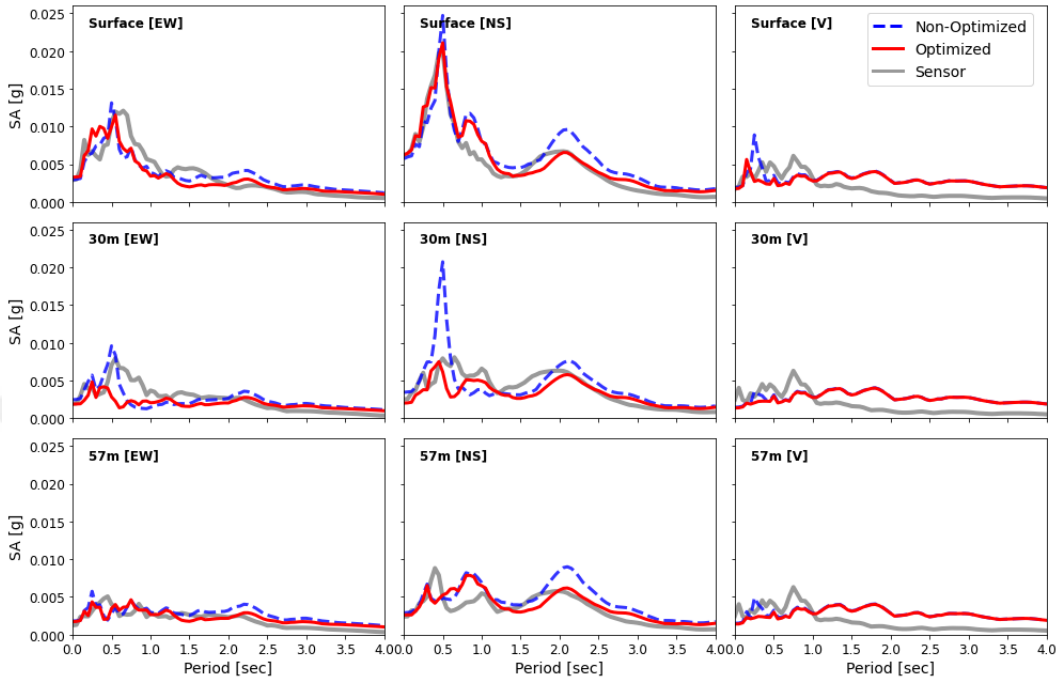

Figure 6.23: *Using optimized soil profile (Zeytinburnu) for 2013 earthquake in 3D SRA.*

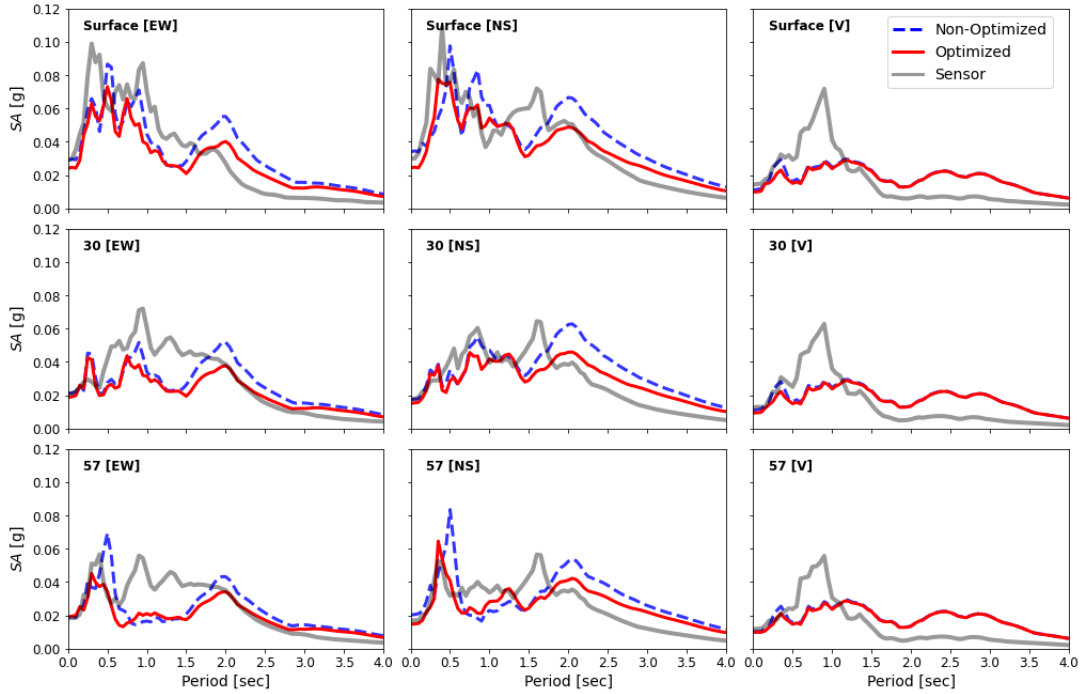

7. CONCLUSIONS

This thesis investigated the effectiveness of proposed three-dimensional site response analyses in modeling seismic ground motions, using detailed soil profiles from Zeytinburnu in Istanbul, Türkiye, and Anchorage in Alaska, United States. By employing real earthquake records in three directions and incorporating uncertainties in soil properties through optimization methods, the study aimed to address existing gaps in geotechnical earthquake engineering research.

7.1 Summary of Work

- **Comparative Site Response Analyses (1D vs.3D):** A series of site response analyses was conducted on both the Zeytinburnu and Alaska soil profiles. One dimensional simulations were performed using DEEPSOIL, while three dimensional analyses were executed using PLAXIS3D and further modeled via OpenSeesPy scripting. The Zeytinburnu profile was examined under the recorded Kütahya earthquake scenario, whereas the Alaska profile was tested against seven distinct earthquakes of varying intensities. This comparative approach provided a comprehensive evaluation of the relative performance and accuracy of 1D and 3D site response methodologies in different boreholes. All analyses incorporated three-component of motion records (East–West, North–South, and Vertical), directly obtained from in situ accelerometers. By simulating full triaxial motion, these assessments closely replicated actual seismic events, thus enhancing the realism, reliability, and applicability of the resulting insights.

- **Proposed Framework under Strong Earthquake Loading:** To further assess the robustness of the proposed 3D framework, the Düzce earthquake—a strong ground motion event—was simulated. This additional evaluation allowed for an in-depth

comparison of modeled surface behaviors between two approaches.

- **Soil Profile Optimization Using Genetic Algorithms:** To address uncertainties in soil properties—particularly shear wave velocity—genetic algorithms were employed for profile optimization. This refinement process was validated against the 2013 Ege Denizli earthquake, confirming that optimized soil profiles significantly improved the predictive capabilities of the site response models.

7.2 Key Findings

1. In the initial phase, the newly developed three-dimensional (3D) site response analysis code, implemented using OpenSeesPy, was rigorously validated against both the outputs of the commercial software Plaxis3D and recorded sensor data. This comparative evaluation confirmed the code's reliability, consistency, and methodological accuracy, thereby establishing its suitability for 3D site response analysis in the subsequent stages of this study.

2. Superiority of 3D SRA modelings over 1D SRA in Both Zeytinburnu and Alaska soil profiles:

• Zeytinburnu Profile: For the Zeytinburnu soil profile, three-dimensional simulations performed using PLAXIS3D and OpenSeesPy displayed strong agreement with recorded sensor data, whereas one-dimensional analyses conducted with DEEPSOIL consistently underestimated the observed responses.

• Alaska Profile with different Earthquakes: For the Alaska soil profile, across multiple seismic events (A.1, A.3, A.4, A.5, A.6, and A.7), the three-dimensional (3D) site response analysis more accurately replicated the observed ground surface behavior. The 3D simulations exhibited strong agreement with recorded data in both the East–West and North–South directions, demonstrating the robustness and reliability of the 3D approach. In contrast, the one-dimensional (1D) site response analysis substantially underestimated

the surface response, highlighting the inherent limitations of 1D methods in capturing the complex dynamic soil behavior under these seismic conditions.

For the case of A.2, both the 3D and 1D site response analyses exhibit underestimations of the ground surface response when compared to the recorded data. However, the 3D modeled site response analysis demonstrates results that are notably closer to the recorded observations, highlighting its superior in capturing the site response.

• Out of a total of 14 results on the ground surface for the East-West and North-South directions across seven earthquakes, 10 results from the 3D site response modelings exhibited better agreement with the recorded data compared to the 1D approach. This corresponds to approximately 71% of the cases, highlighting the effectiveness of the 3D approach in capturing the observed seismic responses.

• Among the total of 14 results at the -4.6 m level for the East-West and North-South directions across seven earthquakes, 9 out of 14 results from the 3D site response analysis showed better agreement with the recorded data compared to the 1D approach. This corresponds to approximately 64.29%, indicating that the 3D approach provides a more reliable prediction in -4.6m level.

• Among the total of 14 results at the -11.6 m level for the East-West and North-South directions across seven earthquakes, 8 out of 14 results from the 3D site response analysis showed better agreement with the recorded data compared to the 1D approach. This corresponds to approximately 57.14%, highlighting the relative advantage of the 3D approach at this depth.

• Applying strong earthquake to the proposed 3D framework: The analysis from trying proposed 3D framework and 1D analysis for Düzce earthquake revealed notable differences between the two approaches, underscoring the importance of considering results of 3D site response analysis.

3. Effectiveness of Soil Profile Optimization:

• The optimization of soil parameters led to improvements in the modeling accuracy of the 3D SRA. For instance, in the Zeytinburnu profile, the error between measured and predicted results was reduced from 0.178g to 0.150g after optimization, demonstrating the framework's capability to enhance model reliability. This optimized soil profile was validated with another earthquake named Ege Denizli earthquake and showed better alignment at ground surface with accelerometers with respect to not optimized soil.

In conclusion, this study has successfully modeled and validated a comprehensive three-dimensional site response analysis (3D SRA) framework using OpenSeesPy, demonstrating both its robustness and accuracy across a range of complex seismic conditions. By applying this model to both Zeytinburnu and Alaska soil profiles, the 3D SRA approach proved markedly superior to conventional one-dimensional (1D) site response analyses, consistently yielding spectral accelerations and response characteristics in closer agreement with recorded sensor data. This enhanced modeling was especially evident under high-magnitude seismic events, where the 3D framework captured the soil response more effectively than its 1D counterpart. Furthermore, the optimization of soil parameters, facilitated by advanced computational methods such as genetic algorithms, enhanced the predictive accuracy of the 3D model. This improvement was exemplified by the reduction in error for the Zeytinburnu profile and validated through stronger alignment of simulation results with recorded ground surface accelerations during the Ege Denizli earthquake.

It is important to acknowledge that the real comparison between 1D and 3D is not the methodologies but the observed results and moreover, the observed discrepancies between the three-dimensional (3D) and one-dimensional (1D) site response analyses are not solely attributable to the inclusion of multi-directional seismic components in the 3D modeling. While considerable effort was made to ensure methodological consistency across the different computational frameworks, it must be acknowledged that the methods

employed in the three-dimensional (3D) and one-dimensional (1D) site response analyses were not entirely identical. In this study, we meticulously calibrated input parameters, soil properties, and boundary conditions to align as closely as possible between the various software platforms (e.g., PLAXIS3D, OpenSeesPy, and DEEPSOIL). However, inherent differences in the numerical approaches and assumptions—such as the treatment of nonlinear versus equivalent linear soil behavior, meshing strategies, and damping formulations—could not be fully eliminated. Additionally, variations in how computational platforms implement boundary conditions and handle strain-dependent behavior may have further contributed to the observed discrepancies between 3D and 1D results. These differences, although minimized to the extent possible, underscore the challenge of achieving perfect methodological parity across distinct analytical tools. Consequently, while the findings of this study robustly demonstrate the superiority of the 3D approach in replicating recorded seismic responses, these underlying methodological nuances must also be considered when interpreting the comparative results.

Collectively, these findings underscore the applicability, reliability, and adaptability of the proposed 3D SRA approach for a wide range of seismic conditions, ultimately advancing our capacity to accurately assess and mitigate seismic hazards. In turn, these advancements not only inform seismic hazard assessments and the engineering design of earthquake-resistant structures but also encourage the broader adoption of more sophisticated computational techniques in geotechnic earthquake engineering—thereby contributing to the development of safer, more resilient infrastructure in seismically active regions such as Istanbul and Alaska.

REFERENCES

[1] Kramer, S.L. (1996) *Geotechnical Earthquake Engineering.* Prentice-Hall Civil Engineering and Engineering Mechanics Series, Prentice Hall, Upper Saddle River, 653. *References - Scientific Research Publishing.* [Online].

[2] Idriss, I. M. and Seed, H. B. (1967) Response of horizontal soil layers during earthquakes.

[3] Tönük, G., Ansal, A., Kurtuluş, A., and Çetiner, B. (2013) Site Specific Response Analysis for Performance Based Design Earthquake Characteristics, *Bulletin of Earthquake Engineering*, vol. 12, no. 3, pp. 1091–1105. doi: 10.1007/s10518-013-9528-5.

[4] Hashash, Y. M. and Groholski, D. R. (2010) Recent advances in non-linear site response analysis, Fifth International Conference on Recent Advances in Geotechnical Earthquake Engineering and Soil Dynamics and Symposium in Honor of Professor I.M. Idriss, vol. 29, no. 6, pp. 1–22.

[5] Tönük, G. and Ansal, A. (2022) Factors Affecting Site-Specific Response Analysis, *Journal of Earthquake Engineering*, vol. 26, no. 16, pp. 8629–8646.

[6] Ansal, A. and Tönük, G. (2018) Selection of Earthquake Input for Site Response Analysis, in *4th Joint Symposium: Seismic Actions for Designing Geotechnical Works: ISO-23469*, ITU-JSCE-TCCE-JSCE/TR Section, pp. 12–15.

[7] Bommer, J. J. and Acevedo, A. B. (2004) The use of real earthquake accelerograms as input to dynamic analysis, *Journal of Earthquake Engineering*, vol. 8, no. spec01, pp. 43–91.

[8] Tönük, G. and Ansal, A. (2010) Selection and scaling of ground motion records for site response analysis, in *14th European Conference of Earthquake Engineering*, Ohrid.

[9] Chopra, A. K. (2007) *Dynamics of Structures*, Prentice-Hall International Series in Civil Engineering and Engineering Mechanics, Pearson Education.

[10] Ansal, A., Tönük, G., and Kurtuluş, A. (2018) Implications of Site Specific Response Analysis, in *Recent Advances in Earthquake Engineering*, K. Pitilakis, Ed., ch. 2.

[11] Ansal, A. and Tönük, G. (2022) Site Characterization for Site Response Analysis in Performance Based Approach, in *Performance Based Design in Earthquake Geotechnical Engineering (Beijing 2022)*, W. Lanmin, Z. Jian-Min, and R. Wang, Eds., ch. 1.

[12] Tönük, G. and Ansal, A. (2023) Probabilistic seismic microzonation for ground shaking intensity: A case study in Turkey, *Journal of Seismology*, vol. 27, pp. 863–874. doi: 10.1007/s10950-023-10170-8.

[13] Schnabel, P. B. (1972) SHAKE: A computer program for earthquake response analysis of horizontally layered sites, EERC Report 72-12, University of California, Berkeley.

[14] Smerzini, C., Paolucci, R., and Stupazzini, M. (2011) Comparison of 3D, 2D, and 1D numerical approaches to predict long period earthquake ground motion in the Gubbio plain, Central Italy, *Bulletin of Earthquake Engineering*, vol. 9, pp. 2007–2029.

[15] Idriss, I. M. and Seed, H. B. (1968) Seismic response of horizontal soil layers, *Journal of the Soil Mechanics and Foundations Division*, vol. 94, no. 4, pp. 1003–1031.

[16] Sadeghzadeh, S., Ansal, A., and Kurtuluş, A. (2022) The Effects of Fault Type for the Selection of Input Acceleration Records for Site Response Analysis.

[17] Malcioglu, F. S., O'Kane, A., Donmez, K., and Aktas, Y. D. (2022) Characteristics of Strong Ground Motions in the 30 October 2020, MW6.9 Aegean Sea Earthquake, *Front Built Environment*, vol. 8, pp. 1–26. doi: 10.3389/fbuil.2022.870279.

[18] Sari, B., Vocational, A., and Services, H. (2024) Disaster Management Following Earthquakes in 2023, Türkiye the Great Kahramanmaraş.

[19] Rathje, E. M., Kottke, A. R., and Trent, W. L. (2010) Influence of input motion and site property variabilities on seismic site response analysis, *Journal of Geotechnical and Geoenvironmental Engineering*.

[20] Kawano, M., Asano, K., Dohi, H., and Matsuda, S. (1995) Verification of predicted

non-linear site response during the 1995 Hyogo-Ken Nanbu earthquake.

[21] Jennings, P. C. and Bielak, J. (1973) Dynamics of building-soil interaction, modeled by a linear elastic half-space and an n-degree-of-freedom building structure.

[22] Li, W. and Assimaki, D. (2010) Site-and motion-dependent parametric uncertainty of site-response analyses in earthquake simulations, *Bulletin of the Seismological Society of America*, vol. 100, no. 3, pp. 954–968.

[23] Abdollahiparsa, H., Homami, P., and Khoshnoudian, F. (2016) Effect of vertical component of an earthquake on steel frames considering soil-structure interaction, *KSCE Journal of Civil Engineering*, vol. 20, no. 7, pp. 2790–2801. doi: 10.1007/s12205-016-0687-y.

[24] Madiai, C., Facciorusso, J., Gargini, E., and Baglione, M. (2016) 1D versus 2D site effects from numerical analyses on a cross section at Barberino di Mugello (Tuscany, Italy), *Procedia Engineering*, vol. 158, pp. 499–504.

[25] McGann, C. R., Bradley, B., Wotherspoon, L., and Lee, R. (2021) Basin effects and limitations of 1D site response analysis from 2D numerical models of the Thorndon basin, *Bulletin of the New Zealand Society for Earthquake Engineering*, vol. 54, no. 1, pp. 21–30.

[26] Makra, K. and Chávez-García, F. J. (2016) Site effects in 3D basins using 1D and 2D models: an evaluation of the differences based on simulations of the seismic response of Euroseistest, *Bulletin of Earthquake Engineering*, vol. 4, pp. 1177–1194.

[27] Pretell, R., Ziotopoulou, K., and Abrahamson, N. A. (2022) Numerical investigation of VS spatial variability effects on the seismic response estimated using 2D and 1D site response analyses, *Geo-Congress 2022*, pp. 205–215.

[28] Timuraglu, M. Ö., Fahjan, Y., and Dogangun, A. (2022) Comparison of one and three dimensional site response analyses, *Pamukkale University Journal of Engineering Sciences*, vol. 28, no. 3, pp. 372–377. doi: 10.5505/pajes.2021.40565.

[29] Lopez-Caballero, F., Modaressi, A., Razavi, F., and Modaressi, H. (2007) Nonlinear numerical method for earthquake site-response analysis I—elastoplastic cyclic model and parameter identification strategy, *Bulletin of Earthquake Engineering*, vol. 5, pp. 303–323.

[30] Semblat, J. F. et al. (2005) Seismic wave amplification: Basin geometry vs soil layering, *Soil Dynamics and Earthquake Engineering*, vol. 25, no. 7, pp. 529–538. doi: https://doi.org/10.1016/j.soildyn.2004.11.003.

[31] Torre, C. D. E. L. A., McGann, C., Bradley, B., and Pletzer, A. (2023) 3D seismic site response with soil heterogeneity and wave scattering in OpenSees.

[32] Alonso, F. et al. (2023) Site Response Analysis (SRA): A Practical Comparison Among Different Dimensional Approaches.

[33] Akinci, A., Aochi, H., Herrero, A., Pischiutta, M., and Karanikas, D. (2017) Physics-based broadband ground-motion simulations for probable Mw¿7.0 earthquakes in the Marmara Sea region (Turkey), *Bulletin of the Seismological Society of America*, vol. 107, pp. 1307–1323.

[34] Douglas, J. and Aochi, H. (2016) Assessing components of ground-motion variability from simulations for the Marmara Sea region (Turkey), *Bulletin of the Seismological Society of America*, vol. 106, no. 1, pp. 300–306.

[35] Seylabi, E., Restrepo, D., Taborda, R., and Asimaki, D. (2021) Deterministic ground motion simulations with shallow crust nonlinearity at Garner Valley in Southern California, *Earthquake Engineering and Structural Dynamics*, vol. 50, no. 1, pp. 43–59.

[36] Zhang, W., Crempien, J. G. F., Kurtulus, A., Chen, P.-Y., Arduino, P., and Taciroglu, E. (2023) A suite of broadband physics-based ground motion simulations for the Istanbul region, *Earthquake Engineering and Structural Dynamics*, pp. 1161–1181.

[37] Smerzini, C. and Pitilakis, K. (2018) Seismic risk assessment at urban scale from 3D physics-based numerical modeling: The case of Thessaloniki, *Bulletin of Earthquake*

Engineering, vol. 16, no. 7, pp. 2609–2631. doi: 10.1007/s10518-017-0287-3.

[38] Ozcebe, A. G. et al. (2019) On the comparison of 3D, 2D, and 1D numerical approaches to predict seismic site amplification: The case of Norcia basin during the M6.5 2016 October 30 earthquake, in *Earthquake Geotechnical Engineering for Protection and Development of Environment and Constructions*, CRC Press, pp. 4251–4258.

[39] Sadeghzadeh, S., and Ansal, A. (2023) A comparison study between 1D and 3D site response analyses based on observed earthquake acceleration records, *Eccomas Proceedia COMPDYN*.

[40] Ansal, A., Tönük, G., and Sadeghzadeh, S. (2024) Site response analysis in performance based approach, *Soil Dynamics and Earthquake Engineering*, vol. 178, p. 108480.

[41] Wikipedia contributors, (n.d.) Robert B. Atwood Building — Wikipedia, The Free Encyclopedia. [Online].

[42] Çelebi, M. (2006) Recorded Earthquake Responses from the Integrated Seismic Monitoring Network of the Atwood Building, Anchorage, Alaska, *Earthquake Spectra*, vol. 22, no. 4, pp. 847–864, doi: 10.1193/1.2359702.

[43] Brinkgreve, R. B. J., and Vermeer, P. A. (1997) Plaxis finite element code for soil and rock analysis-Version, *Balkema*, Rotterdam.

[44] 3D Software, P. (2023) Refer to `https://www.bentley.com/software/plaxis-3d`.

[45] Gu, Q., Conte, J. P., and Barbato, M. (2010) OpenSees Command Language Manual — Response Sensitivity Analysis based on the Direct Differentiation Method (DDM), `http://opensees.berkeley.edu`.

[46] Hashash, Y., Park, D., Tsai, C. C., Philips, C., and Groholski, D. R. (2023) DEEPSOIL - 1-D Wave Propagation Analysis Program for Geotechnical Site Response Analysis of Deep Soil Deposits, Version 7.

[47] Kaklamanos, J., Baise, L. G., Thompson, E. M., and Dorfmann, L. (2014) Comparison of 1D linear, equivalent-linear, and nonlinear site response models at six KiK-net validation sites, *Soil Dynamics and Earthquake Engineering*.

[48] Kaklamanos, J., Baise, L. G., Thompson, E. M., and Dorfmann, L. (2014) Comparison of 1D linear, equivalent-linear, and nonlinear site response models at six KiK-net validation sites, *Soil Dynamics and Earthquake Engineering*.

[49] Phillips, C., and Hashash, Y. M. A. (2009) Damping formulation for nonlinear 1D site response analyses, *Soil Dynamics and Earthquake Engineering*, vol. 29, no. 7, pp. 1143–1158.

[50] Vucetic, B. M. and Dobry, R. (1972) Effect of soil plasticity on cyclic response.

[51] Knabe, T., Datcheva, M., Lahmer, T., Cotecchia, F., and Schanz, T. (2013) Identification of constitutive parameters of soil using an optimization strategy and statistical analysis, *Comput Geotech*, vol. 49, pp. 143–157.

[52] PLAXIS. (2023) Manuals - PLAXIS - GeoStudio.

[53] Celik, S. (2017) Comparison of Mohr-Coulomb and Hardening Soil Models Numerical Estimation of Ground Surface Settlement Caused by Tunneling, *Journal of the Institute of Science and Technology*, vol. 7, pp. 95–102. doi: 10.21597/jist.2017.202.

[54] Çelik, S. (2017) Comparison of Mohr-Coulomb and Hardening Soil Models: Numerical Estimation of Ground Surface Settlement Caused by Tunneling, *Journal of the Institute of Science and Technology*, vol. 7, pp. 95–102, doi: 10.21597/jist.2017.202.

[55] Kondner, R. L. (1963) A hyperbolic stress-strain formulation for sands, in *Proc. 2nd Pan-American Conf. on SMFE*, pp. 289–324.

[56] Duncan, J. M., and Chang, C.-Y. (1970) Nonlinear analysis of stress and strain in soils, *Journal of the Soil Mechanics and Foundations Division*, vol. 96, no. 5, pp. 1629–1653.

[57] Numerical modeling of diaphragm wall behavior in Bangkok soil using hardening

soil model — ISSMGE. [Online].

[58] Tafili, M., Grandas Tavera, C., Triantafyllidis, T., and Wichtmann, T. (2021) On the dilatancy of fine-grained soils, *Geotechnics*, vol. 1, no. 1, pp. 192–215.

[59] Puri, N., Prasad, H. D., and Jain, A. (2018) Prediction of Geotechnical Parameters Using Machine Learning Techniques, in *Procedia Computer Science*, Elsevier B.V., pp. 509–517, doi: 10.1016/j.procs.2017.12.066.

[60] Anbazhagan, P., Uday, A., Moustafa, S. S. R., and Al-Arifi, N. S. N. (2017) Soil void ratio correlation with shear wave velocities and SPT N values for Indo-Gangetic basin, *Journal of the Geological Society of India*, vol. 89, no. 4, pp. 398–406, doi: 10.1007/s12594-017-0621-z.

[61] Hudson, M., Idriss, I. M., Beikae, M., et al. (1994) QUAD4M: a computer program to evaluate the seismic response of soil structures using finite element procedures and incorporating a compliant base, *Center for Geotechnical Modeling, Department of Civil and Environmental Engineering, University of California, Davis*.

[62] Lysmer, J., and Kuhlemeyer, R. L. (1969) Finite dynamic model for infinite media, *Journal of the Engineering Mechanics Division*, vol. 95, no. 4, pp. 859–877.

[63] Zhu, M., McKenna, F., and Scott, M. H. (2018) OpenSeesPy: Python library for the OpenSees finite element framework, *SoftwareX*, vol. 7, pp. 6–11.

[64] Zienkiewicz, O. C., and Taylor, R. L. (2005) *The Finite Element Method for Solid and Structural Mechanics*, Elsevier.

[65] Khosravifar, A., Elgamal, A., Lu, J., and Li, J. (2018) A 3D model for earthquake-induced liquefaction triggering and post-liquefaction response, *Soil Dynamics and Earthquake Engineering*, vol. 110, pp. 43–52, doi: 10.1016/j.soildyn.2018.03.017.

[66] Mazzoni, S., McKenna, F., Scott, M. H., and Fenves, G. L. (2006) OpenSees command language manual, *Pacific Earthquake Engineering Research (PEER) Center*, vol. 264, pp. 137–158.

[67] Elgamal, A., Yan, L., Yang, Z., and Conte, J. P. (2008) Three-Dimensional Seismic Response of Humboldt Bay Bridge-Foundation-Ground System, *Journal of Structural Engineering*.

[68] Khosravifar, A. A note on calibrating Pressure Dependent and Pressure Independent Multi Yield Surface Models.

[69] Joyner, W. B., and Chen, A. T. F. (1975) Calculation of nonlinear ground response in earthquakes, *Bulletin of the Seismological Society of America*, vol. 65, no. 5, pp. 1315–1336. [Online].

[70] Nigbor, R. L., and Imai, T. (1994) The suspension P-S velocity logging method, *The Suspension P-S Velocity Logging Method*, pp. 57–61.

[71] Hardin, B. O., and Drnevich, V. P. (1972) Shear modulus and damping in soils: measurement and parameter effects (Terzaghi Lecture), *Journal of the Soil Mechanics and Foundations Division*, vol. 98, no. 6, pp. 603–624.

[72] Hossain, A. S. M. F. (2015) PS Logging for Site Response Analysis in Dhaka City, *University of Quebec in Chicoutimi*.

[73] Characterization of sites and undefined. (1994) The suspension PS velocity logging method, *pascal-francis.inist.fr*. [Online].

[74] Masters, T. A., Juszkiewicz, P., Mandolini, A., and Christian, H. (2019) A critical appraisal of the benefits of and obstacles to gaining quality data with offshore seismic CPT and P-S logging, *Proceedings of the Annual Offshore Technology Conference*, vol. 2019-May, no. April, doi: 10.4043/29485-ms.

[75] Ameen, M. S., Smart, B. G. D., Somerville, J. Mc., Hammilton, S., and Naji, N. A. (2009) Predicting rock mechanical properties of carbonates from wireline logs (A case study: Arab-D reservoir, Ghawar field, Saudi Arabia), *Marine and Petroleum Geology*.

[76] Rasouli, V., Pallikathekathil, Z. J., and Mawuli, E. (2011) The influence of perturbed stresses near faults on drilling strategy: A case study in Blacktip field, North Australia,

Journal of Petroleum Science and Engineering.

[77] Boonen, P., Bean, C., Tepper, R., and Deady, R. (1998) Important Implications from a Comparison of LWD and Wireline Acoustic Data from a Gulf of Mexico Well, *SPWLA Annual Logging Symposium*.

[78] Eissa, E. A., and Kazi, A. (1988) Relation between static and dynamic Young's moduli of rocks, *International Journal of Rock Mechanics and Mining Geomechanics Abstracts*, vol. 25, no. 6.

[79] McKenna, F., Fenves, G. L., Scott, M. H., and others. (2000) Open system for earthquake engineering simulation, *University of California, Berkeley, CA*.

[80] Michalewicz, Z., and Schoenauer, M. (1996) Evolutionary algorithms for constrained parameter optimization problems, *Evolutionary Computation*, vol. 4, no. 1, pp. 1–32.

[81] Goldberg, D. E. (1986) The Genetic Algorithm Approach: Why, How, and What Next?, *Springer Science+Business Media New York*.

[82] Kumar, V., Chhabra, J. K., and Kumar, D. (2014) Parameter adaptive harmony search algorithm for unimodal and multimodal optimization problems, *Journal of Computational Science*, vol. 5, no. 2, pp. 144–155.

[83] Bonabeau, E., Dorigo, M., and Theraulaz, G. (1999) Swarm intelligence: from natural to artificial systems, *Oxford University Press*.

[84] Kumar, V., and Kumar, D. (2017) An astrophysics-inspired grey wolf algorithm for numerical optimization and its application to engineering design problems, *Advances in Engineering Software*, vol. 112.

[85] Kang, Y. L., Lin, X.-H., and Qin, Q. H. (2004) Inverse/genetic method and its application in identification of mechanical parameters of interface in composite, *Composite Structures*, vol. 66, pp. 449–458.

[86] Wrobel, L. C., and Miltiadou, P. (2004) Genetic algorithms for inverse cathodic protection problems, *Engineering Analysis with Boundary Elements*, vol. 28, no. 3, pp.

267–277.

[87] Liu, D. (2019) Mathematical modeling analysis of genetic algorithms under schema theorem, *Journal of Computational Methods in Sciences and Engineering*.

[88] Wikipedia contributors. Robert B. Atwood Building — Wikipedia, The Free Encyclopedia.

[89] Çelebi, M. (2006) Recorded Earthquake Responses from the Integrated Seismic Monitoring Network of the Atwood Building, Anchorage, Alaska, *Earthquake Spectra*, vol. 22, no. 4, pp. 847–864, doi: 10.1193/1.2359702.

[90] Brinkgreve, R. B. J., and Vermeer, P. A. (1997) Plaxis finite element code for soil and rock analysis-Version, Balkema, Rotterdam.

[91] Bentley 3D Software. (2023) Refer to www.bentley.com.

[92] Gu, Q., Conte, J. P., and Barbato, M. (2010) OpenSees Command Language Manual — Response Sensitivity Analysis based on the Direct Differentiation Method (DDM), `http://opensees.berkeley.edu`. [Online].

[93] Hashash, Y., Park, D., Tsai, C. C., Philips, C., and Groholski, D. R. (2023) DEEPSOIL - 1-D Wave Propagation Analysis Program for Geotechnical Site Response Analysis of Deep Soil Deposits, Version 7.

[94] Kaklamanos, J., Baise, L. G., Thompson, E. M., and Dorfmann, L. (2014) Comparison of 1D linear, equivalent-linear, and nonlinear site response models at six KiK-net validation sites, *Soil Dynamics and Earthquake Engineering*.

[95] Phillips, C., and Hashash, Y. M. A. (2009) Damping formulation for nonlinear 1D site response analyses, *Soil Dynamics and Earthquake Engineering*, vol. 29, no. 7, pp. 1143–1158.

[96] Hudson, M., Idriss, I. M., and Beikae, M. (1994) QUAD4M: A computer program to evaluate the seismic response of soil structures using finite element procedures and incorporating a compliant base, Center for Geotechnical Modeling, Department of Civil

and Environmental Engineering, University of California, Davis.

[97] Vucetic, B. M., and Dobry, R. Effect of Soil Plasticity on Cyclic Response.

[98] Knabe, T., Datcheva, M., Lahmer, T., Cotecchia, F., and Schanz, T. (2013) Identification of constitutive parameters of soil using an optimization strategy and statistical analysis, *Comput Geotech*, vol. 49, pp. 143–157.

[99] Manuals - PLAXIS - GeoStudio — PLAXIS Wiki - GeoStudio — PLAXIS - Bentley Communities. [Online].

[100] Çelik, S. (2017) Comparison of Mohr-Coulomb and Hardening Soil Models Numerical Estimation of Ground Surface Settlement Caused by Tunneling, *Journal of the Institute of Science and Technology*, vol. 7, pp. 95–102, doi: 10.21597/jist.2017.202.

[101] Kondner, R. L. (1963) A hyperbolic stress-strain formulation for sands, in *Proc. 2nd Pan-American Conf. on SMFE*, pp. 289–324.

[102] Duncan, J. M., and Chang, C.-Y. (1970) Nonlinear analysis of stress and strain in soils, *Journal of the Soil Mechanics and Foundations Division*, vol. 96, no. 5, pp. 1629–1653.

[103] ISSMGE. (2023) Numerical modeling of diaphragm wall behavior in Bangkok soil using hardening soil model. [Online].

[104] Tafili, M., Grandas Tavera, C., Triantafyllidis, T., and Wichtmann, T. (2021) On the dilatancy of fine-grained soils, *Geotechnics*, vol. 1, no. 1, pp. 192–215.

[105] Puri, N., Prasad, H. D., and Jain, A. (2018) Prediction of Geotechnical Parameters Using Machine Learning Techniques, in *Procedia Computer Science*, Elsevier B.V., pp. 509–517, doi: 10.1016/j.procs.2017.12.066.

[106] Anbazhagan, P., Uday, A., Moustafa, S. S. R., and Al-Arifi, N. S. N. (2017) Soil void ratio correlation with shear wave velocities and SPT N values for Indo-Gangetic basin, *Journal of the Geological Society of India*, vol. 89, no. 4, pp. 398–406, doi: 10.1007/s12594-017-0621-z.

[107] Hudson, M., Idriss, I. M., and Beikae, M. (1994) QUAD4M: A computer program to evaluate the seismic response of soil structures using finite element procedures and incorporating a compliant base, Center for Geotechnical Modeling, Department of Civil and Environmental Engineering.

[108] Lysmer, J., and Kuhlemeyer, R. L. (1969) Finite dynamic model for infinite media, *Journal of the Engineering Mechanics Division*, vol. 95, no. 4, pp. 859–877.

VITA

Name Surname: Shima Sadeghzadeh

Education:

Ph.D. in Civil Engineering (Geotechnical Earthquake Engineering), Özyeğin University, Turkey (GPA: 4.00)

Master's Degree in Civil Engineering (Geotechnical Engineering), University of Mohaghegh Ardabili, Ardabil,Iran (GPA: 3.91)

Bachelor's degree in Civil Engineering, University of Mohaghegh Ardabili, Ardabil, Iran. (GPA: 3.40)

Awards and Scholarships:

[1] Teaching and Research Assistant, Özyeğin University, Istanbul/Türkiye.

[2] Research Scholarship Tubitak, Özyeğin University, title: ''Assessment of Soil-Foundation-Structure Interaction Effects under Seismic Loads"

[3] Research Scholarship ReLuis (Consorzio della Rete dei Laboratori Universitari di Ingegneria Sismica e Strutturale). Reluis Ponti Program, Roma Tre University, Rome, Italy.

[4] Research Scholarship, Politecnico di Torino, Turin Italy.

[5] OPENSEES Course Certificate awarded in 2022, Politecnico di Torino, Italy.

[6] Bentley PLAXIS3D Course Certificate, awarded in 2022, Istanbul, Türkiye.

Publications:

[1] A. Ansal, G. Tönük, S. Sadeghzadeh "Site Response Analysis in Performance-Based Approach" published at Soil Dynamics and Earthquake Engineering, Elsevier, Volume 178, 2024.

[2] S. Sadeghzadeh, A. P. Sberna, F. Di Trapani, C. Demartino, “Enhancing seismic site response analyses: tuning soil properties via genetic algorithms and Bayesian model updating from downhole array data” submitted at Soil Dynamics and Earthquake Engineering, Elsevier, November 2024. (Under Review)

[3] S. Sadeghzadeh, A. Ansal, “Impact of Long-Duration Earthquakes on Site Response: Comparison of 1D and 3D approaches” submitted to Journal of Seismology, December 2024. (Under Review)

[4] S. Sadeghzadeh, A. Ansal, ”A Comparison Study Between 1D and 3D Site Response Analyses Based on Observed Earthquake Acceleration Records”. COMPDYN 2023, 9th ECCOMAS Thematic Conference on Computational Methods in Structural Dynamics and Earthquake Engineering, Athens, Greece, June 12-14, 2023. (SCOPUS Cited)

[5] S. Sadeghzadeh, A. Ansal, ”Numerical Verification of 3D Site Response Analysis Based on Obtained Seismic Records in Istanbul”. 18th World Conference on Earthquake Engineering (WCEE 2024), July 2024, Milan, Italy.

[6] S. Sadeghzadeh, C. Nuti, C. Demartino, ”Seismic Performance and Residual Life Analysis of Corroded Concrete Bridges in Italy: A Case Study”. Engineering Mechanics Institute and Probabilistic Mechanics and Reliability Conference (EMI/PMC 2024), University of Illinois Urbana-Champaign, Chicago, IL, USA, May 28-31, 2024. (Published at Book of Abstracts R-V$_E MI - PMC 2024.pdf$)

[7] S. Sadeghzadeh, C. Demartino, F. Di Trapani, A. P. Sberna, A. Ansal, “Soil Profile Numerical Model Optimization for Multi-Directional Site Response Analysis Using OpenSees”. 6th Eurasian Conference on OpenSees, OpenSees Days 2024, Beijing, China, July 24-25, 2024.

[8] S. Sadeghzadeh, A. Ansal, A. Kurtulus “The Effects of Fault Type for the Selection of Input Acceleration Records for Site Response Analysis”. ZMGM18 the 18th National Conference on Soil Mechanic and Geotechnical Engineering, Kayseri, Turkey,

September 30, 2022.

[9] S. Sadeghzadeh, A. Negahdar, B. Easazadeh “Thermal and Weather Condition on Confined Compressive test in Fine Grain soils”. 1st International Conference on Water, Environment and sustainable Development, Mohaghegh University of Ardabil, Iran, September 28, 2016.